Spontaneous And Template-Directed Emergence Of Low-Symmetry Foldamers From Dynamic Homomeric Sequences

Charalampos G. Pappas,[a] Pradeep K. Mandal,[b] Bin Liu,[a] Brice Kauffmann,[c] Xiaoming Miao,[a] David Komáromy,[a] Waldemar Hoffmann,[d,e] Christian Manz,[d,e] Rayoon Chang,[d,e] Kai Liu,[a] Kevin Pagel,[d,e] Ivan Huc*[b] and Sijbren Otto*[a]

[a]Centre for Systems Chemistry, Stratingh Institute, Nijenborgh 4, 9747 AG Groningen, The Netherlands. [b]Department of Pharmacy and Center for Integrated Protein Science, Ludwig-Maximilians Universität, Butenandstraße 5-13, D-81377 Munich, Germany. [c]Université de Bordeaux, CNRS, INSERM, UMS3033, Institut Européen de Chimie et Biologie, 2 rue Robert Escarpit, 33600 Pessac, France. [d]Institute of Chemistry and Biochemistry, Freie Universität Berlin, Takustraße 3, 14195 Berlin, Germany. [e]Fritz Haber Institute of the Max Planck Society, Faradayweg 4-6, 14195 Berlin, Germany.

The self-assembly of a defined number of identical molecular units into discrete objects is to some extent understood and amenable to design. No matter how large, these objects generally lack complexity in that their sub-components engage in similar interactions with their neighbors, resulting in high symmetry of the assembly, as various types of rings and cages illustrate.[1-4] Homomeric assemblies with no symmetry may occur in the asymmetric unit of crystals lattices,[5,6] but these assemblies are not discrete and may not exist in solution. Herein, we report the discovery of the self-templated formation of exceptionally large dynamic macrocycles having well-defined folded conformations with low symmetry and substantial structural complexity. Each macrocycle consists of identical subunits, but their roles and interactions with neighbor units in the final structure differ. In the chemical space explored so far of poly-(disulfides) of dipeptidyl aryl-dithiols, the occurrence of such structures is both frequent and diverse. It is driven by folding into well-defined conformations akin to those of biopolymers with the remarkable difference that the sequences described here are homomeric and largely devoid of secondary structure elements. Thus, a 16mer (8.3 kDa) with eight distinct environments and a 23mer (10.9 kDa) with twelve distinct environments spontaneously form from their respective building block at the exclusion of shorter or longer sequences. Upon subtle chemical variations, a 9mer, a 17mer and a 20mer also emerged. Structure elucidation shows that, in contrast with biopolymers, the folded conformations of these macrocycles show limited hierarchy. Metal ions or small molecules template the formation of other ring sizes (12mer and 13mer). The macrocycles were capable of binding their templates.

Dynamic bonds, whether covalent or noncovalent, are essential for accessing discrete self-assembled structures, as they allow for error-correction during assembly processes, giving rise to the thermodynamically most stable object.[7-11] In dynamic combinatorial chemistry these characteristics are combined with the ability to screen structural space for the most stable assemblies from among many related structures.[12-14] Dynamic combinatorial approaches to foldamers[15-18] involve creating mixtures of molecules that exchange building blocks by reversible covalent chemistry. Noncovalent interactions within folded structures cause these to be more stable than their non-folded counterparts, shifting the product distribution of the dynamic combinatorial library (DCL) in the direction of, ideally, the most stably folded structures. Despite early proof-of-principle results,[19] this approach has so far not lived up to the promise of delivering foldamers with unexpected and

unpredictable structures. Encouraged by our recent discovery of a new foldamer based on a chimeric nucleobase-amino-acid conjugate[20] we intensified our exploration of structural space focused on building blocks with a 1,3-dimercaptobenzene core carrying a side chain in the 5-position (Fig. 1). We focused our search on dipeptides as side chains (R).

a

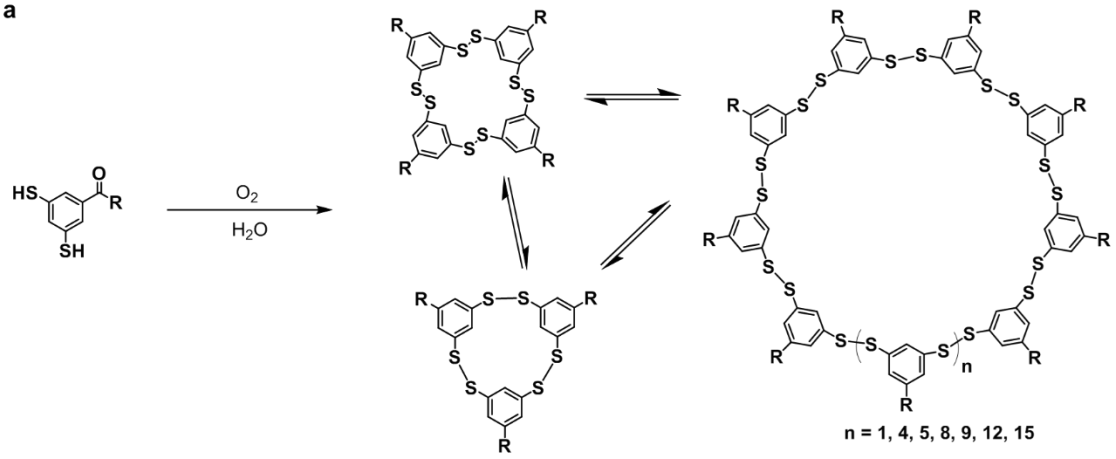

b

Entry	R	Ring size
1a	-OH	3, 4
1b	-Asp-OH	3, 4
1c	-Asp-Lys-OH	3, 4
1d	-4-Pro-Lys-OH	3, 4
2a	-Phe-Lys-OH	4
2b	-Phe(4-CF_3)-Lys-OH	4
2c	-Phe(4-OCH_3)-Lys-OH	4
2d	-Phe(4-F)-Lys-OH	4
2e	-Phe(4-NO_2)-Lys-OH	4
3a	-Phe(4-OH)-Lys-OH	family of oligomers
3b	-Lys-Phe(4-OH)-OH	family of oligomers
3c	-Ser-Lys-OH	family of oligomers
3d	-Phe-OH	family of oligomers
4a	-Phe(4-COOH)-Lys-OH	9, 12, 13
4b	-Phe(4-guanidinium)-Lys-OH	16
4c	-Phe(4-CH_2NH_2)-Lys-OH	16, 23
4d	-Phe(4-NH_2)-Lys-OH	23
4e	-Phe(4-COOH)-Lys(N^6-CH_3)-OH	9
4f	-Phe(4-NH_2)-Lys(N^6-$(CH_3)_2$)-OH	23
4g	-Lys-Phe(4-NH_2)-OH	20
4h	-Lys-Phe(4-guanidinium)-OH	17

c

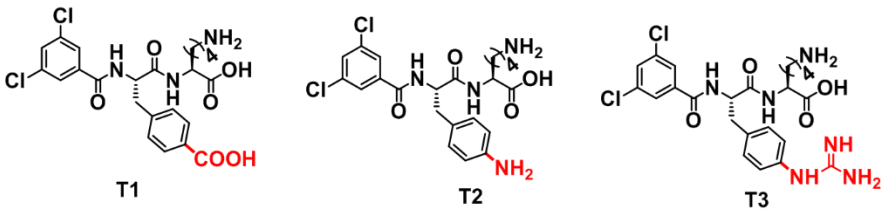

Fig. 1. Foldamers from dynamic combinatorial libraries. **a**, Dithiol building blocks oxidize to form DCLs of differently size disulfide macrocycles. **b**, Product distribution of DCLs prepared from different building blocks. **c**, Chemical structure of peptide templates.

DCLs were generated by dissolving building blocks at 2.0 mM concentration in buffered aqueous solution (pH = 8.0). The presence of oxygen from the air is sufficient to oxidize the thiols into disulfides, which exchange with each other as long as residual thiolate is present in the medium.[21] As benchmark, a small DCL was made from parent derivative **1a**, with a carboxylate group in the 5-position. Analysis of the library composition using Ultra Performance Liquid Chromatography/Mass Spectrometry (UPLC/MS) showed that it was dominated by small three- and four-membered rings (Fig. 2a). This product distribution reflects the entropic tendency of relatively dilute DCLs to be dominated by the smallest non-strained rings. A survey of a series of derivatives of **1a** revealed three types of behavior (Fig. 1, Fig. 2a). DCLs made from building block families **1** (featuring hydrophilic peptides) and **2** (featuring hydrophobic amino-acid side groups) gave rise to small rings, like parent molecule **1a**. Much larger rings form from building block families **3** and **4** which feature an amphiphilic amino-acid side group. For building block family **4** we observed the remarkably selective formation of large rings ranging from 9mers to 23mers, of which several have a prime number of units (13, 17, 23) rarely encountered in self-assembly and incompatible with symmetry elements other than unlikely high order axes (C_{13}, C_{17} or C_{23}, respectively). Specifically, upon modifying building block **2a**, that formed only a small macrocycle, with a carboxylic acid group (to give **4a**) a 9mer macrocycle $(\mathbf{4a})_9$ accounted for 75% of the library material. Analogous building block **4b**, carrying a guanidinium group, selectively yielded 16mers $(\mathbf{4b})_{16}$. The corresponding chromatogram showed two distinct peaks with the same mass. The ^{1}H-NMR spectrum of the early-eluting peak shows sharp signals suggesting a conformationally defined species (Supplementary Fig. 89). UPLC analysis of the original sample after lyophilization, followed by dissolution in DMF gave only one main peak, eluting late (Supplementary Fig. 60). ^{1}H-NMR analysis of this material revealed broad signals (Supplementary Fig. 91), indicating a disordered conformation. Thus, the second peak most likely arises from partial unfolding of the material during analysis. Introducing an aminomethyl substituent on the aromatic ring (**4c**) also gave rise to a 16mer, which was now accompanied by 10% of a 23mer. Substitution by an amino group (**4d**) led to 95% conversion into 23mer $(\mathbf{4d})_{23}$. Methylation of the lysine residue in **4a** and **4d** (to give **4e** and **4f**, respectively) had limited impact on the library composition. In contrast, monomers **4h** and **4g**, the constitutional isomers of **4b** and **4d**, respectively, in which the amino-acid sequence was reserved, yielded macrocycles $(\mathbf{4g})_{20}$ and $(\mathbf{4h})_{17}$. UPLC/MS characterization of the samples above is provided in Supplementary Information (Supplementary Figs. 1-87).

The selectivity with which the large rings form for building block family **4** suggests that the rings benefit from specific non-covalent interactions that occur most efficiently with the particular observed ring size; i.e. these rings appear to be foldamers. This hypothesis was confirmed through circular dichroism (CD) and NMR spectroscopy, ion mobility-mass spectrometry (IM-MS) and x-ray crystallography. Initial evidence suggesting that the large macrocycles adopt specific folded conformation came from IM-MS. The change in rotationally averaged collision cross-sections (CCS) as a function of the number of subunits in a macrocycle provides information regarding the extent of folding. If the macrocycles can be approximated as two-dimensional objects, the CCS is expected to increase linearly with the number of subunits, whereas the formation of compact three-dimensional shapes gives rise to a smaller CCS than predicted by the linear growth trend.[22] Regardless of the building block used, the smaller macrocycles of all libraries follow such a linear growth trend up to hexamers. In contrast, $(\mathbf{4a})_9$ and in particular $(\mathbf{4b})_{16}$ and $(\mathbf{4d})_{23}$ adopt significantly more compact structures than predicted by the linear growth trend (Figs. 2c-e, Supplementary Tables 1-3).

Further evidence suggesting well-defined assemblies came from CD and NMR. While solutions of the monomers **4a**, **4b** and **4d** show only very weak CD signals, intense and distinct CD bands were observed for $(\mathbf{4a})_9$, $(\mathbf{4b})_{16}$ and $(\mathbf{4d})_{23}$ indicating that these structures have substantially different folds (Fig. 2f). Solution-phase ^{1}H-NMR spectra of the three large macrocycles (D_2O, 298K) also demonstrated well-defined conformations and limited flexibility, as evident from the presence of remarkably sharp peaks (Supplementary Figs. 88-90). Temperature dependent NMR (Supplementary Figs. 92-94) and CD experiments (Fig. 2g) show that $(\mathbf{4b})_{16}$ and $(\mathbf{4d})_{23}$ start to unfold only upon heating above 60°C, whereas $(\mathbf{4a})_9$ unfolds at lower temperatures. Refolding was observed in all cases after a heat-cool cycle (Supplementary Figs. 95-98) and subsequent UPLC measurements revealed that the composition remained unchanged.

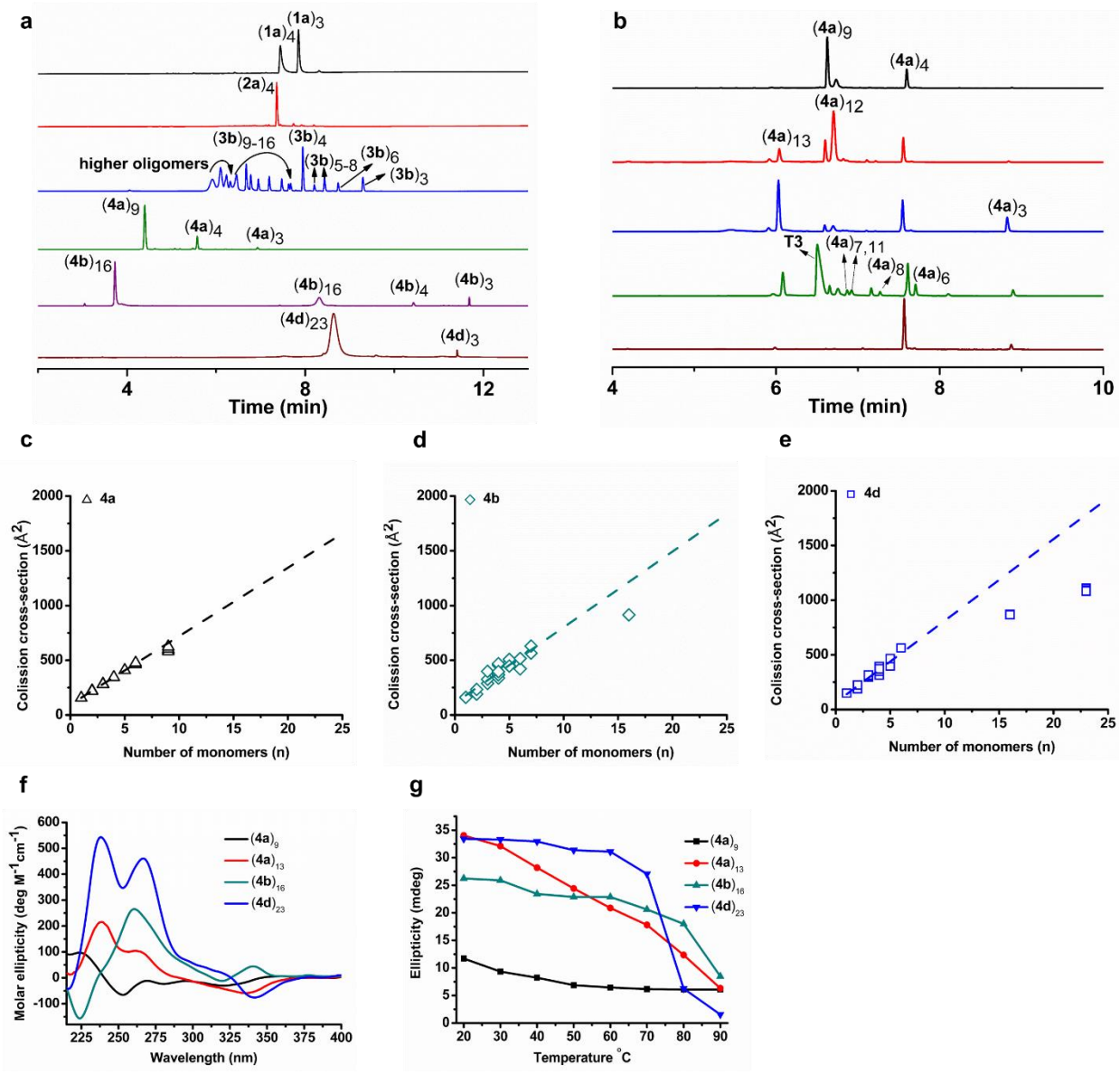

Fig. 2. Spontaneous formation of large folded macrocycles. **a**, UPLC chromatograms (absorption at 254 nm) showing compositions after 16 days of stirring of DCLs made from 2.0 mM of (from top to bottom) **1a**, **2a**, **3b**, **4a**, **4b** and **4d** in 12.5 mM borate buffer pH = 8.0. **b**, UPLC chromatograms made from 2.0 mM of **4a** in presence of (from top to bottom): 1.0 M NaCl; 1.0 M $MgCl_2$, 1.0 M $MnCl_2$, 5.0 mM template **T3** and 1.0 M guanidinium chloride. Collision cross-sections for library members,

indicating the formation of compact conformations for **c**, (**4a**)$_9$, **d**, (**4b**)$_{16}$ and **e** (**4d**)$_{23}$. **f**, CD spectra of the libraries prepared from **4a**, **4b** and **4d** after 16 days. **g**, Changes in ellipticity at specified wavelengths in CD spectra of the libraries prepared from **4a** (at 252 nm for (**4a**)$_9$ and 238 nm for (**4a**)$_{13}$), **4b** (at 260 nm) and **4d** (at 266 nm) upon heating, indicating different unfolding temperatures. For (**4a**)$_9$ the absolute value of CD signal at 252 nm was taken for a better comparison.

Decisive evidence for foldamer formation came from analysis by x-ray crystallography of macrocycles (**4b**)$_{16}$ and (**4d**)$_{23}$ (Fig. 3, Supplementary Figs. 99-108). Each structure revealed a well-defined and novel fold. In both cases, the 1,3-dimercaptobenzene macrocycle collapsed to form a dense hydrophobic core as observed in globular proteins. However, unlike proteins, no hierarchy between secondary and tertiary folding can be distinguished, as distinct secondary elements (such as helices and sheets) are lacking. The dipeptides have peripheral positions and form multiple hydrogen bonds. The phenylalanine side chains partially shield the hydrophobic cores and 4-substituents are often involved in intramolecular interaction networks. The charged functions are exposed to the solvent and frequently disordered. The overall structure of (**4b**)$_{16}$ has only one crystallographic C_2 axis, thus defining eight distinct environments for **4b**. The symmetry of the core is higher and reflected in the ^{1}H NMR spectrum (Supplementary Fig. 89) suggesting that the arrays of dipeptide side-chains exchange rapidly on the NMR timescale. Similarly, a pseudo-C_2 axis in the structure of (**4d**)$_{23}$ defines twelve distinct environments for **4d**. This low symmetry contrast with the C_5-symmetrical, propeller-shaped, chimeric nucleobase-amino-acid conjugate found previously,[20] and with all self-assembled homomeric structures described to date. It appears to be the result of a balance between two antagonistic parameters: (i) the high potential of each monomer for forming strong interactions *via* hydrophobic effects, hydrogen bonds, chalcogen bonds, and salt bridges, and (ii) the geometrical constraints imposed by the semi-rigidity of the 1,3-dimercaptobenzene backbone and macrocyclization. Small macrocycles may not provide enough degrees of freedom to fulfill a large number of interactions intramolecularly. It is remarkable that, for many derivatives, a unique structure exists that fulfills interactions so much better than others that it constitutes a dominant product. This is not always the case though and **3a**-**3d**, which possess fewer hydrogen bonding units than **4a**-**4h**, produce a range of large rings. Remarkably, macrocycle growth and folding occur in preference over aggregation which may have constituted alternate pathways to fulfill interactions.[21]

The dynamic combinatorial approach to folded macromolecules has as yet unrealized potential for the development of functional foldamers. Specifically, addition of a template molecule that can bind to a constitutionally dynamic foldamer should lead to the amplification of this species at the expense of other library members. After isolation the amplified foldamer should be able to selectively recognize and bind to its template. Our attempts to implement this strategy focused on the DCL prepared from **4a**, which gave foldamer (**4a**)$_9$. We reasoned that the relatively low stability of this foldamer (Supplementary Figure 92) would make the template-induced formation of other foldamers easier. Furthermore, the presence of carboxylate groups in **4a** makes this building block potentially suitable for binding to metal ions. Indeed, the addition of NaCl, $MgCl_2$ or $MnCl_2$ resulted in the formation of (**4a**)$_{12}$ and (**4a**)$_{13}$ (top three traces in Fig. 2b). In the presence of 1.0 M guanidinium chloride (a widely used denaturant of proteins) these effects were suppressed (bottom trace in Fig. 2b). These template effects are due to the metal cations, as different anions did not affect the composition of library, except for I^-, which favored (**4a**)$_4$ (Supplementary Fig. S109). Macrocycle (**4a**)$_{13}$ was isolated in 90% purity using flash column chromatography (Supplementary Fig. 110) and its binding to $MnCl_2$ was investigated using Isothermal Titration Calorimetry (ITC) revealing a binding

constant of 4×10^4 M^{-1} (Supplementary Fig. 111). Interestingly, (**4a**)$_9$ and (**4a**)$_{13}$ exhibit substantially different folds and unfolding temperatures (Figs. 2f, g), even though they are made from the same building block.

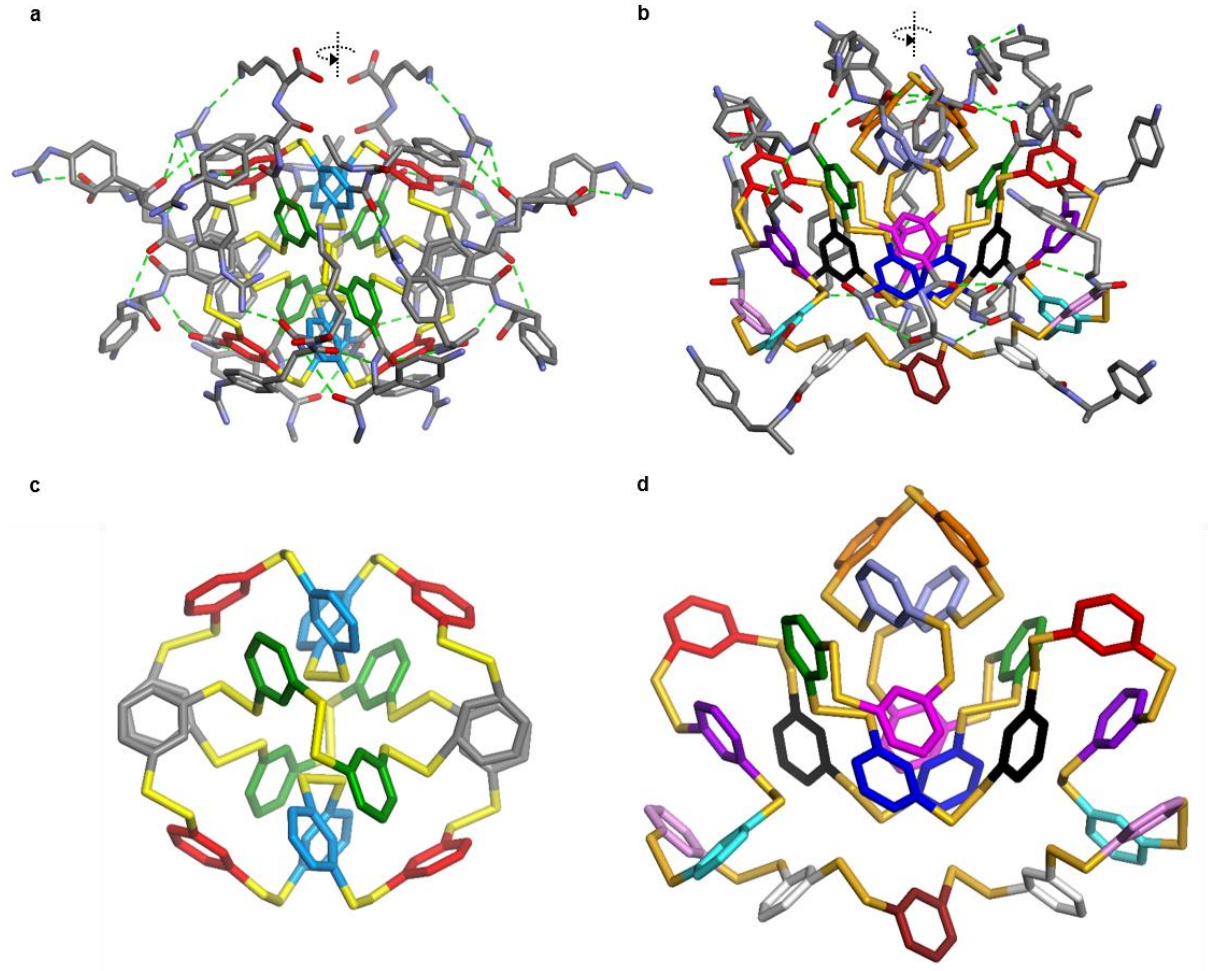

Fig. 3. Crystal structures of (**4b**)$_{16}$ (**a**,**c**) and (**4d**)$_{23}$ (**b**,**d**). Hydrogen bonds involving peptidic side chains are shown as green dashed lines in **a** and **b**. The views in **c** and **d** show the 1,3-dimercaptobenzene hydrophobic backbones alone. Benzene rings are color coded according to their environment. The core of (**4b**)$_{16}$ (**c**) possesses three apparent C_2 symmetry axes but two of them do not apply to the dipeptide appendages eventually generating eight different environments.

We also investigated whether peptides resembling the dithiol monomers would template the formation of foldamers. Thus, dipeptides **T1**-**T3** were mixed with libraries made from building blocks **4a**, **4b** or **4d**. We found that **T3** strongly influenced the macrocyclization of **4a**, eventually favoring (**4a**)$_{13}$ (35% conversion at 1:2.5 **4a**/**T3** ratio, Fig. 2b). ITC experiments (Supplementary Fig. 112) revealed that (**4a**)$_{13}$ binds to **T3** with a K_a of 8.1×10^3 M^{-1}. **T1** and **T2** showed considerably lower affinity (Supplementary Figs. 113, 114). Additionally, smaller rings such as (**4a**)$_4$ showed limited affinity to **T3** (Supplementary Fig. 115). No template effects were observed in libraries made from **4b** and **4d** (Supplementary Figs. 116-122), possibly due to the higher thermodynamic stability of (**4b**)$_{16}$ and (**4d**)$_{23}$ compared to(**4a**)$_9$.

Using a systems chemistry approach, we have thus discovered the spontaneous or template-induced formation of foldamers of unprecedented complexity. The 1,3-dimercaptobenzene core proved to be versatile, adopting varied conformations depending on the side-chain it carries. This is similar to how peptide side chains direct protein folding with the major difference that complex folds are shown here to emerge from homomeric sequences. Rules are starting to emerge for the design of the building blocks that give rise to foldamers in DCLs. Folding is a cooperative phenomenon, requiring large molecules. Thus, the inherent tendency to form small-ring assemblies needs to be overcome, which can be achieved using hydrophobically frustrated building blocks that are unable to shield their hydrophobic parts from water when part of a small oligomer. The preferential formation of one particular foldamer requires it to be substantially more stable than other potential foldamers of similar sizes. Such differences in stability likely require the presence of a sufficiently large number of non-covalent interactions with relatively strong angle- and distance dependence, such as, for example, hydrogen bonds. Indeed, the main difference between the behavior of building blocks in family **3** (forming a range of large rings) and family **4** (forming one specific foldamer) is the higher propensity for forming hydrogen bonds in the latter. Our results have bearing in diverse areas of chemistry. The spontaneous and uniquely selective oligomerization of simple monomer units into oligomers that are of uniform length and are conformationally well-defined, as demonstrated here, has been a long-standing objective in polymer science. Our work also makes it possible to obtain, for the first time, molecularly imprinted polymers[23] that are uniform and have well-defined conformations, addressing two long-standing challenges in the field.

Data Availability

The raw datasets generated during and/or analysed during the current study are available from the corresponding author upon reasonable request.

Author information

Reprints and permissions information is available at www.nature.com/reprints. The authors declare no competing financial interests. Correspondence and requests for materials should be addressed to I.H. (ivan.huc@cup.lmu.de) and S.O. (s.otto@rug.nl).

Acknowledgments

We thank Dr. I. Melnikov (ID23-1, ESRF, Grenoble, France) and Dr. G. Pompidor (PETRA III, DESY, Hamburg, Germany) for assistance during data collection at synchrotron beamlines. This research was supported by the ERC (AdG 741774), the EU (MCIF 745805−DSR), NWO (VICI grant), Zernike Dieptestrategie and the Dutch Ministry of Education, Culture and Science (Gravitation program 024.001.035).

Author Contributions

S.O. and I.H. supervised the overall project. C.G.P. conceived and designed the study, synthesized the building blocks, analyzed the DCL compositions by UPLC and isolated and characterized the foldamers by CD and NMR. B.L. performed the UPLC-MS experiments and analyzed the data. P.K.M. and B.K. carried out crystallographic studies. X.M. and K.L. performed the ITC experiments. D.K., W.H., C.M., R.C. and K.P. performed the ion mobility-mass experiments and analyzed the data. C.G.P., I.H. and S.O. co-wrote the paper. All authors discussed the results and commented on the manuscript.

References

1. Fujita, D. et al. Self-assembly of tetravalent Goldberg polyhedra from 144 small components. *Nature* **540**, 563-566 (2016).
2. Bale, J. B. et al. Accurate design of megadalton-scale two-component icosahedral protein complexes. *Science* **353**, 389-394 (2016).
3. Pasquale, S., Sattin, S., Escudero-Adan, E. C., Martinez-Belmonte, M. & de Mendoza, J. Giant regular polyhedra from calixarene carboxylates and uranyl. *Nat. Commun.* **3**, 785 (2012).
4. Sasaki, E. et al. Structure and assembly of scalable porous protein cages. *Nat. Commun.* **8**, 14663 (2017).
5. Anderson, K. M., Goeta, A. E. & Steed, J. W. Supramolecular Synthon Frustration Leads to Crystal Structures with Z' > 1. *Cryst. Growth Des.* **8**, 2517-2524 (2008).
6. Banerjee, R., Bhatt, P. M., Kirchner, M. T. & Desiraju, G. R. Structural studies of the system Na(saccharinate)n H_2O: a model for crystallization. *Angew. Chem. Int. Ed.* **44**, 2515-2520 (2005).
7. Whitesides, G. M. & Ismagilov, R. F. Complexity in Chemistry. *Science* **284**, 89-92 (1999).
8. Lehn, J.-M. From supramolecular chemistry towards constitutional dynamic chemistry and adaptive chemistry. *Chem. Soc. Rev.* **36**, 151-160 (2007).
9. Lehn, J. M. Constitutional dynamic chemistry: bridge from supramolecular chemistry to adaptive chemistry. *Top. Curr. Chem.* **322**, 1-32 (2012).
10. Vantomme, G. & Meijer, E. W. The construction of supramolecular systems. *Science* **363**, 1396-1397 (2019).
11. Nitschke, J. R. Systems chemistry: Molecular networks come of age. *Nature* **462**, 736-738 (2009).
12. Li, J., Nowak, P. & Otto, S. Dynamic Combinatorial Libraries: From Exploring Molecular Recognition to Systems Chemistry. *J. Am. Chem. Soc.* **135**, 9222-9239 (2013).
13. Corbett, P. T. et al. Dynamic Combinatorial Chemistry. *Chem. Rev.* **106**, 3652-3711 (2006).
14. Cougnon, F. B. L. & Sanders, J. K. M. Evolution of Dynamic Combinatorial Chemistry. *Acc. Chem. Res.* **45**, 2211-2221 (2012).
15. Tsiamantas, C. et al. Selective Dynamic Assembly of Disulfide Macrocyclic Helical Foldamers with Remote Communication of Handedness. *Angew. Chem. Int. Ed.* **55**, 6848-6852 (2016).
16. Steinkruger, J. D., Woolfson, D. N. & Gellman, S. H. Side-chain pairing preferences in the parallel coiled-coil dimer motif: insight on ion pairing between core and flanking sites. *J. Am. Chem. Soc.* **132**, 7586-7588 (2010).
17. Hadley, E. B., Testa, O. D., Woolfson, D. N. & Gellman, S. H. Preferred side-chain constellations at antiparallel coiled-coil interfaces. *Proc. Natl. Acad. Sci. U.S.A.* **105**, 530-535 (2008).
18. Krishnan-Ghosh, Y. & Balasubramanian, S. Dynamic covalent chemistry on self-templating peptides: formation of a disulfide-linked beta-hairpin mimic. *Angew. Chem. Int. Ed.* **42**, 2171-2173 (2003).
19. Oh, K., Jeong, K. S. & Moore, J. S. Folding-driven synthesis of oligomers. *Nature* **414**, 889-893 (2001).
20. Liu, B. et al. Complex Molecules That Fold Like Proteins Can Emerge Spontaneously. *J. Am. Chem. Soc.* **141**, 1685-1689 (2019).
21. Sadownik, J. W., Mattia, E., Nowak, P. & Otto, S. Diversification of self-replicating molecules. *Nat. Chem.* **8**, 264-269 (2016).
22. Seo, J. et al. An infrared spectroscopy approach to follow β-sheet formation in peptide amyloid assemblies. *Nat. Chem.* **9**, 39-44 (2016).
23. BelBruno, J. J. Molecularly Imprinted Polymers. *Chem. Rev.* **119**, 94-119 (2019).

METHODS

General procedures. All chemicals, unless otherwise stated, were purchased from Sigma-Aldrich and used as received. Amino-acid resins were purchased from Novabiochem and Fmoc modified phenylalanine amino-acid residues from Chem Impex International and Iris Biotech. Acetonitrile (ULC-MS grade), water (ULC-MS grade) and trifluoroacetic acid (HPLC grade) were purchased from Biosolve BV. Flash column chromatography was performed on a Reveleris® X2 Flash Chromatography System (Grace Davison Discovery Sciences, Deerfield IL) on normal or reversed phase silica cartridges. NMR spectra were recorded on Bruker 500 and 600 MHz spectrometers.

Peptide Synthesis. Synthesis of monomers was performed using conventional Solid Phase Peptide Synthesis (SPPS) using the Fmoc/tBu protecting group strategy on Wang resin. Amino-acids were introduced protected as Fmoc-Lys(Boc)-OH, Fmoc-Tyr(Boc)-OH, Fmoc-Phe(4-NH-Boc)-OH or Fmoc-Phe(4-COOtBu)-OH. Fmoc deprotection steps were carried out with 20 % piperidine in DMF (v/v) for 15 min. Coupling of Fmoc amino-acids was performed in DMF using N-diisopropylcarbodiimide (DIC) and ethyl cyano(hydroxyimino)acetate (oxyma). Deprotection from resin and removal of the protecting groups on the side chains of the amino-acids was performed using a cocktail of 95% TFA, 2.5% 1,2-ethanedithiol (EDT), 1.25% water and 1.25% triisopropylsilane (TIS) for 3 hours. Crude peptides were purified using flash column chromatography and obtained at a purity level> 97%. The ≤3 % impurities were dominated by disulfide oligomers.

Library Preparation. Building blocks were dissolved in borate buffer (12.5 mM in $Na_2B_4O_7$ pH = 8.0). Where necessary, the pH of the solution was adjusted by the addition of 1.0 M NaOH. All libraries were set up in an HPLC vial (12×32 mm) with a Teflon-coated screw cap. All HPLC vials were equipped with a cylindrical stirrer bar (2×5 mm, Teflon coated, purchased from VWR) and stirred at 1200 rpm using an IKA RCT basic hot plate stirrer. All experiments were performed at ambient conditions.

Buffer preparation. Borate buffer (12.5 mM in $Na_2B_4O_7$, pH = 8.0) was prepared by dissolving boric acid anhydride (87.0 mg, B_2O_3) in 50 mL doubly distilled water. The pH was adjusted to 8.0 using concentrated NaOH.

UPLC analysis. UPLC analyses were performed on a Waters Acquity H and I-class system equipped with a PDA detector, at a detection wavelength of 254 nm. Samples were injected on an Aeris WIDEPORE 3.6 µm BEH-C18 (150 × 2.1 mm) column, using ULC-MS grade water (eluent A) and ULC-MS grade acetonitrile (eluent B), containing 0.1 V/V % TFA as modifier. A flow rate of 0.3 mL/min and a column temperature of 35 °C were applied. Sample preparation was performed by diluting 5 µL library to 100 µL with double distilled water.

UPLC-MS analysis. UPLC-MS analyses were performed using a Waters Acquity UPLC H-class system coupled to a Waters Xevo-G2 TOF. The mass spectrometer was operated in positive electrospray ionization mode with the following ionization parameters: capillary voltage: 3 kV; sampling cone voltage: 20 V; extraction cone voltage: 4 V; source gas temperature: 120 °C; desolvation gas temperature: 450 °C; cone gas flow (nitrogen): 1 L/h; desolvation gas flow (nitrogen): 800 L/h.

Circular Dichroism (CD) Spectroscopy. Spectra were recorded on a Jasco J-810 spectrometer with a Peltier temperature controller. Heat-cool cycles were applied from 20 to 90°C in steps of 1 degree at a rate of 0.1 degree/min and maintained for 10 min at every temperature before measuring. Spectra were obtained as averages of 3 measurements from 200 to 400 nm with a scanning speed of 150 nm/min and a bandwidth of 1 nm.

Isothermal Titration Calorimetry (ITC). The binding studies were conducted using VP-ITC (Microcal LLC, GE Healthcare). Solutions of $MnCl_2$ and templates **T1-T3** (in 12.5 mM borate buffer pH = 8.0) were titrated into solutions of hosts $(\mathbf{4a})_{13}$ and $(\mathbf{4a})_4$ (in 12.5 mM borate buffer pH = 8.0). Binding constants and enthalpies of binding were obtained by curve fitting of the titration data using the one-site binding model available in the Origin 2.9 software as shown in the Supplementary Information.

Ion mobility-mass spectrometry (IM-MS). Linear drift tube (DT) IM-MS measurements were performed on a modified Synapt G2-S HDMS (Waters Corporation, Manchester, UK) and on a home-built instrument (iMob), both described in detail elsewhere.[24, 25] For nano-electrospray typically 5 µL of sample were loaded and electrosprayed by applying 0.4-0.8 kV capillary voltage. Further parameters on the modified Synapt instrument were: 100 V sampling cone voltage, 1 V source offset voltage, 30 °C source temperature, 150 °C desolvation gas temperature, 50 L/h cone gas flow, 500

L/h desolvation gas flow, 0 V trap CE, 0 V transfer CE, 3 mL/min trap gas flow. Ion mobility parameters were: 2.2 Torr helium IMS gas, 27-29°C IMS temperature, 2.0 V trap DC entrance voltage, 5.0 V trap DC bias voltage, -10.0 V trap DC voltage, 5.0 V trap DC exit voltage, -25.0 V IMS DC entrance voltage, 60-200 V helium cell DC voltage, -40.0 V helium exit voltage, 60 V IMS bias voltage, 0 V IMS DC exit voltage, 5.0 V transfer DC entrance voltage, 15.0 V transfer DC exit voltage, 150 m/s trap wave velocity, 2.0 V trap wave height voltage, 200 m/s transfer wave velocity, 5.0 V transfer wave height voltage. Further parameters on the iMob instrument were: 10-20 V/cm electric field inside the ion mobility tubes, ~ 4 mbar helium IMS gas, ~ 23 °C IMS temperature. IM-MS spectra were recorded in the positive ion mode (except for the **4a** library which was measured in negative ion polarity) and measured drift times were converted to rotationally-averaged collision cross-sections (CCS) using the Mason-Schamp equation.[26]

Crystallization of L-(4b)$_{16}$ and L/D-(4d)$_{23}$. Aqueous solutions of L-(**4b**)$_{16}$ and of L/D-(**4d**)$_{23}$ were prepared using pure water to a final concentration of 25mg/ml. Racemic (**4d**)$_{23}$ was prepared by mixing the enantiopure solutions of L-(**4d**)$_{23}$ and D-(**4d**)$_{23}$. Crystallization trials of each of these solutions was carried out with commercial sparse matrix screens- JBScreen Basic from Jena Bioscience using the standard sitting drop vapour diffusion method at 293 K. X-ray quality crystals of L-(**4b**)$_{16}$ (Supplementary Fig. 99) were observed after 5 days by the addition of 1µL of L-(**4b**)$_{16}$ and 1µL of 30% w/v PEG 4000, 100mM Tris buffer (pH = 8.5) and 200mM magnesium chloride from the reservoir solution. X-ray quality crystals of L/D-(**4d**)$_{23}$ (Supplementary Fig. 99) were optimized using the hanging drop method by mixing 0.8µL of and 2.2µL of 30% w/v PEG 4000, 100mM Tris buffer (pH = 8.0) and 200mM lithium sulfate from the reservoir solution. Crystals for both L-(**4b**)$_{16}$ and L/D-(**4d**)$_{23}$ were fished using micro loops and plunged into liquid nitrogen directly such that the respective mother liquor served as cryo-protectant.

Data collection and structure determination of L-(4b)$_{16}$. The X-ray diffraction data were collected at ID23-1 beamline in ESRF, Grenoble with a Dectris Pilatus 6M detector.[27] Diffraction data were measured at T = 100 K and λ = 0.972 Å. The crystal was exposed for 0.1 s and 0.15° oscillation per frame. Diffraction data was processed using the program *XDS*.[28] The crystal belonged to the space group $P6_2$ with unit cell parameters: $a = b$ = 36.980 (5) Å and c = 44.071 (9) Å; V = 52194 (15) Å^3 and ½ molecule per asymmetric unit (Z = 3). The structure was solved with the program *SHELXT*[29] and refined by full-matrix least-squares method on F^2 with *SHELXL-2014*[30] within *Olex2*.[31] After each refinement step, visual inspection of the model and the electron-density maps were carried out using *Olex2* and *Coot*.[32] Some side chain atoms of phenyl guanidium and lysine were observed to be

severely disordered and were either omitted or refined with partial occupancy and isotropic displacement parameters. AFIX, DFIX and FLAT instructions were used to improve the geometry of molecules. Restraints on anisotropic displacement parameters were implemented with DELU, SIMU, RIGU and ISOR instructions. After several attempts to model the disordered side chains, *SQUEEZE* procedure was used to flatten the electron density map.[33] Very disordered side chains and solvent molecules were removed. Calculated total potential solvent accessible void volume and electron count per cell are 26111 Å^3 and 9476 respectively. Hydrogen atoms were placed at idealized positions except for those at disordered/missing side chains.

Data collection and structure determination of L/D-(4d)$_{23}$. The X-ray diffraction data were collected at EMBL P13 beamline in Hamburg, with a Dectris Pilatus 6M detector.[34] Diffraction data were measured at T = 100 K and λ = 0.980 Å. The crystal was exposed for 0.04 s and 0.1° oscillation per frame. Diffraction data was processed using the program *CrysAlis^{Pro}*.[35] The crystal belonged to the space group *P*1 with unit cell parameters: *a* = 35.114 (2) Å; *b* = 49.232 (3) Å; *c* = 61.528 (5) Å; *α* = 77.641 (1)°; *β* = 89.369 (1)°; *γ* = 71.229 (1)°; V = 98185.4 (14) Å^3 and 4 molecules per unit cell (Z = 4). The structure was solved with the program *SHELXT*[29] and refined by full-matrix least-squares method on F^2 with *SHELXL-2014*[30] within *Olex2*.[31] The initial structure revealed most of the main chain atoms and few of the side chains of two macrocycles out of four. After several iterations of least square refinement, the main chain trace improved for the 3rd and 4th macrocycle. Anisotropic refinement was carried out only for the sulfur atoms. AFIX, DFIX and FLAT instructions were used to improve the geometry of molecules. After several attempts to model the disordered side chains, *SQUEEZE* procedure was used to flatten the electron density map.[33] Very disordered side chains were removed. Calculated total potential solvent accessible void volume and electron count per cell are 72418.1 Å^3 and 2951 respectively. Hydrogen atoms were not added due to the poor quality of data.

Crystallographic data, refinement statistics, and comments on checkcif alerts obtained from IUCr's checkcif algorithm are reported in Supplementary Tables 4 and 5.

24. Allen, S. J., Giles, K., Gilbert, T. & Bush, M. F. Ion mobility mass spectrometry of peptide, protein, and protein complex ions using a radio-frequency confining drift cell. *Analyst* **141**, 884-891 (2016).
25. Warnke, S., von Helden, G. & Pagel, K. Analyzing the higher order structure of proteins with conformer-selective ultraviolet photodissociation. *Proteomics* **15**, 2804-2812 (2015).
26. Revercomb, H. E. & Mason, E. A. Theory of plasma chromatography/gaseous electrophoresis. Review. *Anal. Chem.* **47**, 970-983 (1975).
27. Nurizzo, D., Mairs, T., Guijarro, M., Rey, V., Meyer, J., Fajardo, P., Chavanne, J., Biasci, J-C., McSweeney, S., Mitchell, E. The ID23-1 structural biology beamline at the ESRF. *J. Synchrotron Rad.* **13**, 227–238 (2000).
28. Kabsch, W. XDS. *Acta Crystallogr.* D**66**, 125–132 (2010).

29. Sheldrick, G. M. SHELXT-Integrated space-group and crystal-structure determination. *Acta Crystallogr.* A**71**, 3-8 (2015).
30. Sheldrick, G. M. Crystal structure refinement with SHELXL. *Acta Crystallogr.* C**71**, 3-8 (2015).
31. Dolomanov, O. V., Bourhis, L. J., Gildea, R. J., Howard, J. A. K., Puschmann, H. OLEX2: a complete structure solution, refinement and analysis program. *J. Appl. Cryst.* **42**, 339-341 (2009).
32. Emsley, P., Lohkamp, B., Scott, W.G., Cowtan, K. Features and development of Coot. *Acta Crystallogr.* D**66**, 486-501 (2010).
33. Spek, A. L. Structure validation in chemical crystallography. *Acta Crystallogr.* D**65**, 148-155 (2009).
34. Cianci, M., Bourenkov, G., Pompidor, G., Karpics, I., Kallio, J., Bento, I., Roessle, M., Cipriani, F., Fiedler, S., Schneider, T. R. P13, the EMBL macromolecular crystallography beamline at the low-emittance PETRA III ring for high- and low-energy phasing with variable beam focussing. *J. Synchrotron Rad.* **24**, 323-332 (2017).
35. Agilent, CrysAlisPRO. Agilent Technologies Ltd, Yarnton, Oxfordshire, England (2014).

Supplementary Information for

Spontaneous and Template-Directed Emergence Of Low-Symmetry Foldamers From Dynamic Homomeric Sequences.

Charalampos G. Pappas,[a] Pradeep K. Mandal,[b] Bin Liu,[a] Brice Kauffmann,[c] Xiaoming Miao,[a] David Komáromy,[a] Waldemar Hoffmann,[d,e] Christian Manz,[d,e] Rayoon Chang,[d,e] Kai Liu,[a] Kevin Pagel,[d,e] Ivan Huc*[b] and Sijbren Otto*[a]

[a]Centre for Systems Chemistry, Stratingh Institute, Nijenborgh 4, 9747 AG Groningen, The Netherlands. [b]Department of Pharmacy and Center for Integrated Protein Science, Ludwig-Maximilians Universität, Butenandstraße 5-13, D-81377 Munich, Germany. [c]Université de Bordeaux, CNRS, INSERM, UMS3033, Institut Européen de Chimie et Biologie, 2 rue Robert Escarpit, 33600 Pessac, France. [d]Institute of Chemistry and Biochemistry, Freie Universität Berlin, Takustraße 3, 14195 Berlin, Germany. [e]Fritz Haber Institute of the Max Planck Society, Faradayweg 4-6, 14195 Berlin, Germany.

Contents

1. UPLC Methods 16
2. UPLC/MS analyses 17
3. Kinetic Profile and total UPLC peak areas for libraries prepared from building blocks 4a, 4b and 4d 103
4. NMR analysis of building blocks **4a**, **4b** and **4d** and the foldamers made from these 104
5. Temperature dependent NMR and CD for the foldamers made from building blocks **4a**, **4b** and **4d** 108
6. Collision cross-sections for the macrocycles present in libraries prepared from building blocks **4a**, **4b** and **4d** 115
7. X-ray crystallography of $(\mathbf{4b})_{16}$ and $(\mathbf{4d})_{23}$ 118
8. Salt effect on **4a** 130
9. Isolation of $(\mathbf{4a})_{13}$ 131
10. ITC data for titration of $(\mathbf{4a})_{13}$ with $MnCl_2$ 132
11. ITC data for titration of $(\mathbf{4a})_{13}$ with T1-T3 133
12. UPLC/MS analyses of peptide template effects 137
References 143

1. UPLC Methods

Method for the analysis of DCLs made from building blocks **2a-e**:

t / min	% B
0	10
1	20
11	80
13	95
13.5	95
14	10
17	10

Method for the analysis of DCLs made from building blocks **1c, 1d**, **3a-c**, **4a, 4e**:

t / min	% B
0	10
1	15
11	50
13	95
13.5	95
14	10
17	10

Method for the analysis of DCLs made from building blocks **4b-4d and 4f-h**:

t / min	% B
0	10
1	15
9	24
12.5	60
13	95
13.5	95
14	10
17	10

2. UPLC/MS analyses

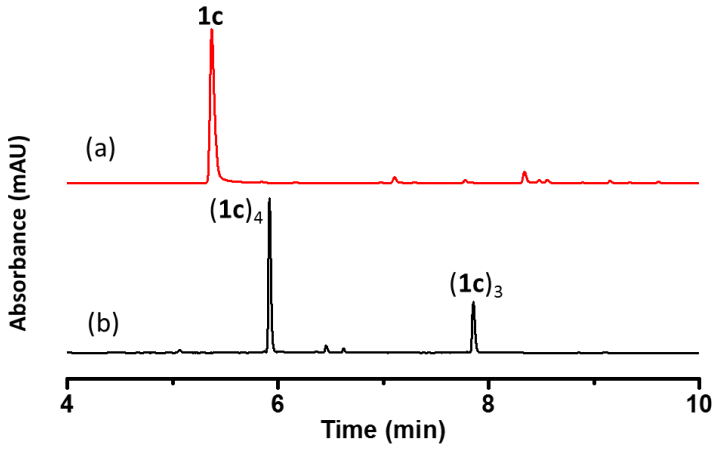

Supplementary Figure 1. UPLC analyses of the DCL made from **1c** (2.0 mM) in borate buffer (12.5 mM, pH = 8.0): (a) immediately after dissolving and (b) after stirring for 14 days.

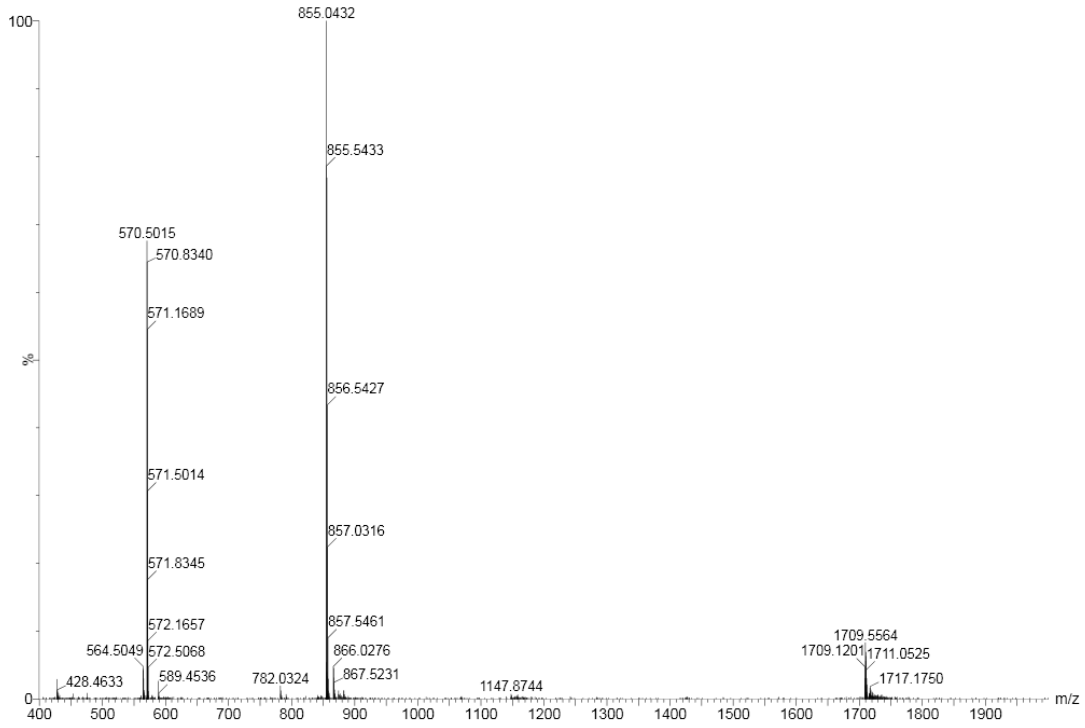

Supplementary Figure 2. Mass spectrum of $(\mathbf{1c})_4$ (retention time 5.92 min in Supplementary Figure 1b) from the LC-MS analysis of a DCL made from **1c** (2.0 mM). $(\mathbf{1c})_4$: m/z calculated: 1709.36 $[M+1H]^+$, 855.18 $[M+2H]^{2+}$, 570.46 $[M+3H]^{3+}$; m/z observed: 1709.56 $[M+1H]^+$, 855.04 $[M+2H]^{2+}$, 570.50 $[M+3H]^{3+}$.

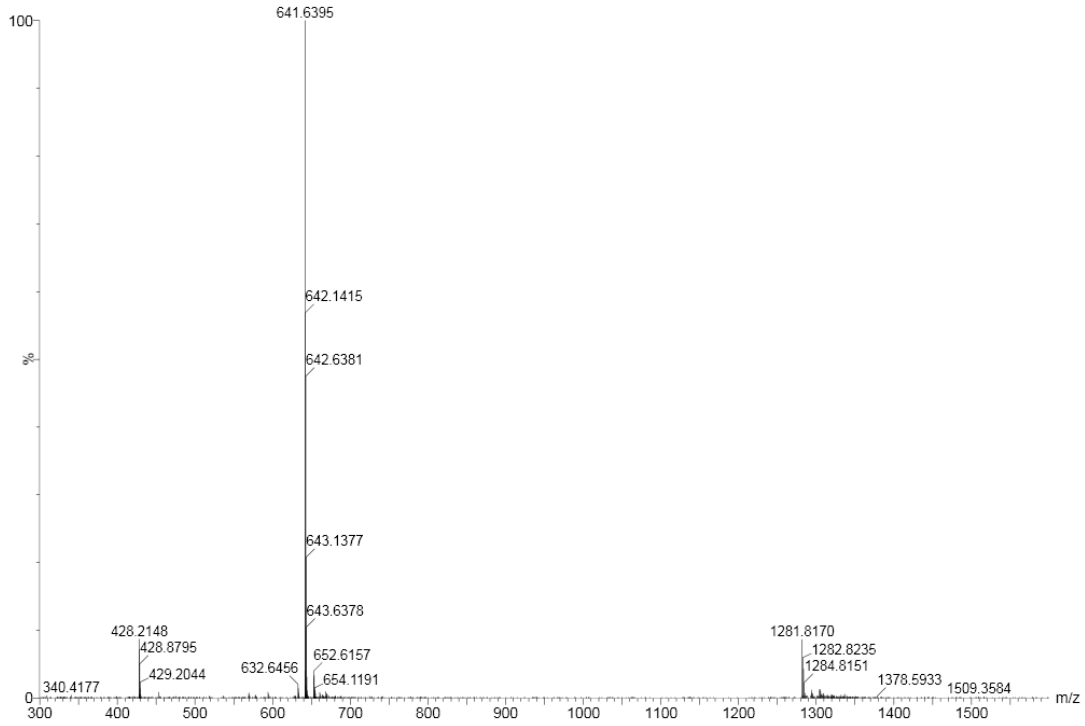

Supplementary Figure 3. Mass spectrum of $(\mathbf{1c})_3$ (retention time 7.85 min in Supplementary Figure 1b) from the LC-MS analysis of a DCL made from **1c** (2.0 mM). $(\mathbf{1c})_3$: m/z calculated: 641.64 $[M+2H]^{2+}$, 428.09 $[M+3H]^{3+}$; m/z observed: 641.64 $[M+2H]^{2+}$, 428.21 $[M+3H]^{3+}$.

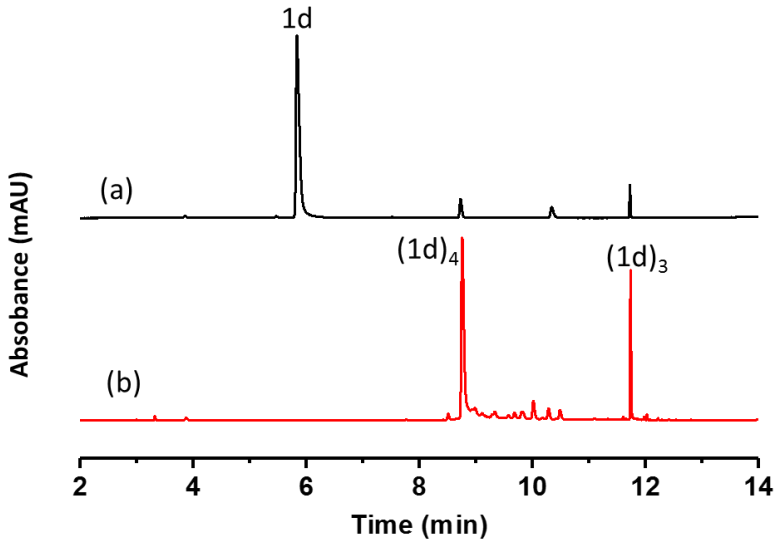

Supplementary Figure 4. UPLC analyses of the DCL made from **1d** (2.0 mM) in borate buffer (12.5 mM, pH = 8.0): (a) immediately after dissolving and (b) after stirring for 14 days.

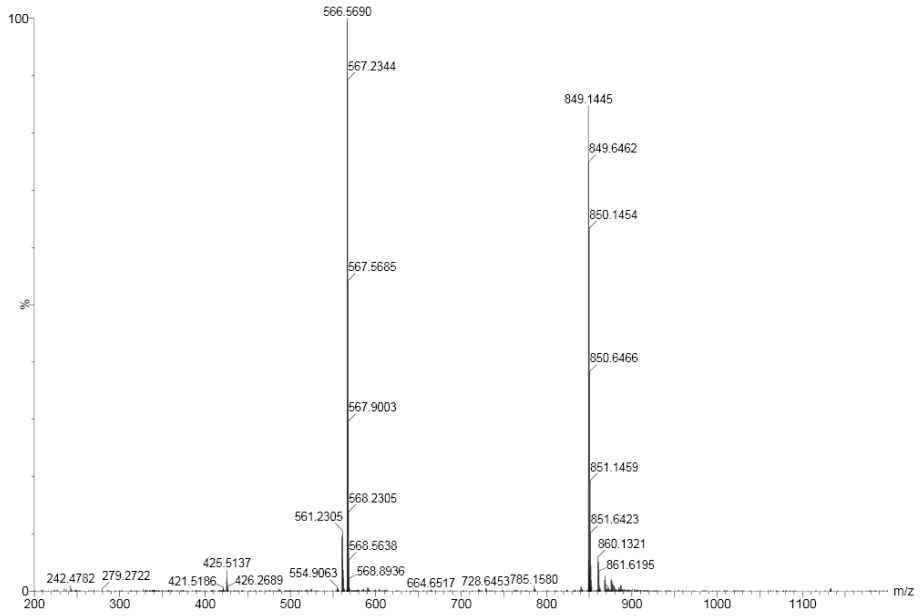

Supplementary Figure 5. Mass spectrum of $(\mathbf{1d})_4$ (retention time 8.75 min in Supplementary Figure 4b) from the LC-MS analysis of a DCL made from **1d** (2.0 mM). $(\mathbf{1d})_4$: m/z calculated: 849.26 $[M+2H]^{2+}$, 566.51 $[M+3H]^{3+}$; m/z observed: 849.14 $[M+2H]^{2+}$, 566.57 $[M+3H]^{3+}$.

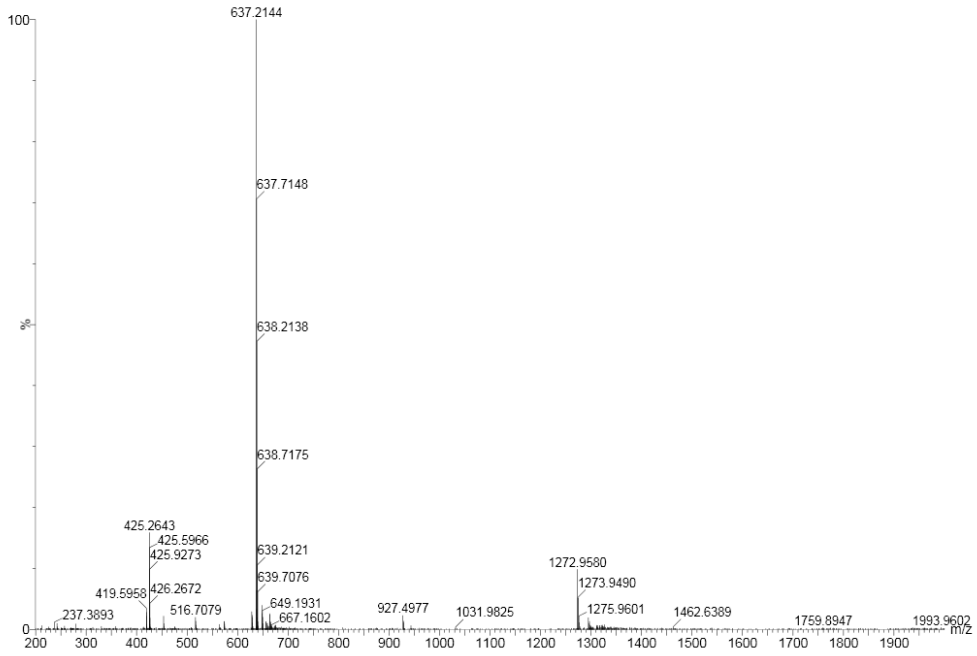

Supplementary Figure 6. Mass spectrum of (**1d**)$_3$ (retention time 11.76 min in Supplementary Figure 4b) from the LC-MS analysis of a DCL made from **1d** (2.0 mM). (**1d**)$_3$: m/z calculated: 637.19 $[M+2H]^{2+}$, 425.13 $[M+3H]^{3+}$; m/z observed: 637.21 $[M+2H]^{2+}$, 425.26 $[M+3H]^{3+}$.

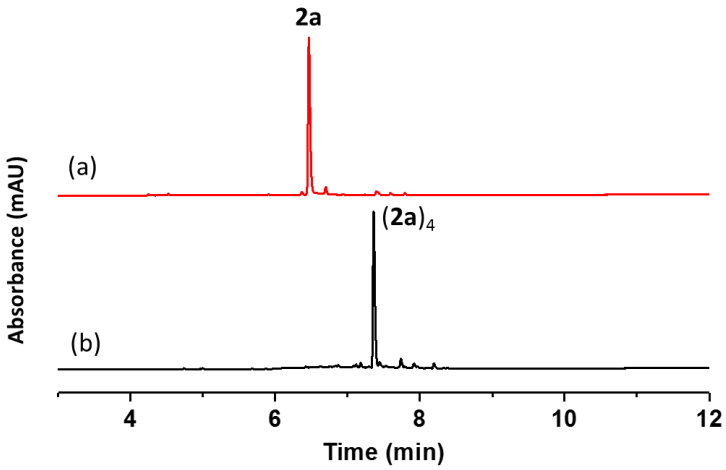

Supplementary Figure 7. UPLC analyses of a DCL made from **2a** (2.0 mM) in borate buffer (12.5 mM, pH = 8.0): (a) immediately after dissolving and (b) after stirring for 16 days.

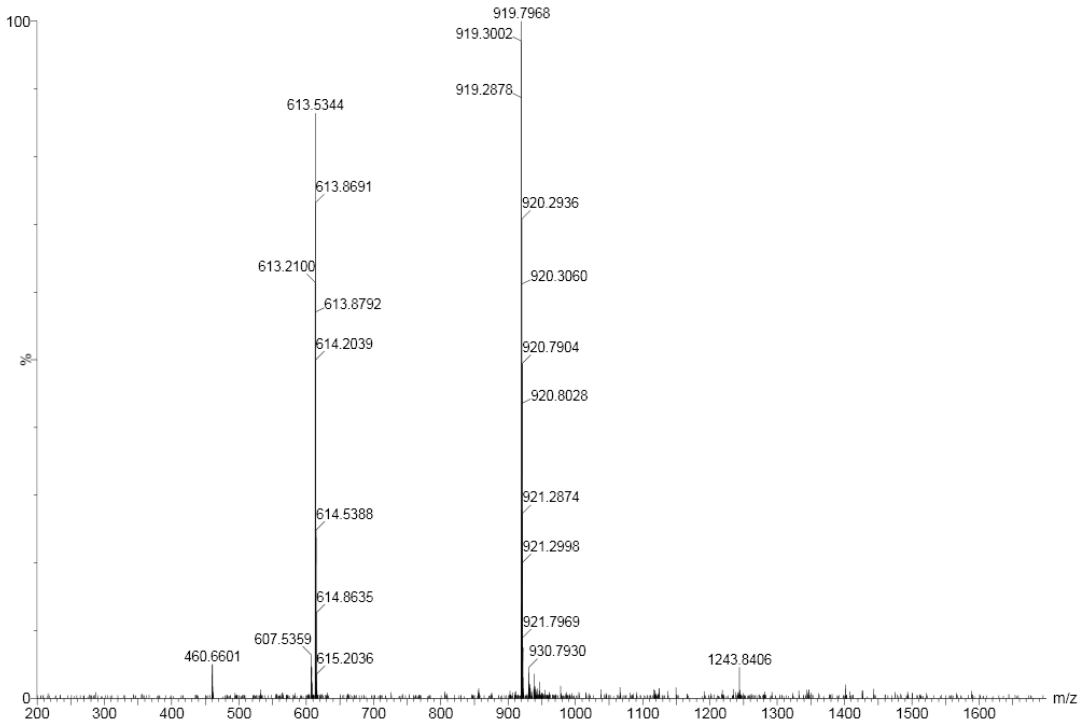

Supplementary Figure 8. Mass spectrum of $(\mathbf{2a})_4$ (retention time 7.35 min in Supplementary Figure 7b) from the LC-MS analysis of a DCL made from **2a** (2.0 mM). $(\mathbf{2a})_4$: m/z calculated: 919.26 $[M+2H]^{2+}$, 613.18 $[M+3H]^{3+}$; m/z observed: 919.28 $[M+2H]^{2+}$, 613.21 $[M+3H]^{3+}$.

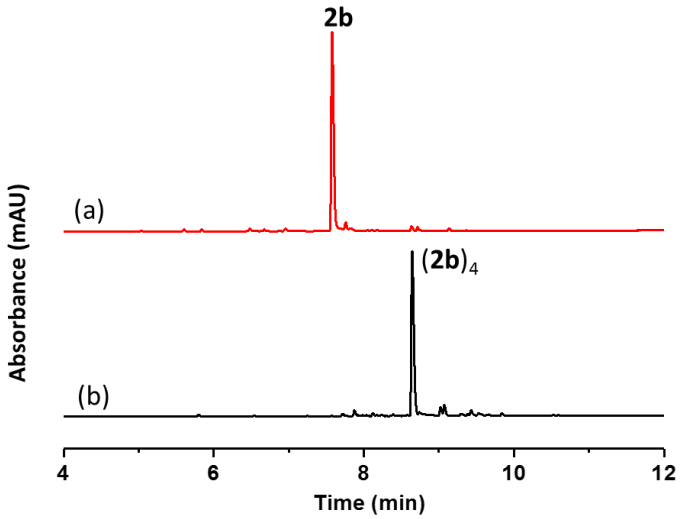

Supplementary Figure 9. UPLC analyses of a DCL made from **2b** (2.0 mM) in borate buffer (12.5 mM, pH = 8.0): (a) immediately after dissolving and (b) after stirring for 16 days.

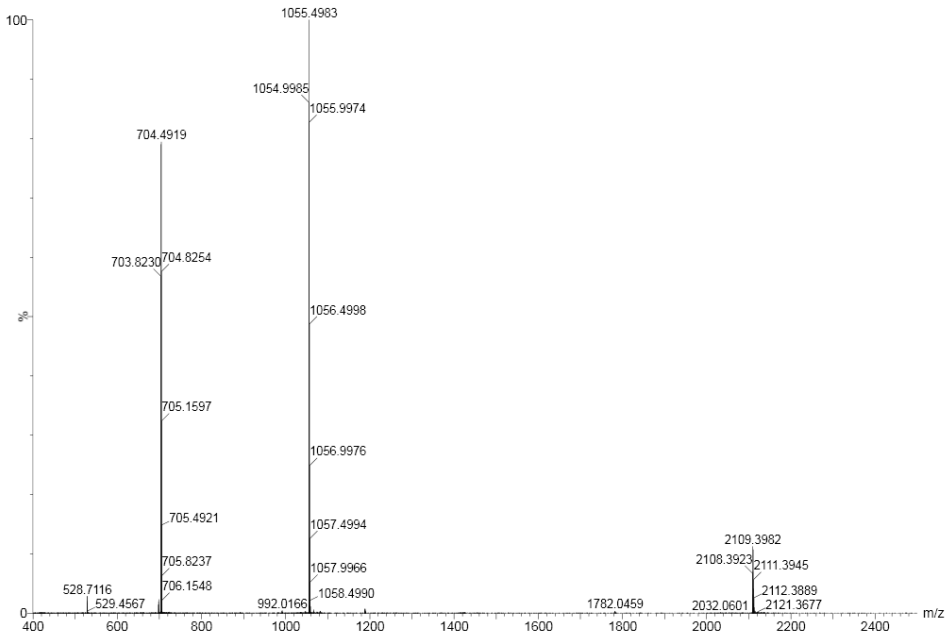

Supplementary Figure 10. Mass spectrum of (**2b**)$_4$ (retention time 8.65 min in Supplementary Figure 9b) from the LC-MS analysis of a DCL made from **2b** (2.0 mM). (**2b**)$_4$: m/z calculated: 2109.47 $[M+1H]^+$, 1055.24 $[M+2H]^{2+}$, 703.83 $[M+3H]^{3+}$; m/z observed: 2109.40 $[M+1H]^+$, 1055.50 $[M+2H]^{2+}$, 703.82 $[M+3H]^{3+}$.

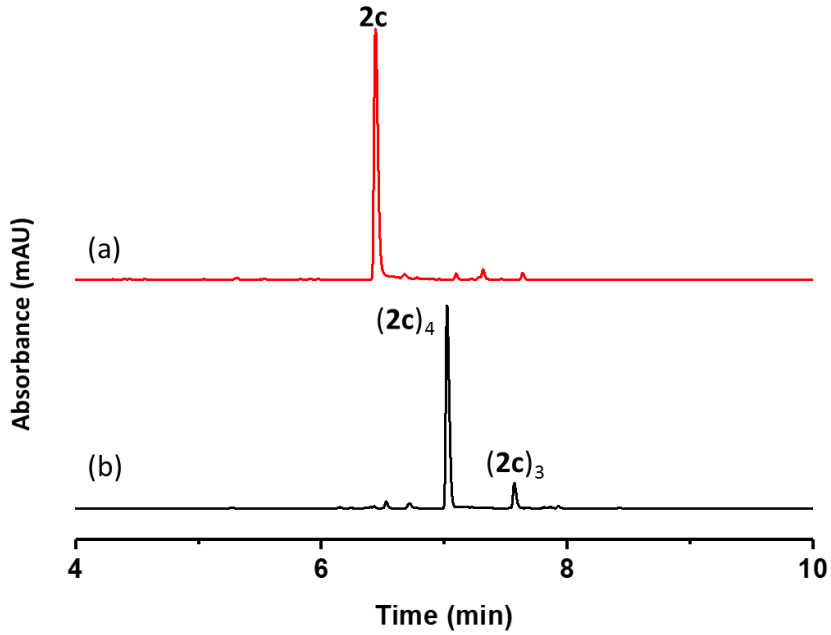

Supplementary Figure 11. UPLC analyses of a DCL made from **2c** (2.0 mM) in borate buffer (12.5 mM, pH = 8.0): (a) after stirring for 1 day and (b) after stirring for 16 days.

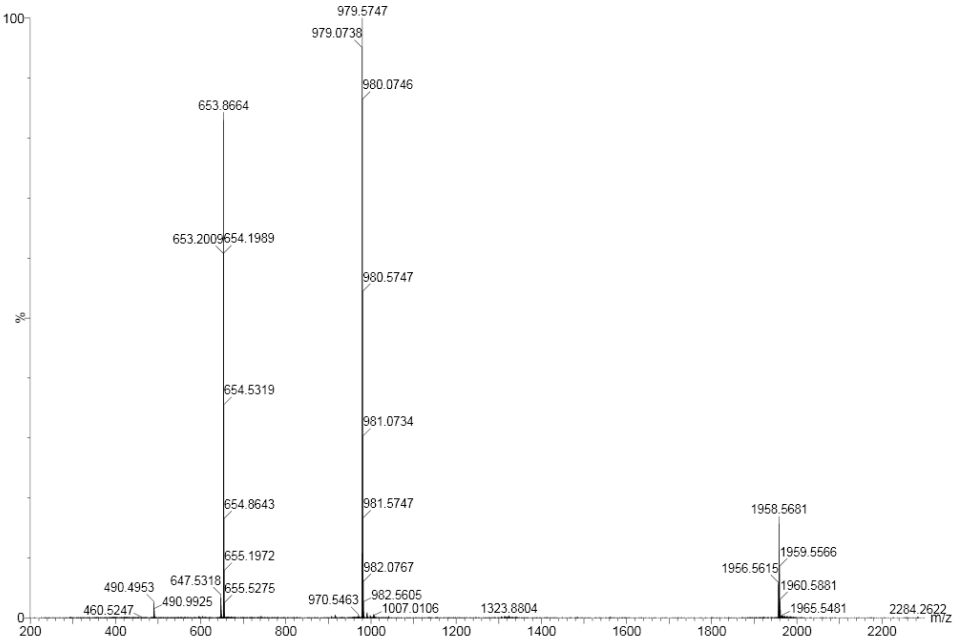

Supplementary Figure 12. Mass spectrum of $(\mathbf{2c})_4$ (retention time 7.02 min in Supplementary Figure 11b) from the LC-MS analysis of a DCL made from **2c** (2.0 mM). $(\mathbf{2c})_4$: m/z calculated: 979.29 $[M+2H]^{2+}$, 653.19 $[M+3H]^{3+}$; m/z observed: 979.57 $[M+2H]^{2+}$, 653.20 $[M+3H]^{3+}$.

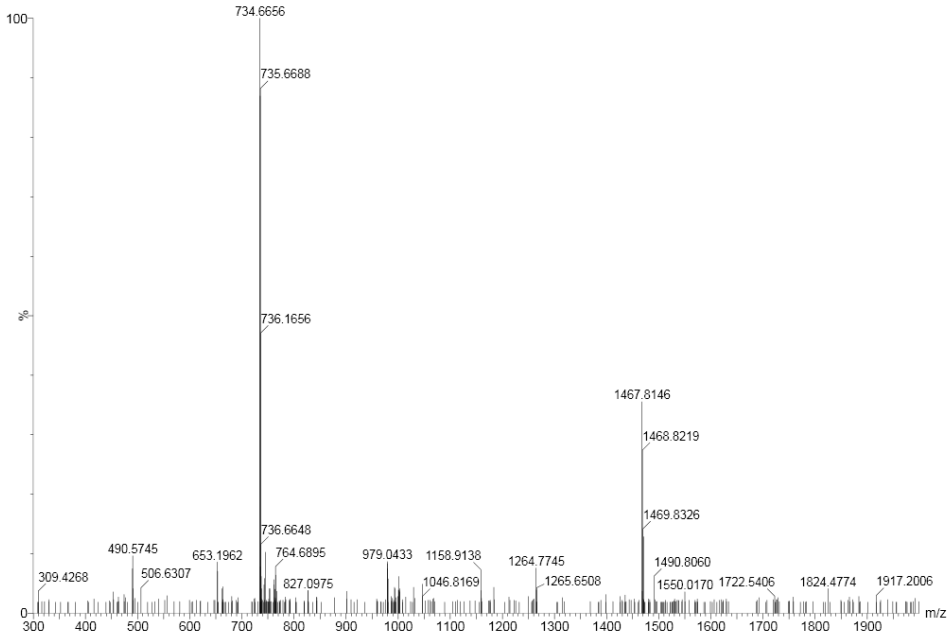

Supplementary Figure 13. Mass spectrum of (**2c**)$_3$ (retention time 7.56 min in Supplementary Figure 11b) from the LC-MS analysis of a DCL made from **2c** (2.0 mM). (**2c**)$_3$: m/z calculated: 734.72 $[M+2H]^{2+}$; m/z observed: 734.67 $[M+2H]^{2+}$.

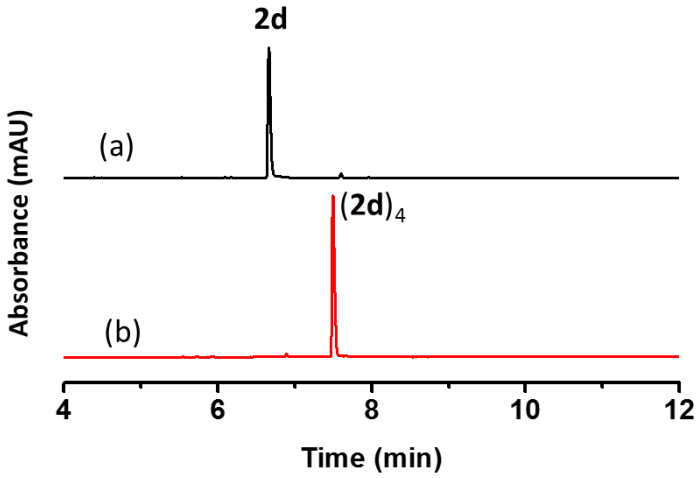

Supplementary Figure 14. UPLC analyses of a DCL made from **2d** (2.0 mM) in borate buffer (12.5 mM, pH = 8.0): (a) immediately after dissolving and (b) after stirring for 16 days.

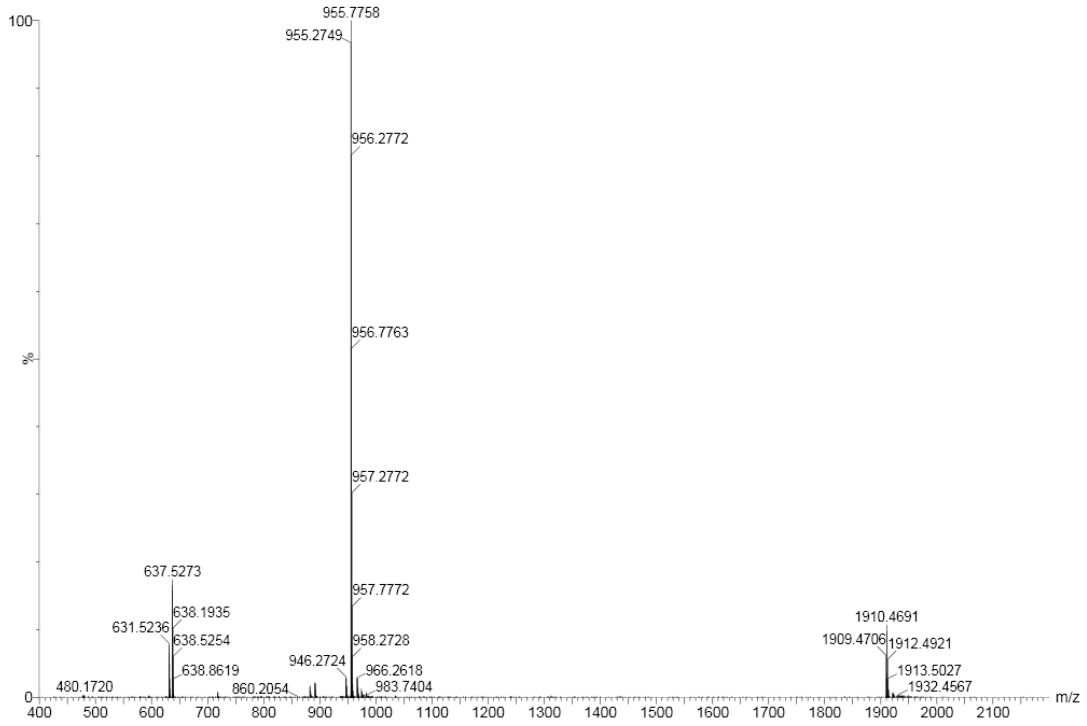

Supplementary Figure 15. Mass spectrum of $(\mathbf{2d})_4$ (retention time 7.51 min in Supplementary Figure 14b) from the LC-MS analysis of a DCL made from **2d** (2.0 mM). $(\mathbf{2d})_4$: m/z calculated: 955.25 $[M+2H]^{2+}$, 637.17 $[M+3H]^{3+}$; m/z observed: 955.27 $[M+2H]^{2+}$, 637.53 $[M+3H]^{3+}$.

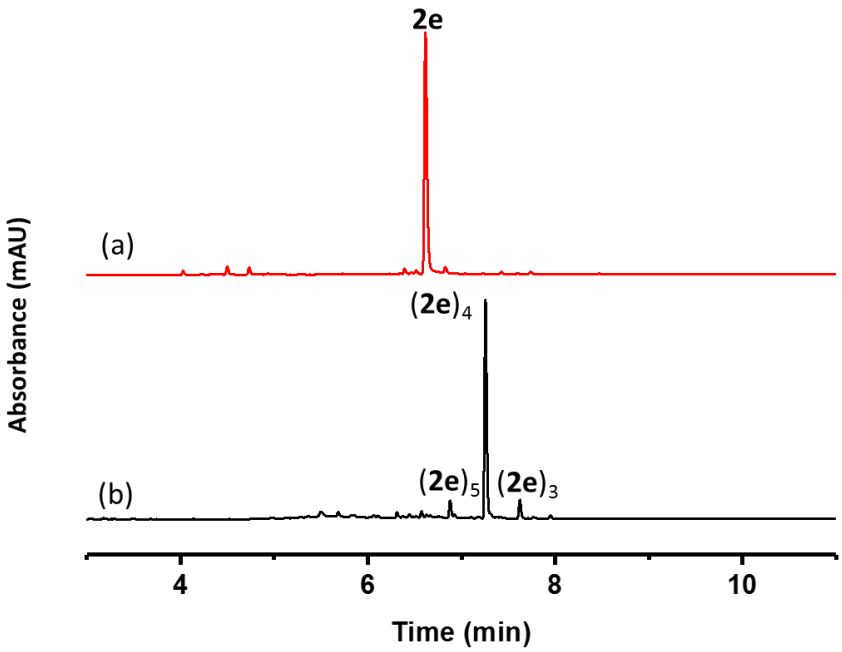

Supplementary Figure 16. UPLC analyses of a DCL made from **2e** (2.0 mM) in borate buffer (12.5 mM, pH = 8.0): (a) immediately after dissolving and (b) after stirring for 16 days.

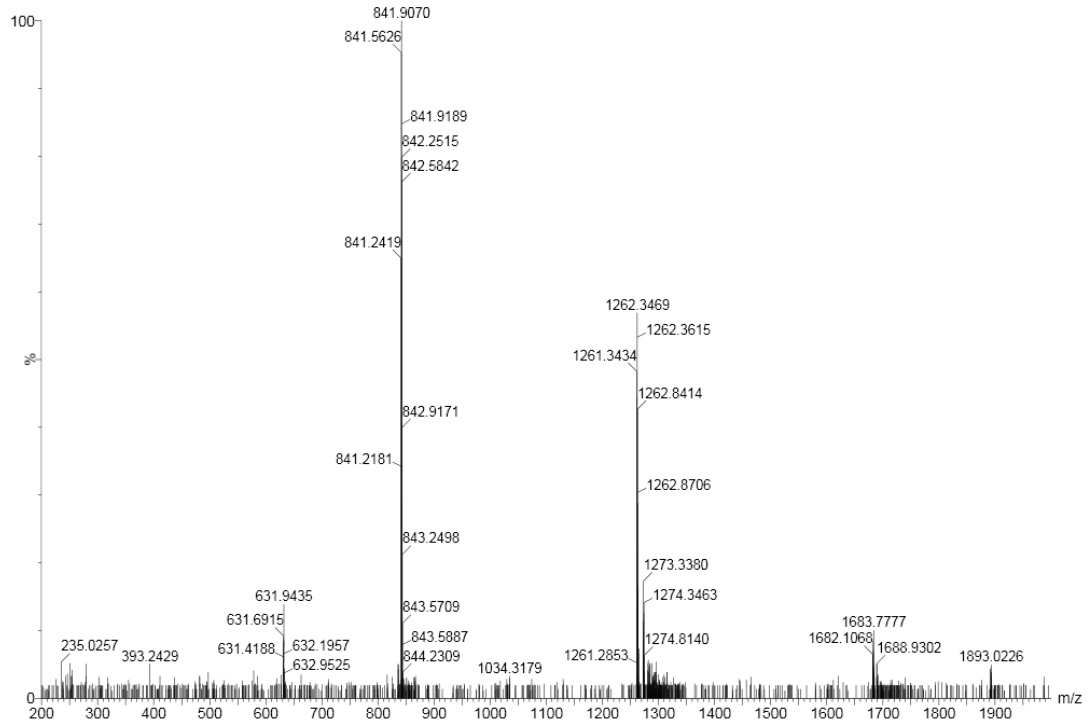

Supplementary Figure 17. Mass spectrum of $(\mathbf{2e})_5$ (retention time 6.87 min in Supplementary Figure 16b) from the LC-MS analysis of a DCL made from **2e** (2.0 mM). $(\mathbf{2e})_5$: m/z calculated: 1261.29 $[M+2H]^{2+}$, 841.20 $[M+3H]^{3+}$; m/z observed: 1261.34 $[M+2H]^{2+}$, 841.24 $[M+3H]^{3+}$.

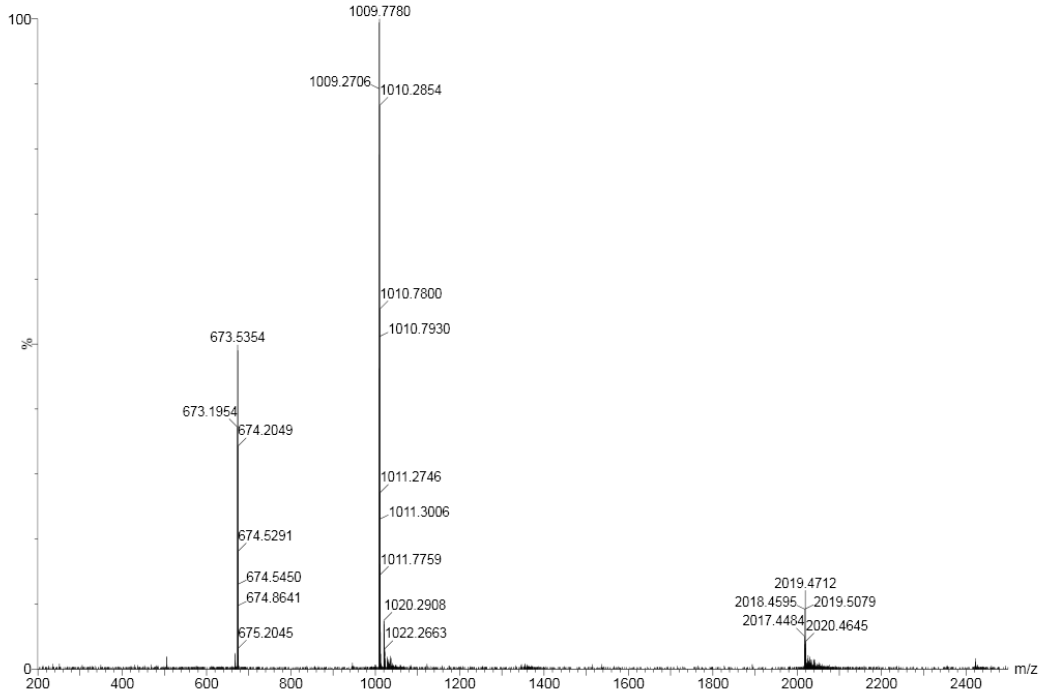

Supplementary Figure 18. Mass spectrum of $(\mathbf{2e})_4$ (retention time 7.27 min in Supplementary Figure 16b) from the LC-MS analysis of a DCL made from **2e** (2.0 mM). $(\mathbf{2e})_4$: m/z calculated: 1009.24 $[M+2H]^{2+}$, 673.16 $[M+3H]^{3+}$; m/z observed: 1009.27 $[M+2H]^{2+}$, 673.20 $[M+3H]^{3+}$.

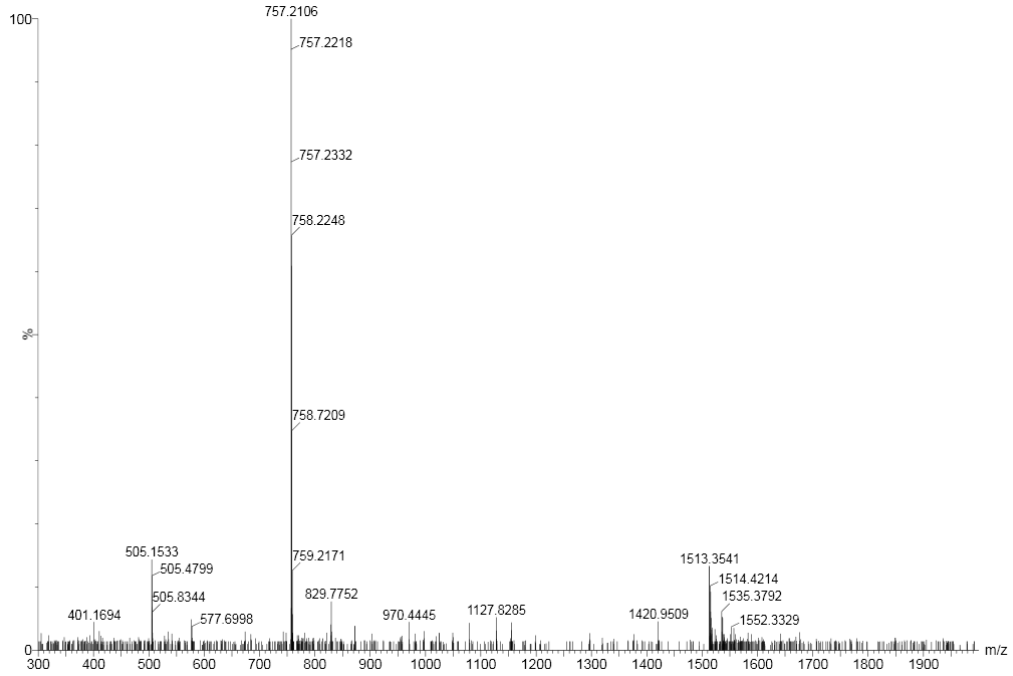

Supplementary Figure 19. Mass spectrum of (**2e**)$_3$ (retention time 7.62 min in Supplementary Figure 16b) from the LC-MS analysis of a DCL made from **2e** (2.0 mM). (**2e**)$_3$: m/z calculated: 757.18 $[M+2H]^{2+}$, 505.12 $[M+3H]^{3+}$; m/z observed: 757.21 $[M+2H]^{2+}$, 505.15 $[M+3H]^{3+}$.

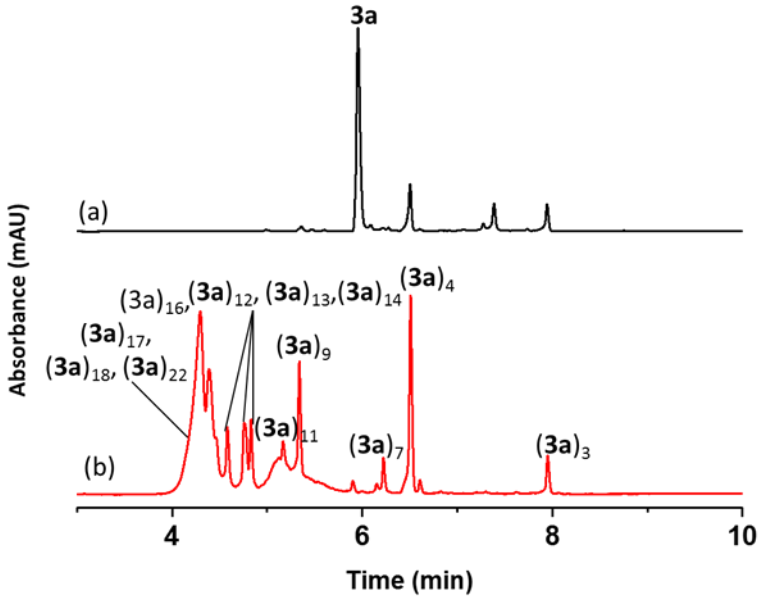

Supplementary Figure 20. UPLC analyses of a DCL made from **3a** (2.0 mM) in borate buffer (12.5 mM, pH = 8.0): (a) after stirring for 1 day and (b) after stirring for 16 days.

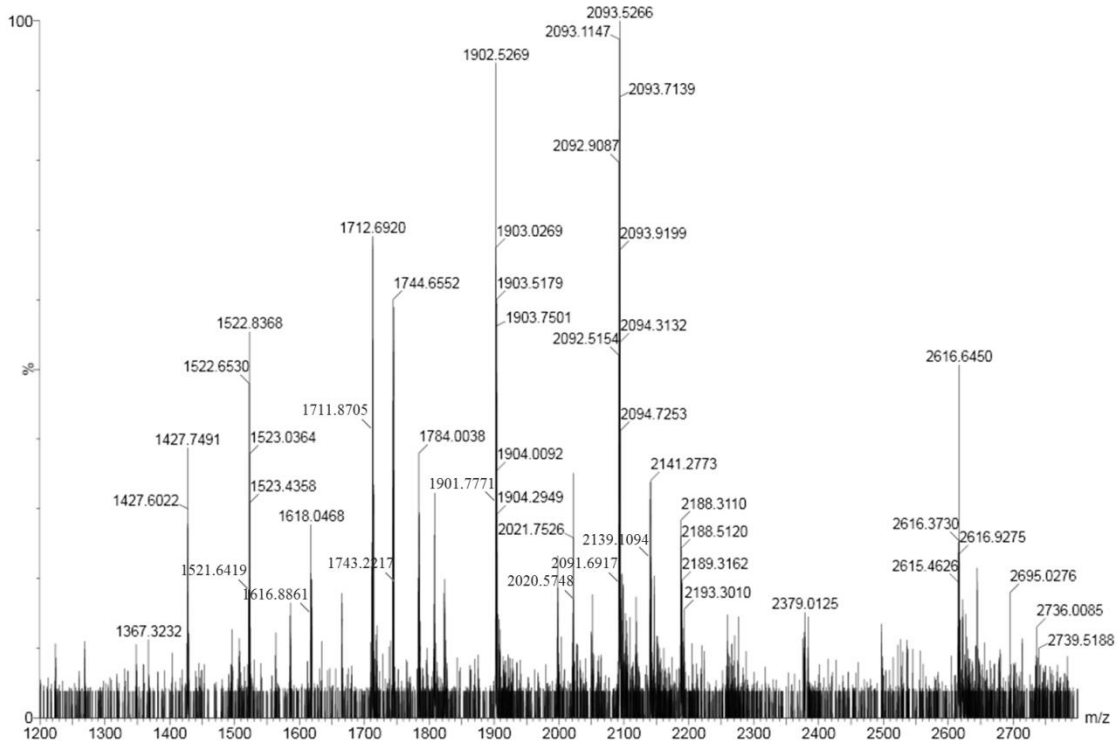

Supplementary Figure 21. Mass spectrum of $(\mathbf{3a})_{16}$, $(\mathbf{3a})_{17}$, $(\mathbf{3a})_{18}$ and $(\mathbf{3a})_{22}$ (retention time 4.12-4.47 min in Supplementary Figure 20b) from the LC-MS analysis of a DCL made from **3a** (2.0 mM). Due to the similar retention time of these macrocycles, they are analyzed in a single mass spectrum. $(\mathbf{3a})_{16}$: m/z calculated: 1901.50 $[M+4H]^{4+}$, 1521.40 $[M+5H]^{5+}$; m/z observed: 1901.78 $[M+3H]^{3+}$, 1521.64 $[M+4H]^{4+}$. $(\mathbf{3a})_{17}$: m/z calculated: 2020.28 $[M+4H]^{4+}$, 1616.43 $[M+5H]^{5+}$; m/z observed: 2020.57 $[M+3H]^{3+}$, 1616.89 $[M+4H]^{4+}$. $(\mathbf{3a})_{18}$: m/z calculated: 2139.06 $[M+4H]^{4+}$, 1711.45 $[M+5H]^{5+}$; m/z observed: 2139.11 $[M+4H]^{4+}$, 1711.87 $[M+5H]^{5+}$. $(\mathbf{3a})_{22}$: m/z calculated: 2091.55 $[M+5H]^{5+}$, 1743.13 $[M+6H]^{6+}$; m/z observed: 2091.69 $[M+5H]^{5+}$, 1743.22 $[M+6H]^{6+}$.

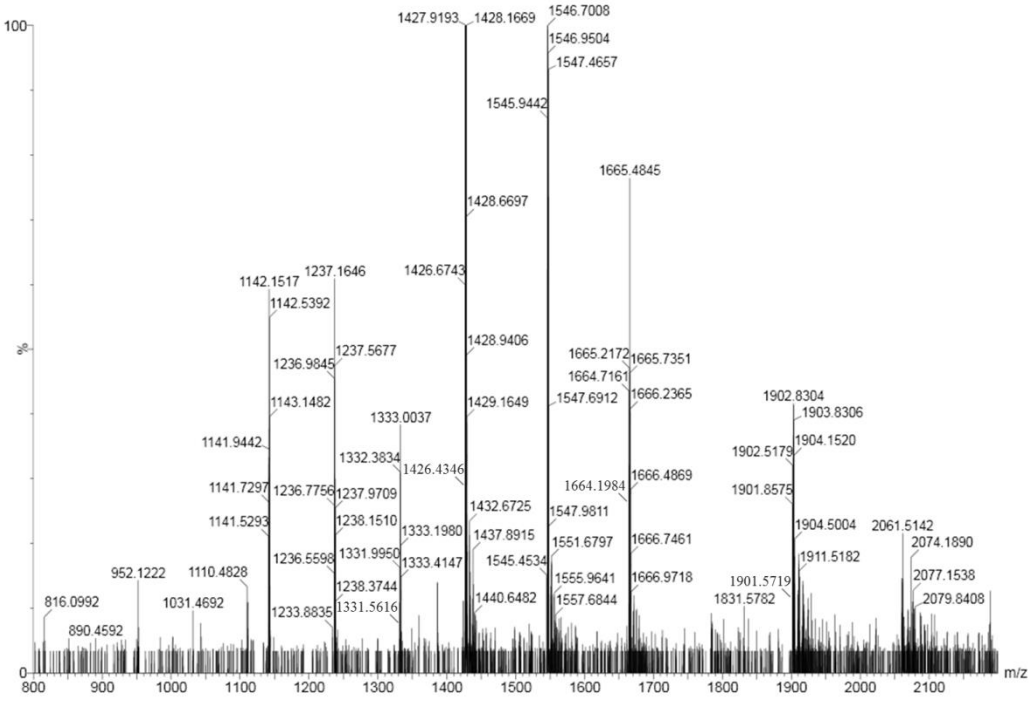

Supplementary Figure 22. Mass spectrum of $(\mathbf{3a})_{12}$, $(\mathbf{3a})_{13}$ and $(\mathbf{3a})_{14}$ (retention time 4.59-4.82 min in Supplementary Figure 20b) from the LC-MS analysis of a DCL made from **3a** (2.0 mM). Due to the similar retention time of these macrocycles, they are analyzed in a single mass spectrum. $(\mathbf{3a})_{12}$: m/z calculated: 1901.50 $[M+3H]^{3+}$, 1426.37 $[M+4H]^{4+}$, 1141.30 $[M+5H]^{5+}$; m/z observed: 1901.57 $[M+3H]^{3+}$, 1426.43 $[M+4H]^{4+}$, 1141.53 $[M+5H]^{5+}$. $(\mathbf{3a})_{13}$: m/z calculated: 1545.16 $[M+4H]^{4+}$, 1236.33 $[M+5H]^{5+}$; m/z observed: 1545.34 $[M+4H]^{4+}$, 1236.56 $[M+5H]^{5+}$. $(\mathbf{3a})_{14}$: m/z calculated: 1663.94 $[M+4H]^{4+}$, 1331.35 $[M+5H]^{5+}$; m/z observed: 1664.20 $[M+4H]^{4+}$, 1331.56 $[M+5H]^{5+}$.

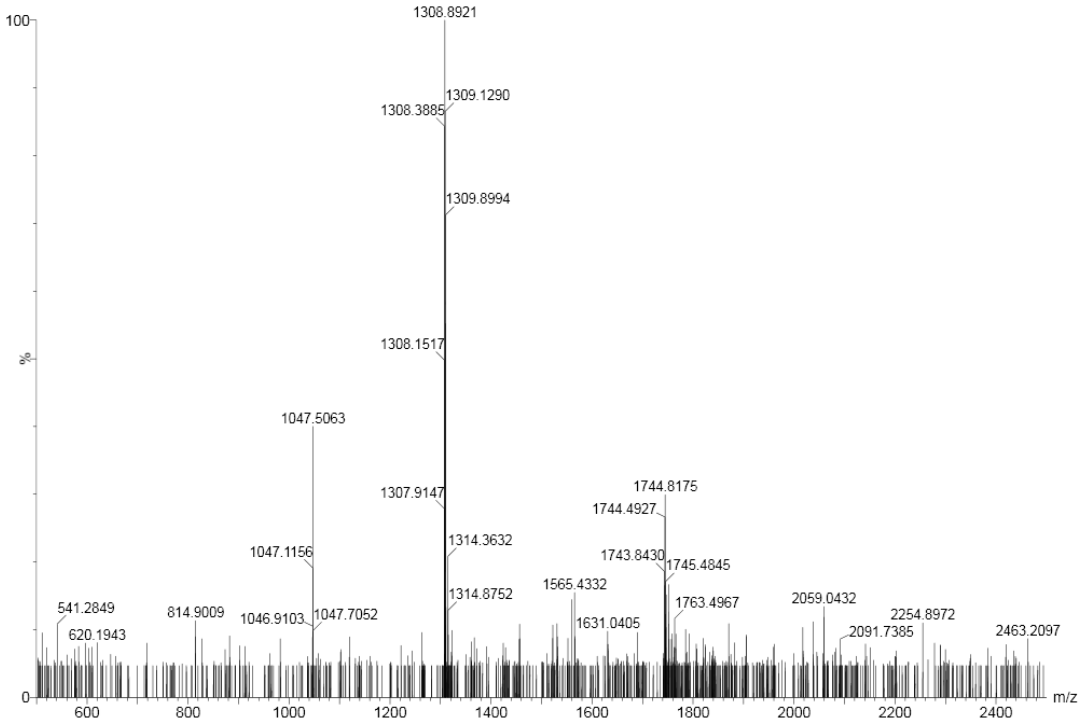

Supplementary Figure 23. Mass spectrum of $(\mathbf{3a})_{11}$ (retention time 5.16 min in Supplementary Figure 20b) from the LC-MS analysis of a DCL made from **3a** (2.0 mM). $(\mathbf{3a})_{11}$: m/z calculated: 1307.60 $[M+4H]^{4+}$, 1046.28 $[M+5H]^{5+}$; m/z observed: 1307.63 $[M+4H]^{4+}$, 1046.31 $[M+5H]^{5+}$.

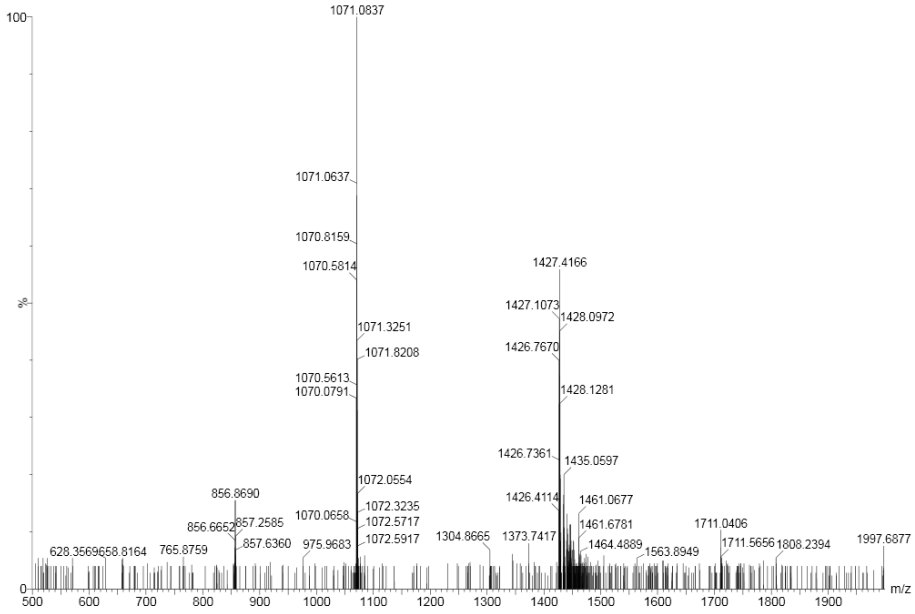

Supplementary Figure 24. Mass spectrum of $(\mathbf{3a})_9$ (retention time 5.34 min in Supplementary Figure 20b) from the LC-MS analysis of a DCL made from **3a** (2.0 mM). $(\mathbf{3a})_9$: m/z calculated: 1426.38 $[M+3H]^{3+}$, 1070.04 $[M+4H]^{4+}$; m/z observed: 1426.41 $[M+3H]^{3+}$, 1070.08 $[M+4H]^{4+}$.

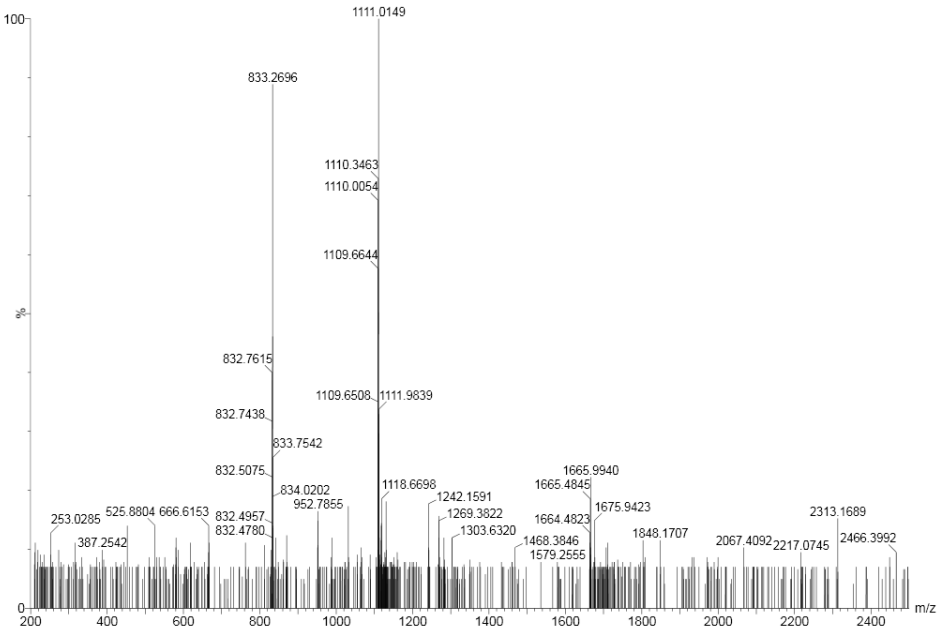

Supplementary Figure 25. Mass spectrum of $(\mathbf{3a})_7$ (retention time 6.22 min in Supplementary Figure 20b) from the LC-MS analysis of a DCL made from **3a** (2.0 mM). $(\mathbf{3a})_7$: m/z calculated: 1109.63 $[M+3H]^{3+}$, 832.47 $[M+4H]^{4+}$; m/z observed: 1109.66 $[M+3H]^{3+}$, 832.51 $[M+4H]^{4+}$.

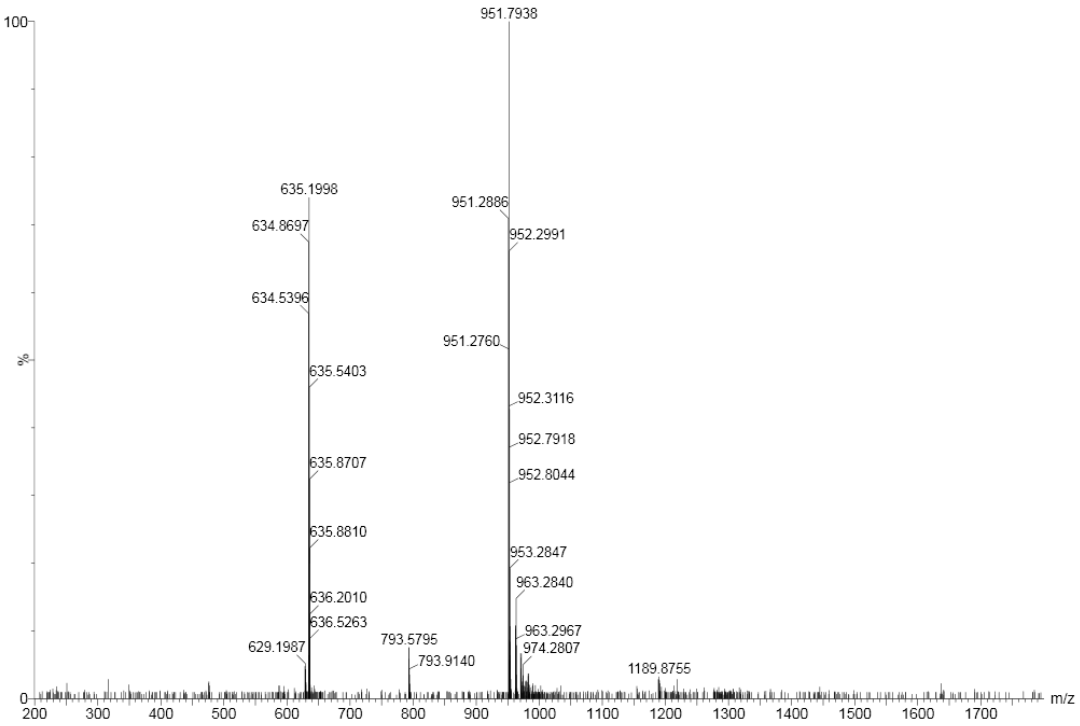

Supplementary Figure 26. Mass spectrum of (**3a**)$_4$ (retention time 6.50 min in Supplementary Figure 20b) from the LC-MS analysis of a DCL made from **3a** (2.0 mM). (**3a**)$_4$: m/z calculated: 951.25 $[M+2H]^{2+}$, 634.51 $[M+3H]^{3+}$; m/z observed: 951.27 $[M+2H]^{2+}$, 634.54 $[M+3H]^{3+}$.

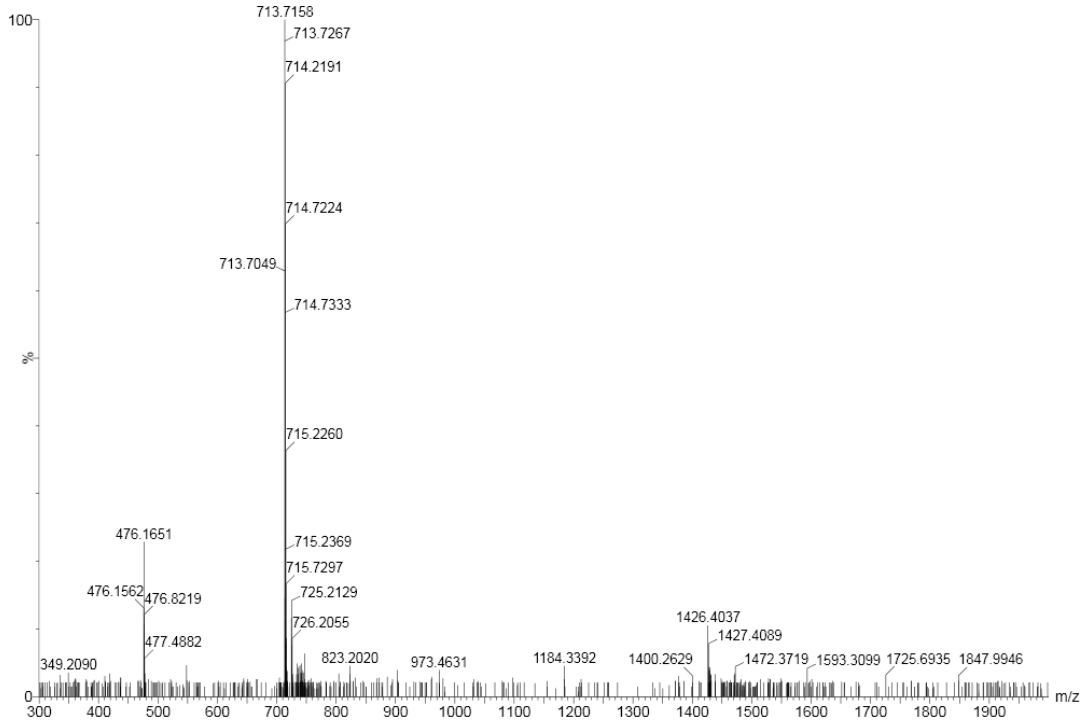

Supplementary Figure 27. Mass spectrum of (**3a**)$_3$ (retention time 7.94 min in Supplementary Figure 20b) from the LC-MS analysis of a DCL made from **3a** (2.0 mM). (**3a**)$_3$: m/z calculated: 713.69 $[M+2H]^{2+}$, 476.13 $[M+3H]^{3+}$; m/z observed: 713.72 $[M+2H]^{2+}$, 476.17 $[M+3H]^{3+}$.

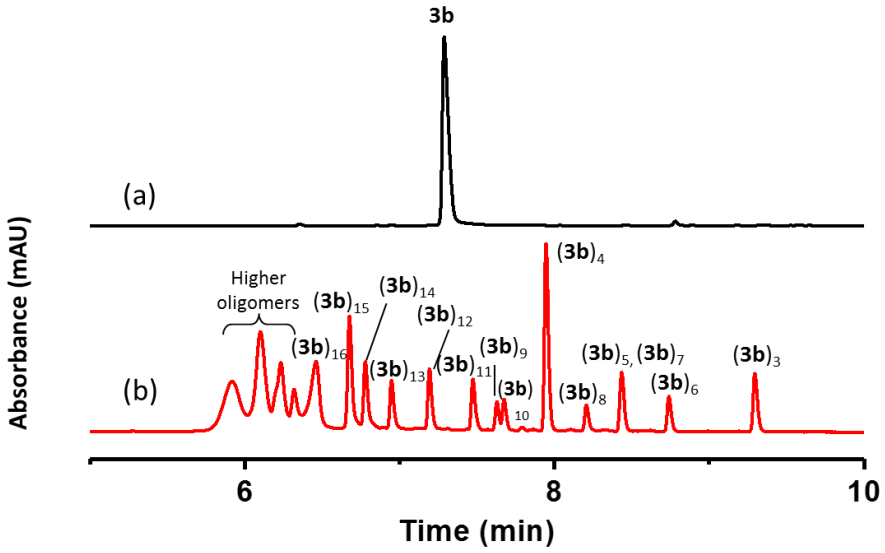

Supplementary Figure 28. UPLC analyses of the DCL made from **3b** (2.0 mM) in borate buffer (12.5 mM, pH = 8.0): (a) immediately after dissolving and (b) after stirring for 16 days.

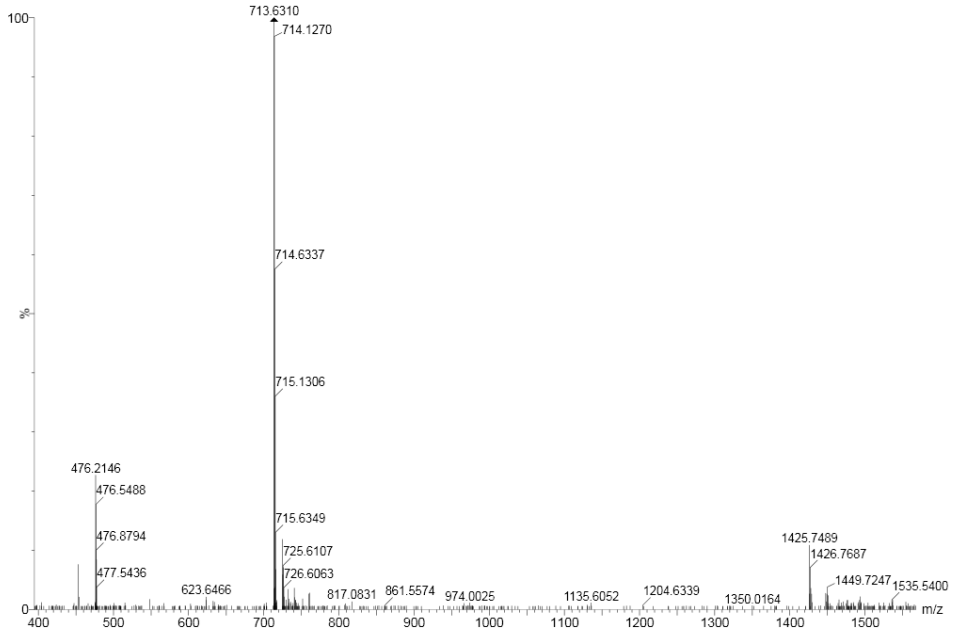

Supplementary Figure 29. Mass spectrum of $(\mathbf{3b})_3$ (retention time 9.3 min in Supplementary Figure 28b) from the LC-MS analysis of a DCL made from **3b** (2.0 mM). $(\mathbf{3b})_3$: m/z calculated: 713.69 $[M+2H]^{2+}$, 476.13 $[M+3H]^{3+}$; m/z observed: 713.63 $[M+2H]^{2+}$, 476.21 $[M+3H]^{3+}$.

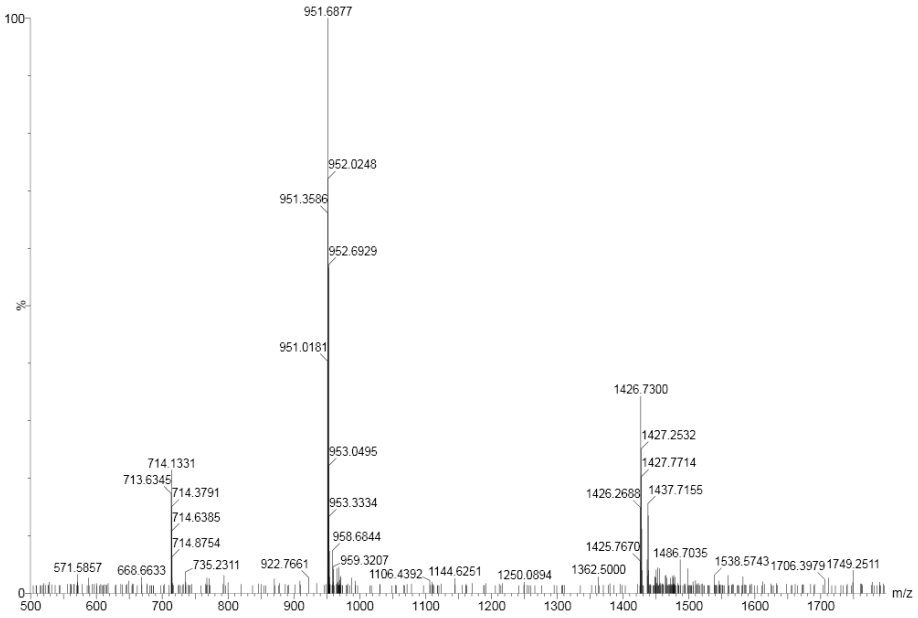

Supplementary Figure 30. Mass spectrum of $(\mathbf{3b})_6$ (retention time 8.75 min in Supplementary Figure 28b) from the LC-MS analysis of a DCL made from **3b** (2.0 mM). $(\mathbf{3b})_6$: m/z calculated: 1426.38 $[M+2H]^{2+}$, 951.25 $[M+3H]^{3+}$, 713.69 $[M+4H]^{4+}$; m/z observed: 1426.27 $[M+2H]^{2+}$, 951.36 $[M+3H]^{3+}$, 713.63 $[M+4H]^{4+}$.

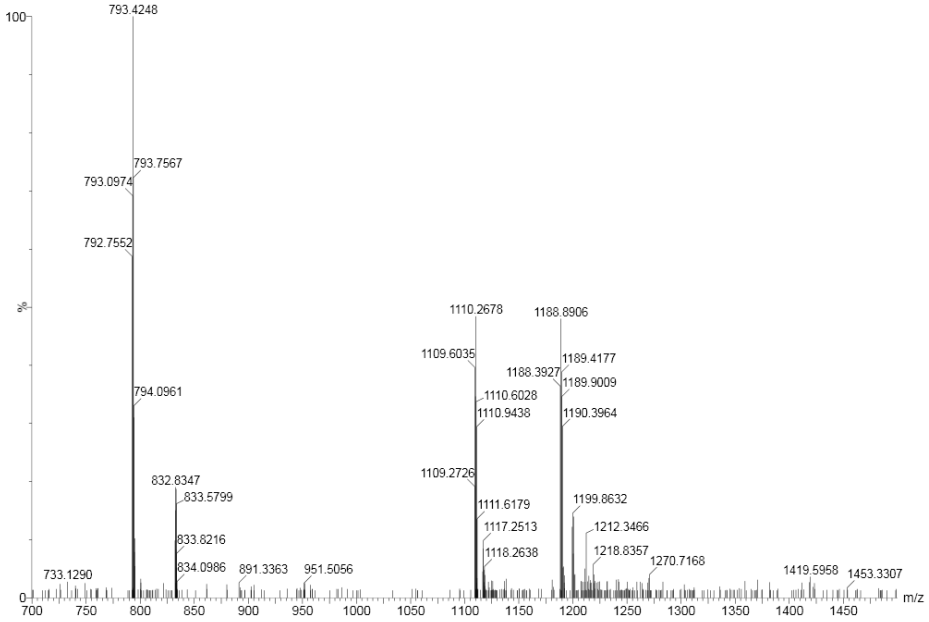

Supplementary Figure 31. Mass spectrum of $(\mathbf{3b})_5$ and $(\mathbf{3b})_7$ (retention time 8.42 min in Supplementary Figure 28b) from the LC-MS analysis of a DCL made from **3b** (2.0 mM). Due to similar retention time of these macrocycles, they are analyzed in a single mass spectrum. $(\mathbf{3b})_5$: m/z calculated: 1188.82 $[M+2H]^{2+}$, 792.88 $[M+3H]^{3+}$; m/z observed: 1188.89 $[M+2H]^{2+}$, 792.76 $[M+3H]^{3+}$. $(\mathbf{3b})_7$: m/z calculated: 1109.63 $[M+3H]^{3+}$, 832.47 $[M+4H]^{4+}$; m/z observed: 1109.60 $[M+3H]^{3+}$, 832.83 $[M+4H]^{4+}$.

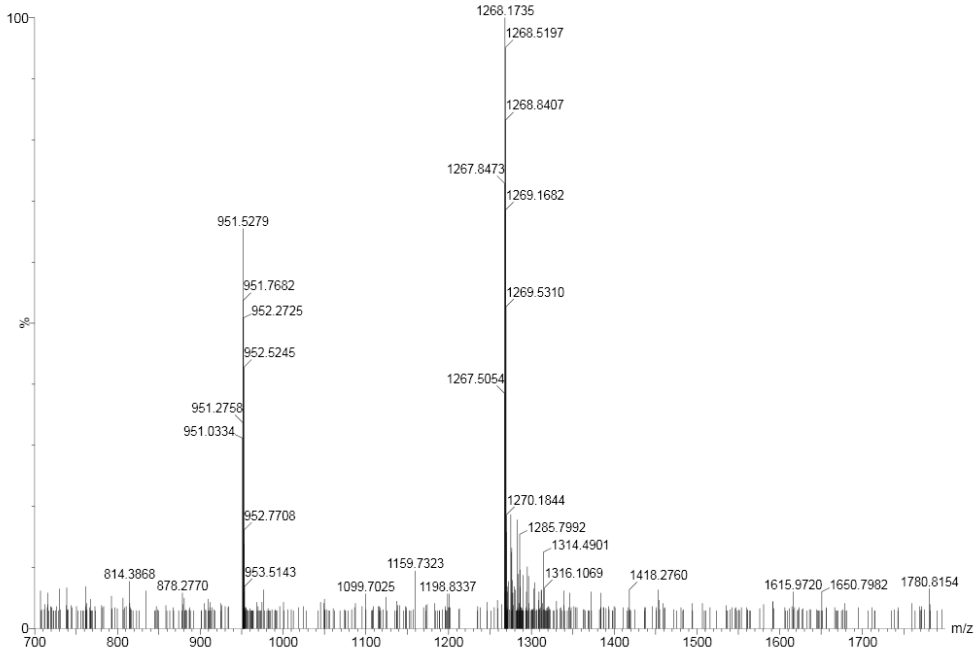

Supplementary Figure 32. Mass spectrum of (**3b**)$_8$ (retention time 8.21 min in Supplementary Figure 28b) from the LC-MS analysis of a DCL made from **3b** (2.0 mM). (**3b**)$_8$: m/z calculated: 1268.00 $[M+3H]^{3+}$, 951.25 $[M+4H]^{4+}$; m/z observed: 1268.17 $[M+3H]^{3+}$, 951.27 $[M+4H]^{4+}$.

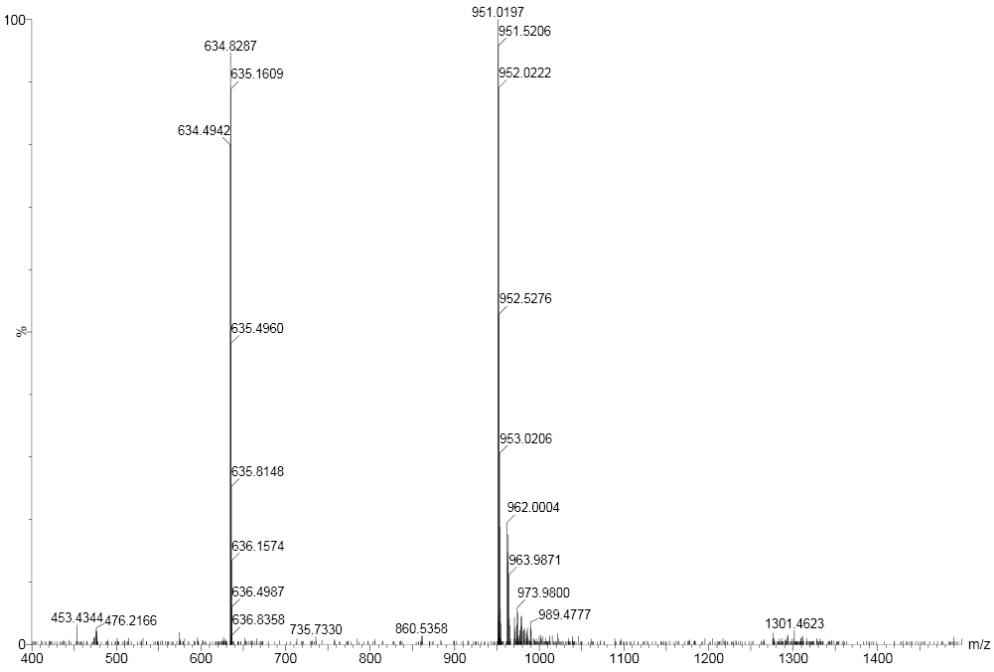

Supplementary Figure 33. Mass spectrum of (**3b**)$_4$ (retention time 7.95 min in Supplementary Figure 28b) from the LC-MS analysis of a DCL made from **3b** (2.0 mM). (**3b**)$_4$: m/z calculated: 951.25 $[M+2H]^{2+}$, 634.51 $[M+3H]^{3+}$; m/z observed: 951.02 $[M+2H]^{2+}$, 634.49 $[M+3H]^{3+}$.

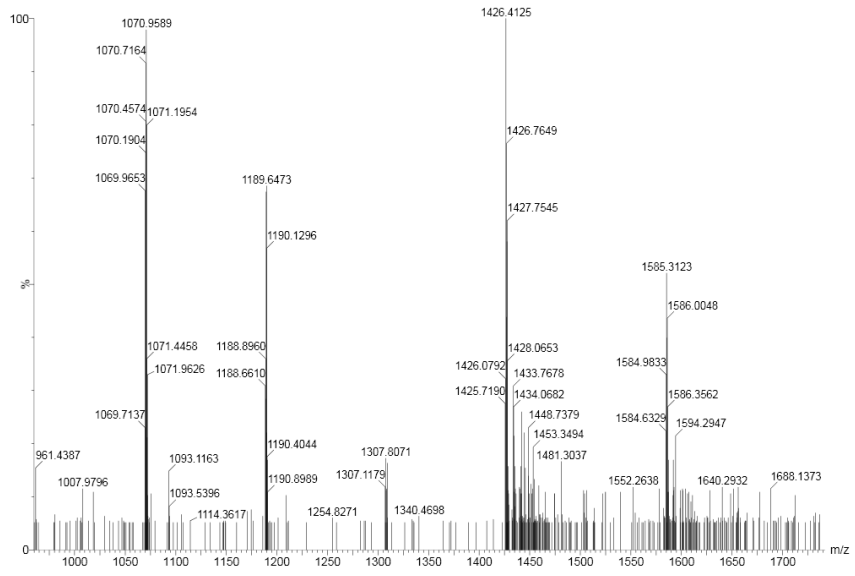

Supplementary Figure 34. Mass spectrum of $(\mathbf{3b})_9$ and $(\mathbf{3b})_{10}$ (retention time 7.63-7.67 min in Supplementary Figure 28b) from the LC-MS analysis of a DCL made from **3b** (2.0 mM). Due to similar retention time of these macrocycles, they are analyzed in a single mass spectrum. $(\mathbf{3b})_9$: m/z calculated: 1426.38 $[M+3H]^{3+}$, 1070.04 $[M+4H]^{4+}$; m/z observed: 1426.41 $[M+3H]^{3+}$, 1070.19 $[M+4H]^{4+}$. $(\mathbf{3b})_{10}$: m/z calculated: 1584.75 $[M+3H]^{3+}$, 1188.82 $[M+4H]^{4+}$; m/z observed: 1584.98 $[M+3H]^{3+}$, 1188.90 $[M+4H]^{4+}$.

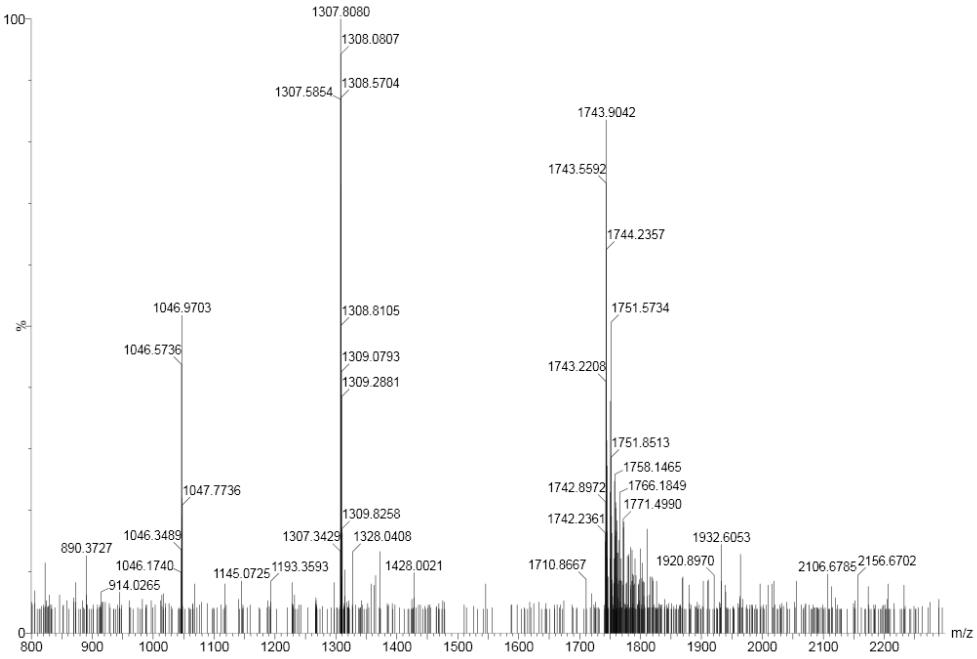

Supplementary Figure 35. Mass spectrum of $(\mathbf{3b})_{11}$ (retention time 7.47 min in Supplementary Figure 28b) from the LC-MS analysis of a DCL made from **3b** (2.0 mM). $(\mathbf{3b})_{11}$: m/z calculated: 1743.13 $[M+3H]^{3+}$, 1307.60 $[M+4H]^{4+}$, 1046.28 $[M+5H]^{5+}$; m/z observed: 1743.22 $[M+3H]^{3+}$, 1307.81 $[M+4H]^{4+}$, 1046.35 $[M+5H]^{5+}$.

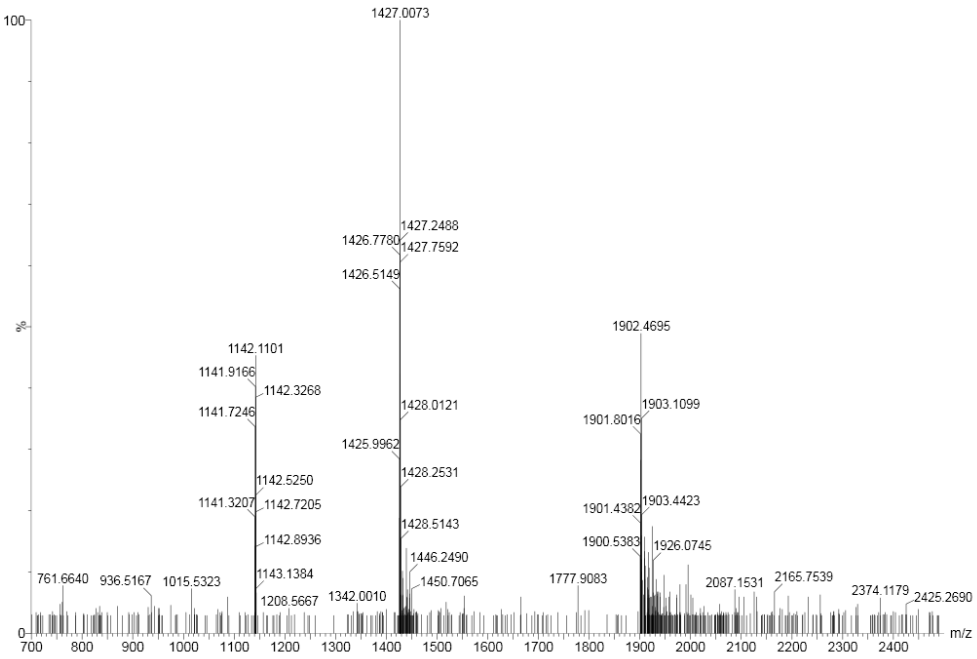

Supplementary Figure 36. Mass spectrum of $(\mathbf{3b})_{12}$ (retention time 7.2 min in Supplementary Figure 28b) from the LC-MS analysis of a DCL made from **3b** (2.0 mM). $(\mathbf{3b})_{12}$: m/z calculated: 1901.50 $[M+3H]^{3+}$, 1426.38 $[M+4H]^{4+}$, 1141.30 $[M+5H]^{5+}$; m/z observed: 1901.44 $[M+3H]^{3+}$, 1426.51 $[M+4H]^{4+}$, 1141.32 $[M+5H]^{5+}$.

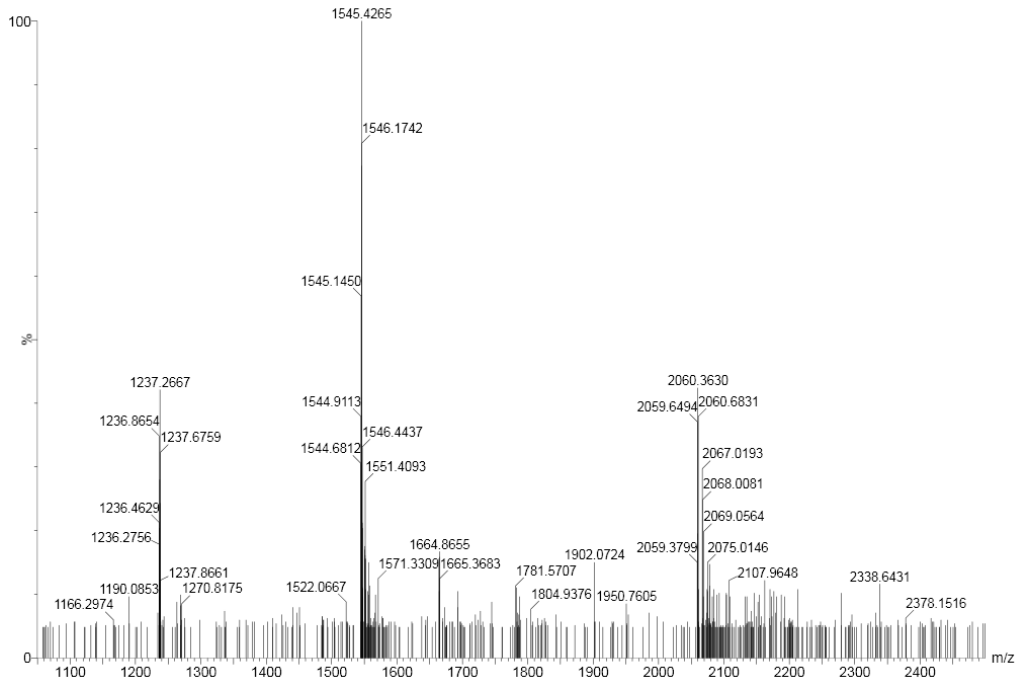

Supplementary Figure 37. Mass spectrum of $(\mathbf{3b})_{13}$ (retention time 6.95 min in Supplementary Figure 28b) from the LC-MS analysis of a DCL made from **3b** (2.0 mM). $(\mathbf{3b})_{13}$: m/z calculated: 2059.87 $[M+3H]^{3+}$, 1545.16 $[M+4H]^{4+}$, 1236.33 $[M+5H]^{5+}$; m/z observed: 2059.65 $[M+3H]^{3+}$, 1545.14 $[M+4H]^{4+}$, 1236.28 $[M+5H]^{5+}$.

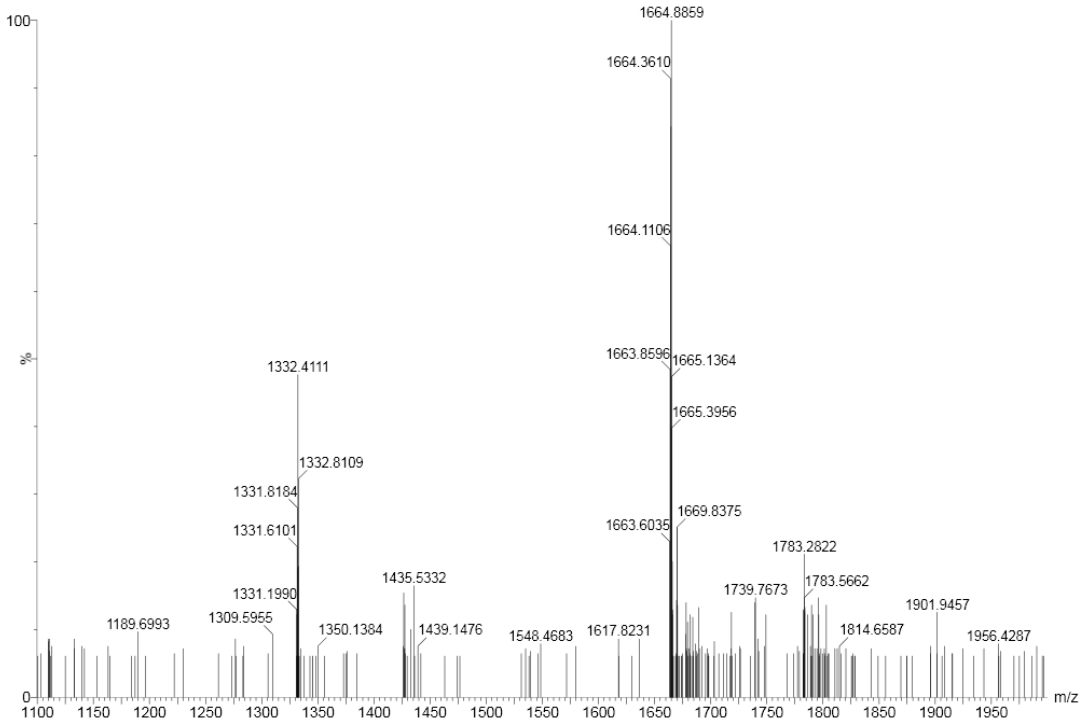

Supplementary Figure 38. Mass spectrum of $(\mathbf{3b})_{14}$ (retention time 6.78 min in Supplementary Figure 28b) from the LC-MS analysis of a DCL made from **3b** (2.0 mM). $(\mathbf{3b})_{14}$: m/z calculated: 1663.94 $[M+4H]^{4+}$, 1331.35 $[M+5H]^{5+}$; m/z observed: 1663.86 $[M+4H]^{4+}$, 1331.20 $[M+5H]^{5+}$.

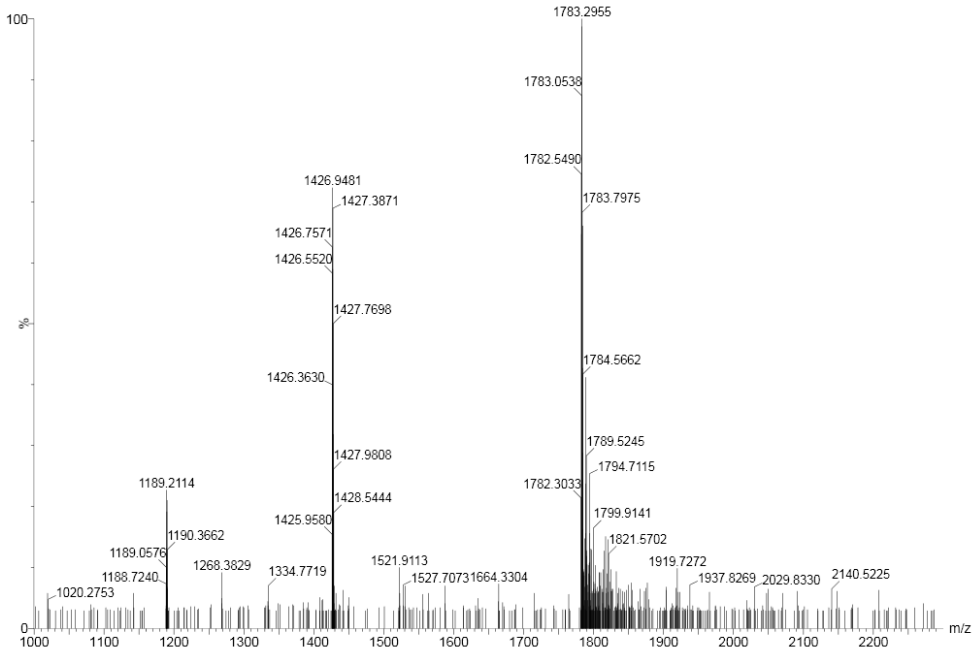

Supplementary Figure 39. Mass spectrum of (**3b**)$_{15}$ (retention time 6.67 min in Supplementary Figure 28b) from the LC-MS analysis of a DCL made from **3b** (2.0 mM). (**3b**)$_{15}$: m/z calculated: 1782.72 $[M+4H]^{4+}$, 1426.38 $[M+5H]^{5+}$, 1188.82 $[M+6H]^{6+}$; m/z observed: 1782.55 $[M+4H]^{4+}$, 1426.36 $[M+5H]^{5+}$, 1188.72 $[M+6H]^{6+}$.

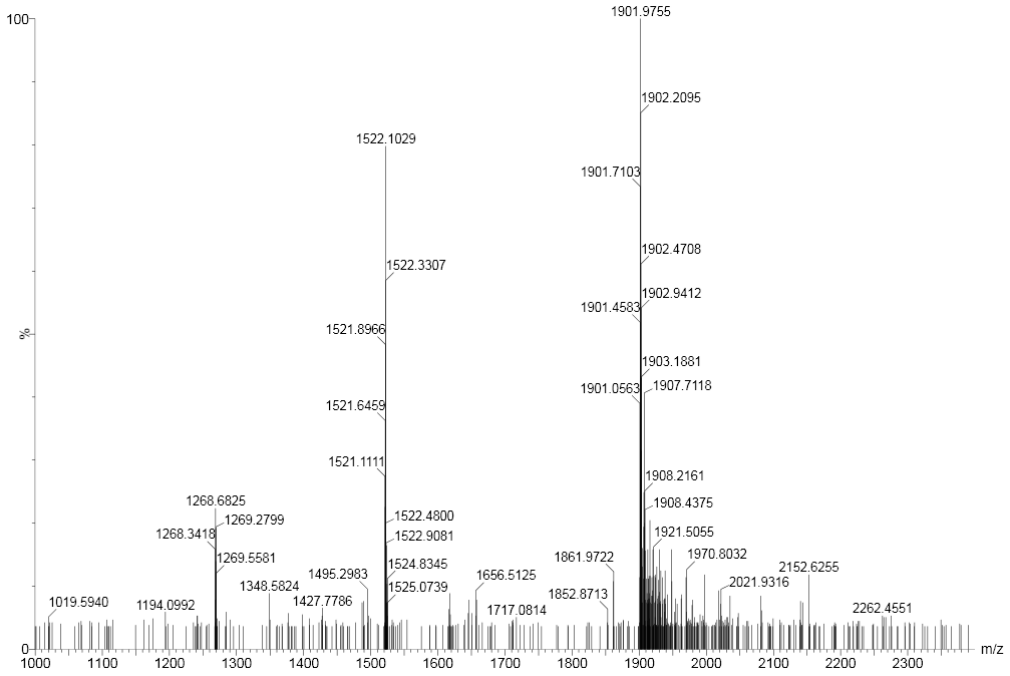

Supplementary Figure 40. Mass spectrum of $(\mathbf{3b})_{16}$ (retention time 6.45 min in Supplementary Figure 28b) from the LC-MS analysis of a DCL made from **3b** (2.0 mM). $(\mathbf{3b})_{16}$: m/z calculated: 1901.50 $[M+4H]^{4+}$, 1521.40 $[M+5H]^{5+}$, 1268.00 $[M+6H]^{6+}$; m/z observed: 1901.45 $[M+4H]^{4+}$, 1521.65 $[M+5H]^{5+}$, 1268.34 $[M+6H]^{6+}$.

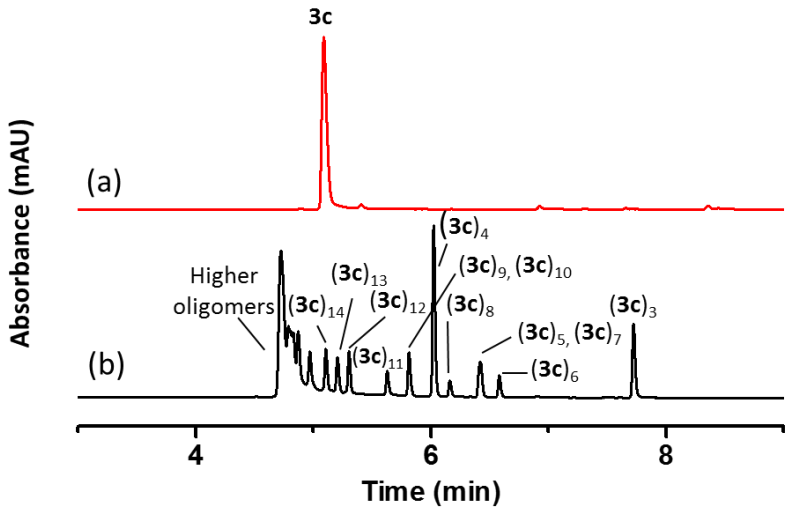

Supplementary Figure 41. UPLC analyses of the DCL made from **3c** (2.0 mM) in borate buffer (12.5 mM, pH = 8.0): (a) immediately after dissolving and (b) after stirring for 16 days.

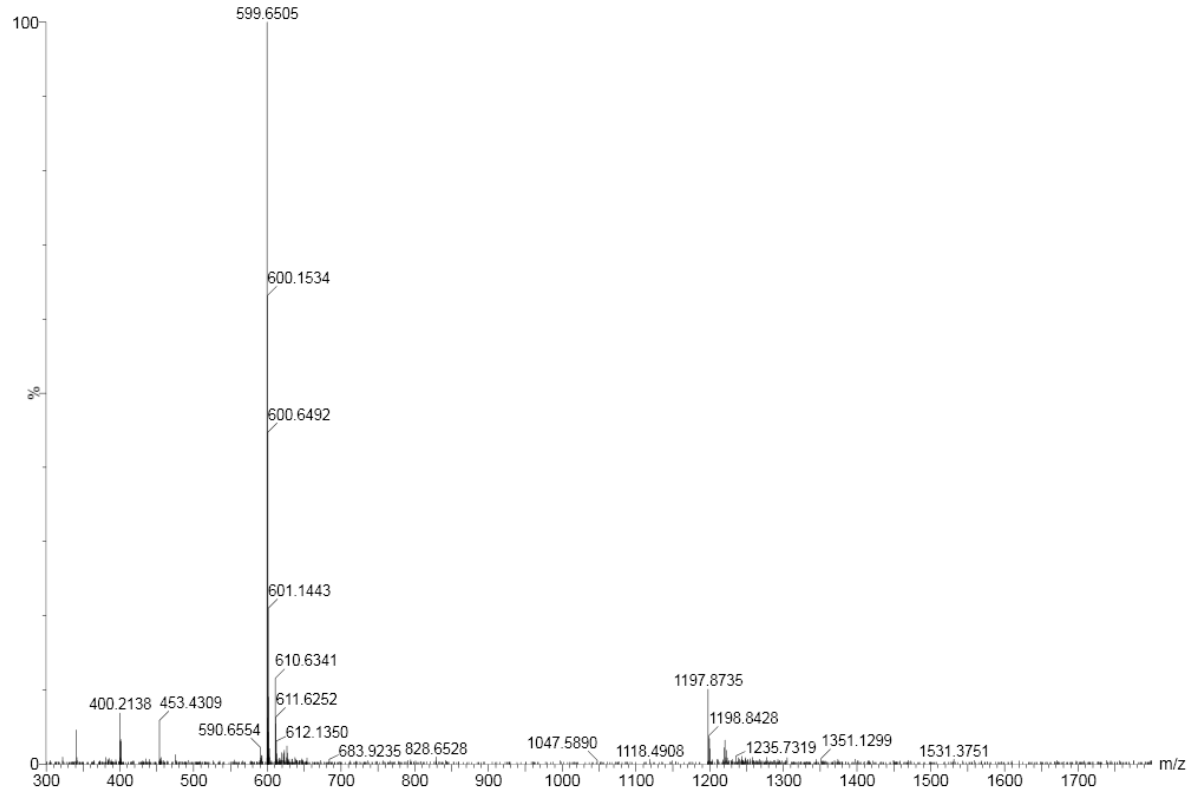

Supplementary Figure 42. Mass spectrum of (**3c**)$_3$ (retention time 7.73 min in Supplementary Figure 41b) from the LC-MS analysis of a DCL made from **3c** (2.0 mM). (**3c**)$_3$: m/z calculated: 599.65 $[M+2H]^{2+}$; m/z observed: 599.65 $[M+2H]^{2+}$.

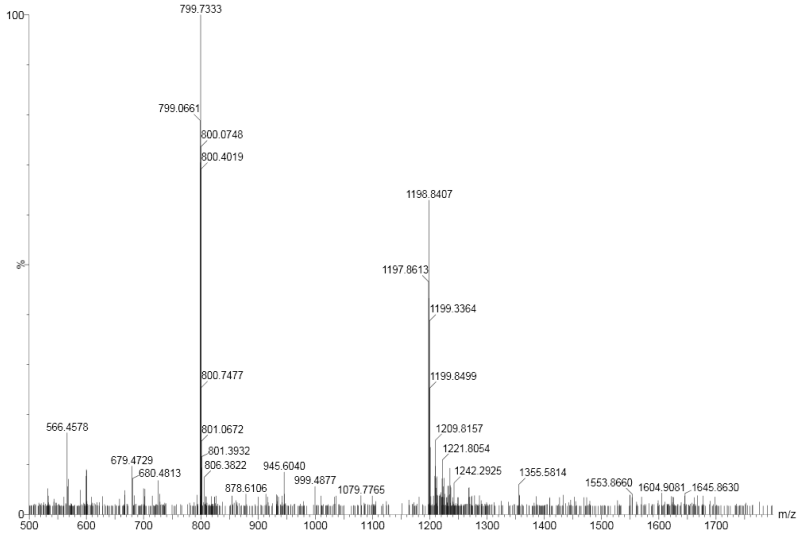

Supplementary Figure 43. Mass spectrum of $(\mathbf{3c})_6$ (retention time 6.56 min in Supplementary Figure 41b) from the LC-MS analysis of a DCL made from **3c** (2.0 mM). $(\mathbf{3c})_6$: m/z calculated: 799.19 $[M+2H]^{2+}$; m/z observed: 799.07 $[M+2H]^{2+}$.

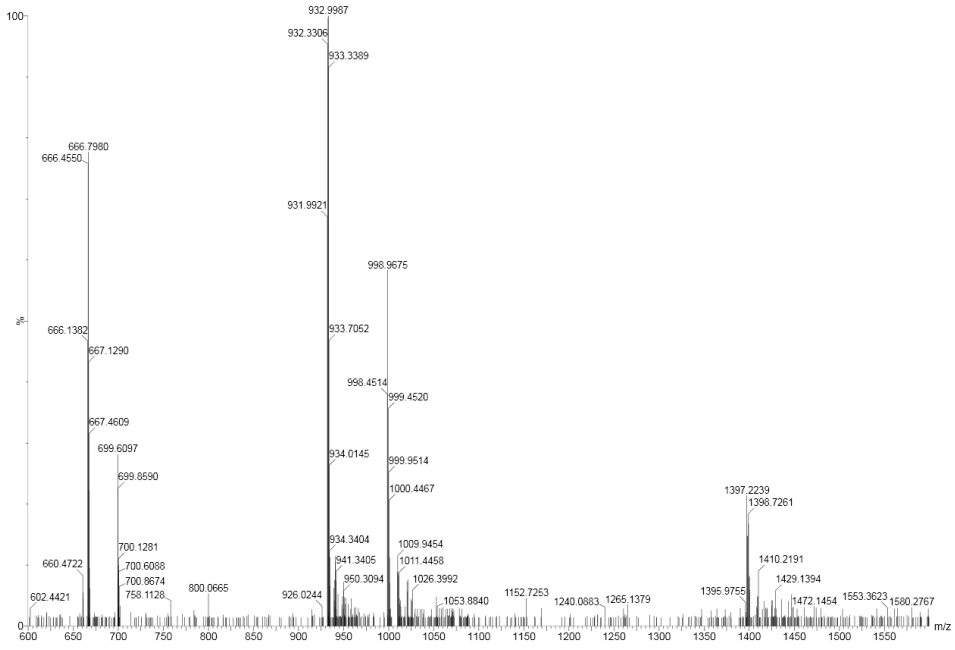

Supplementary Figure 44. Mass spectrum of $(\mathbf{3c})_5$ and $(\mathbf{3c})_7$ (retention time 6.42 min in Supplementary Figure 41b) from the LC-MS analysis of a DCL made from **3c** (2.0 mM). Due to similar retention time of these macrocycles, they are analyzed in a single mass spectrum. $(\mathbf{3c})_5$: m/z calculated: 998.74 $[M+2H]^{2+}$, 666.16 $[M+3H]^{3+}$; m/z observed: 998.97 $[M+2H]^{2+}$, 666.14 $[M+3H]^{3+}$. $(\mathbf{3c})_7$: m/z calculated: 932.22 $[M+3H]^{3+}$, 699.42 $[M+4H]^{4+}$; m/z observed: 932.33 $[M+3H]^{3+}$, 699.61 $[M+4H]^{4+}$.

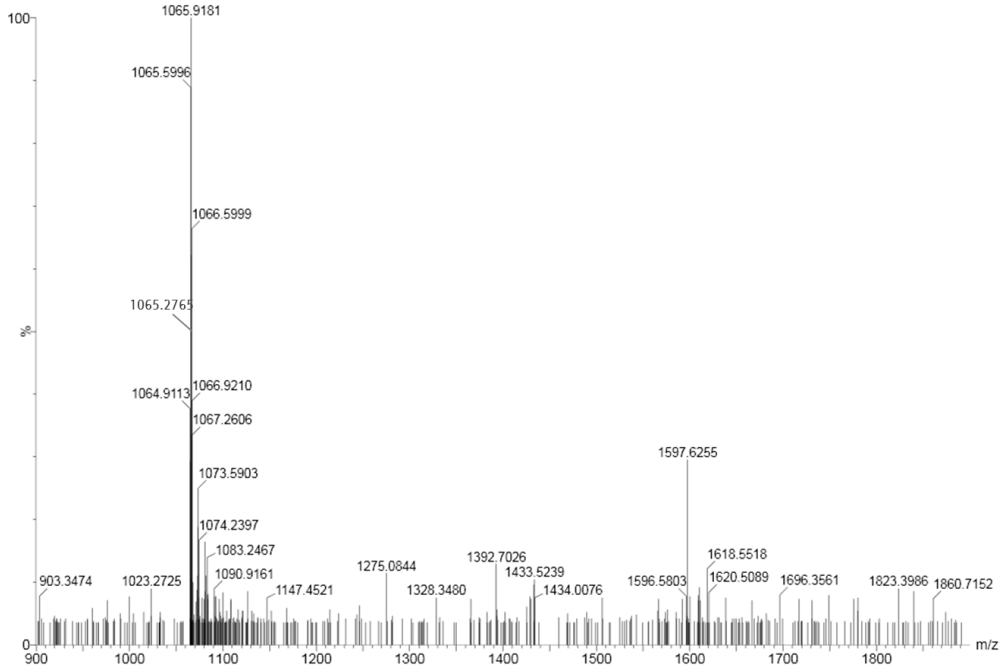

Supplementary Figure 45. Mass spectrum of $(\mathbf{3c})_8$ (retention time 6.17 min in Supplementary Figure 41b) from the LC-MS analysis of a DCL made from **3c** (2.0 mM). $(\mathbf{3c})_8$: m/z calculated: 1065.25 $[M+3H]^{3+}$, 799.19 $[M+4H]^{4+}$; m/z observed: 1065.28 $[M+3H]^{3+}$, 799.07 $[M+4H]^{4+}$.

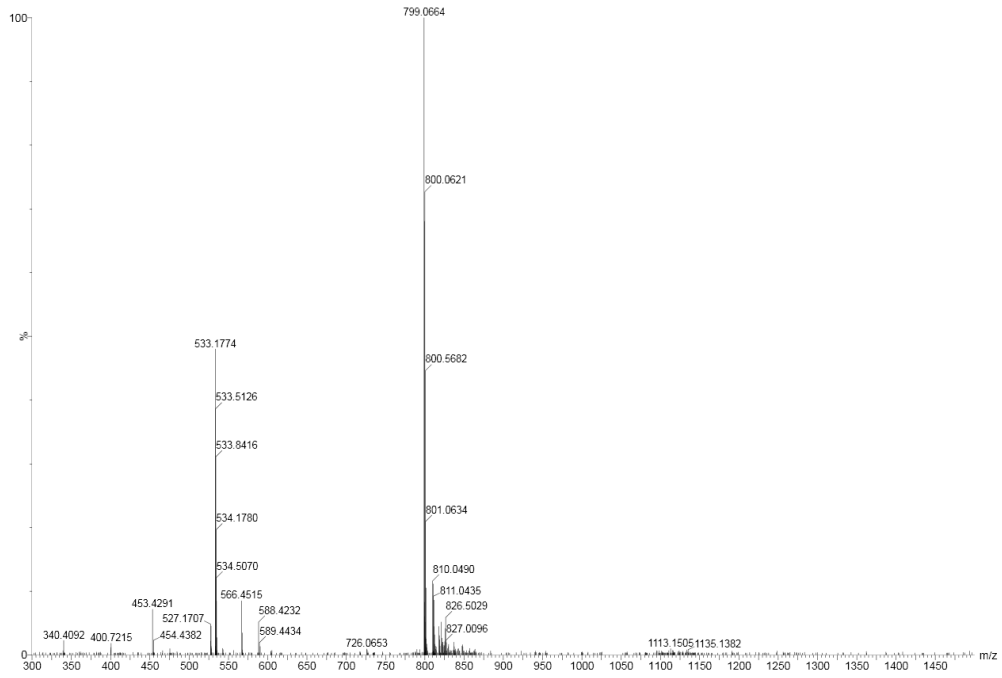

Supplementary Figure 46. Mass spectrum of (**3c**)$_4$ (retention time 6.17 min in Supplementary Figure 41b) from the LC-MS analysis of a DCL made from **3c** (2.0 mM). (**3c**)$_4$: m/z calculated: 799.19 $[M+2H]^{2+}$, 533.13 $[M+3H]^{3+}$; m/z observed: 799.07 $[M+2H]^{2+}$, 533.18 $[M+3H]^{3+}$.

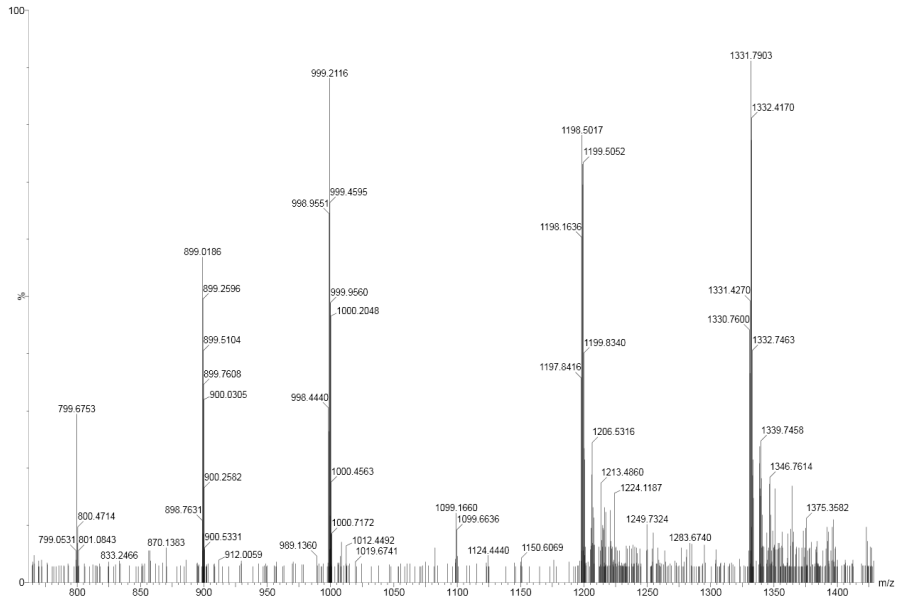

Supplementary Figure 47. Mass spectrum of $(\mathbf{3c})_9$ and $(\mathbf{3c})_{10}$ (retention time 5.81 min in Supplementary Figure 41b) from the LC-MS analysis of a DCL made from **3c** (2.0 mM). Due to similar retention time of these macrocycles, they are analyzed in a single mass spectrum. $(\mathbf{3c})_9$: m/z calculated: 1198.28 $[M+3H]^{3+}$, 898.97 $[M+4H]^{4+}$; m/z observed: 1198.50 $[M+3H]^{3+}$, 899.02 $[M+4H]^{4+}$. $(\mathbf{3c})_{10}$: m/z calculated: 1331.32 $[M+3H]^{3+}$, 998.74 $[M+4H]^{4+}$, 799.19 $[M+5H]^{5+}$; m/z observed: 1131.42 $[M+3H]^{3+}$, 998.96 $[M+4H]^{4+}$, 799.05 $[M+5H]^{5+}$.

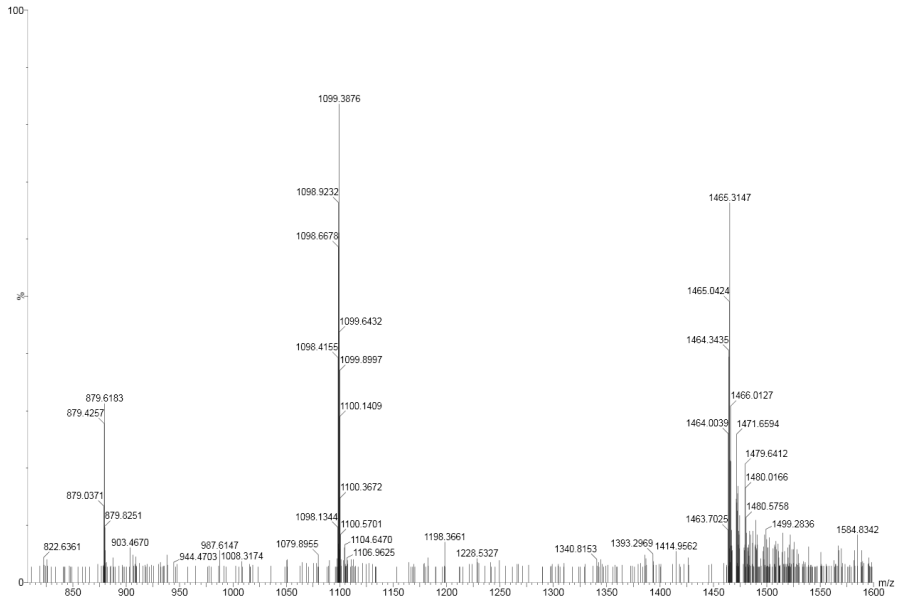

Supplementary Figure 48. Mass spectrum of $(\mathbf{3c})_{11}$ (retention time 5.63 min in Supplementary Figure 41b) from the LC-MS analysis of a DCL made from **3c** (2.0 mM). $(\mathbf{3c})_{11}$: m/z calculated: 1464.35 $[M+3H]^{3+}$, 1098.51 $[M+4H]^{4+}$, 879.01 $[M+5H]^{5+}$; m/z observed: 1464.10 $[M+3H]^{3+}$, 1098.67 $[M+4H]^{4+}$, 879.04 $[M+5H]^{5+}$.

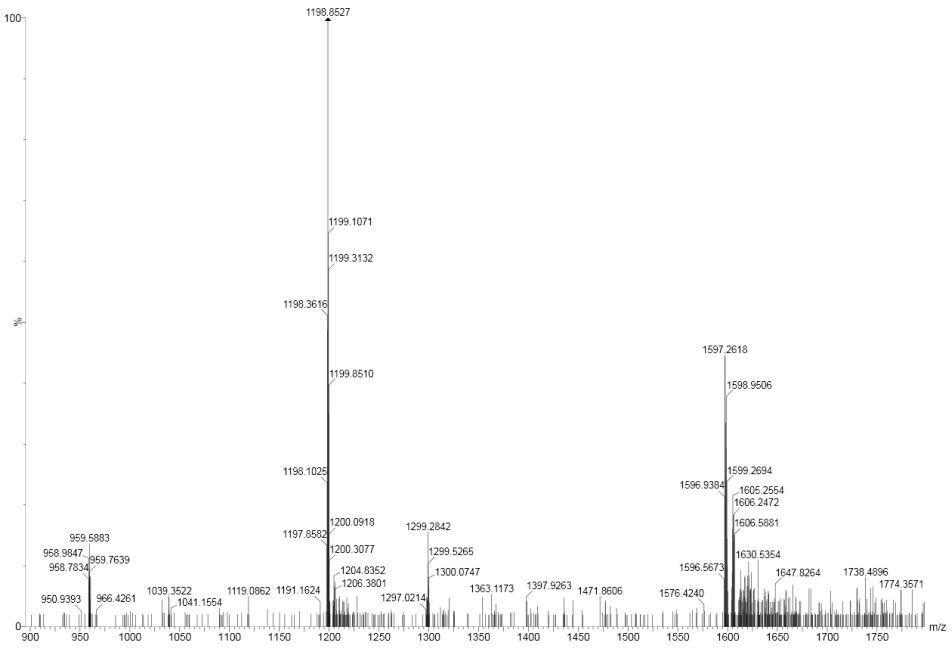

Supplementary Figure 49. Mass spectrum of $(\mathbf{3c})_{12}$ (retention time 5.3 min in Supplementary Figure 41b) from the LC-MS analysis of a DCL made from **3c** (2.0 mM). $(\mathbf{3c})_{12}$: m/z calculated: 1597.38 $[M+3H]^{3+}$, 1198.28 $[M+4H]^{4+}$, 958.83 $[M+5H]^{5+}$; m/z observed: 1597.26 $[M+3H]^{3+}$, 1198.36 $[M+4H]^{4+}$, 958.78 $[M+5H]^{5+}$.

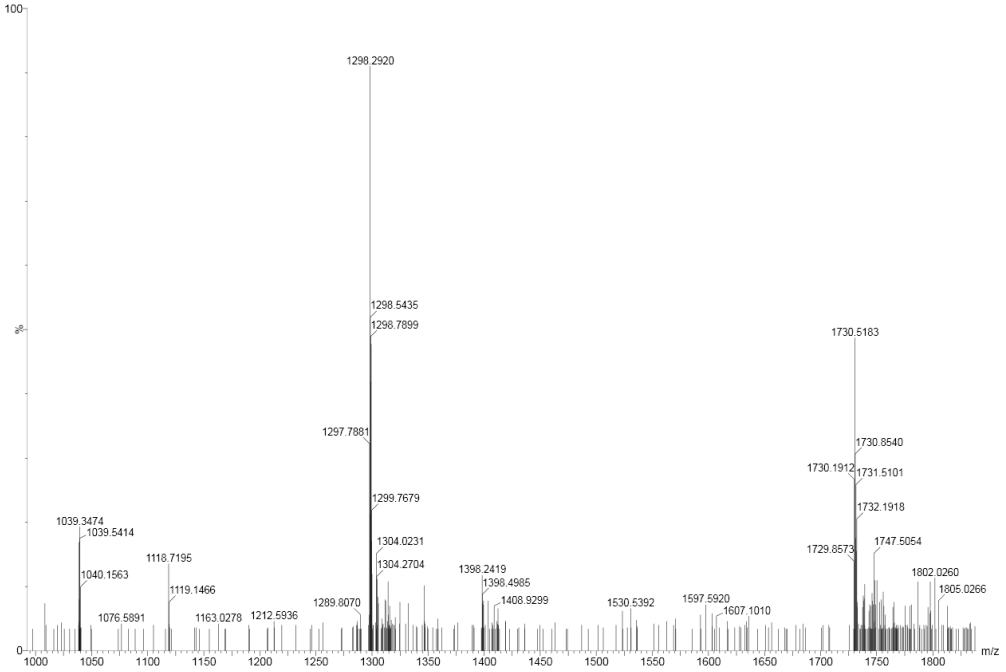

Supplementary Figure 50. Mass spectrum of $(\mathbf{3c})_{13}$ (retention time 5.19 min in Supplementary Figure 41b) from the LC-MS analysis of a DCL made from **3c** (2.0 mM). $(\mathbf{3c})_{13}$: m/z calculated: 1730.41 $[M+3H]^{3+}$, 1298.06 $[M+4H]^{4+}$; m/z observed: 1730.52 $[M+3H]^{3+}$, 1298.29 $[M+4H]^{4+}$.

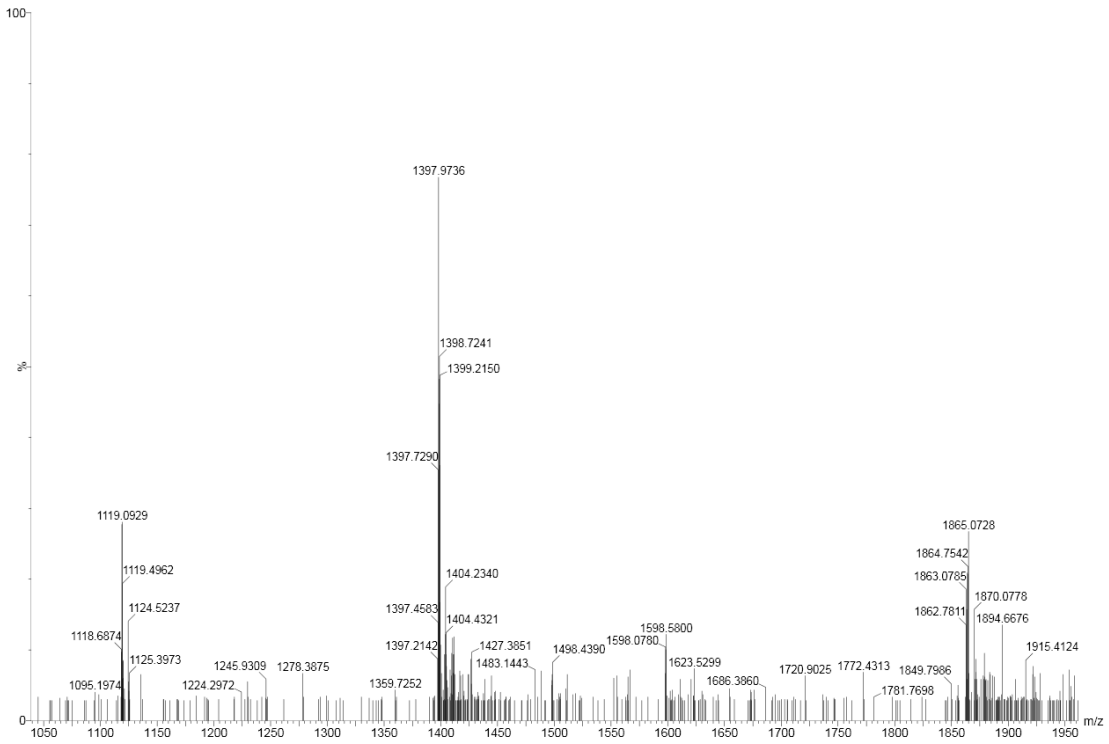

Supplementary Figure 51. Mass spectrum of (**3c**)$_{14}$ (retention time 5.1 min in Supplementary Figure 41b) from the LC-MS analysis of a DCL made from **3c** (2.0 mM). (**3c**)$_{14}$: m/z calculated: 1863.44 $[M+3H]^{3+}$, 1397.83 $[M+4H]^{4+}$, 1118.47 $[M+5H]^{5+}$; m/z observed: 1863.08 $[M+3H]^{3+}$, 1397.73 $[M+4H]^{4+}$, 1118.68 $[M+5H]^{5+}$.

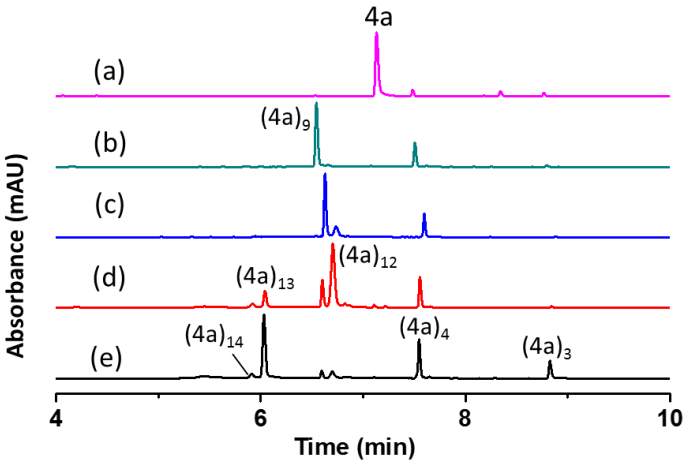

Supplementary Figure 52. UPLC analyses of a DCL made from **4a** (2.0 mM) in borate buffer (12.5 mM, pH = 8.0): (a) immediately after dissolving and (b) after 16 days of stirring, in the presence of (c) 1.0 M NaCl, (d) 1.0 M $MgCl_2$ and (e) 1.0 M $MnCl_2$.

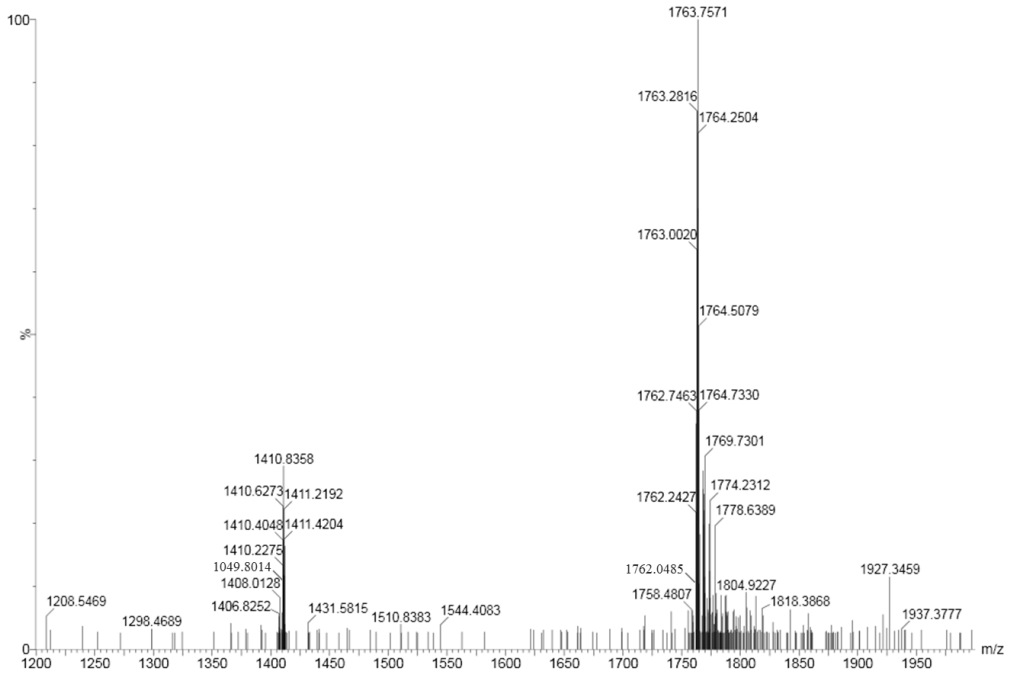

Supplementary Figure 53. Mass spectrum of $(\mathbf{4a})_{14}$ (retention time 5.90 min in Supplementary Figure 52e) from the LC-MS analysis of a DCL made from **4a** (2.0 mM). $(\mathbf{4a})_{14}$: m/z calculated: 1761.92 $[M+4H]^{4+}$, 1409.74 $[M+5H]^{5+}$; m/z observed: 1762.05 $[M+4H]^{4+}$, 1409.80 $[M+5H]^{5+}$.

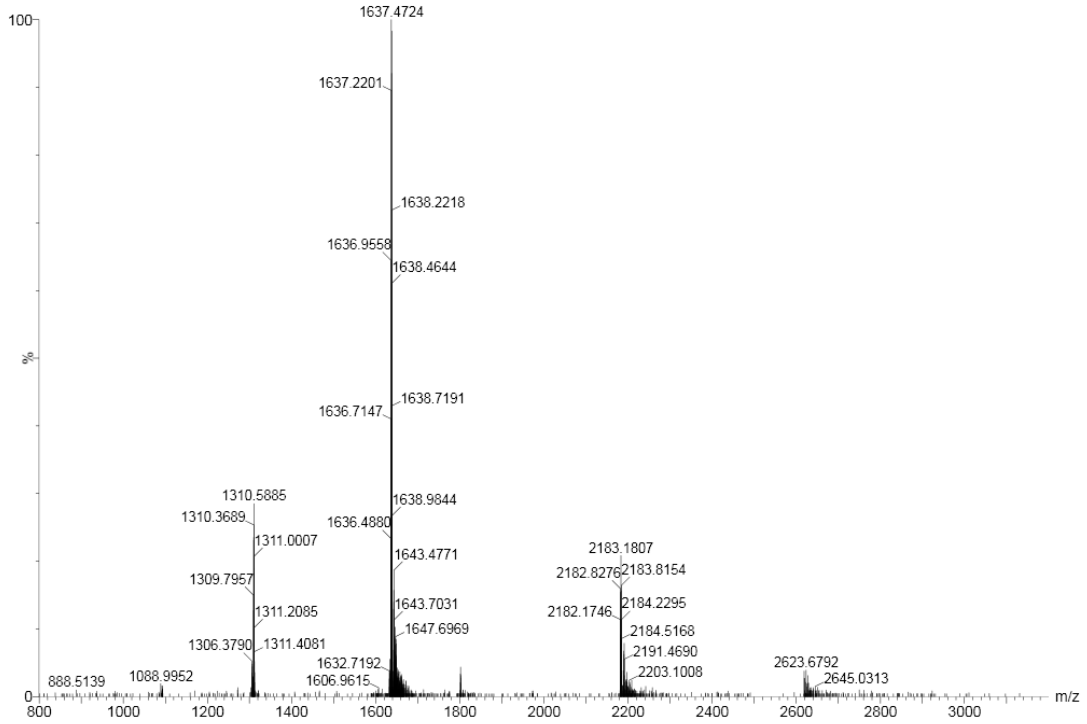

Supplementary Figure 54. Mass spectrum of (**4a**)$_{13}$ (retention time 6.02 min in Supplementary Figure 52e) from the LC-MS analysis of a DCL made from **4a** (2.0 mM). (**4a**)$_{13}$: m/z calculated: 2181.19 $[M+3H]^{3+}$, 1636.14 $[M+4H]^{4+}$; m/z observed: 2181.65 $[M+3H]^{3+}$, 1636.18 $[M+4H]^{4+}$.

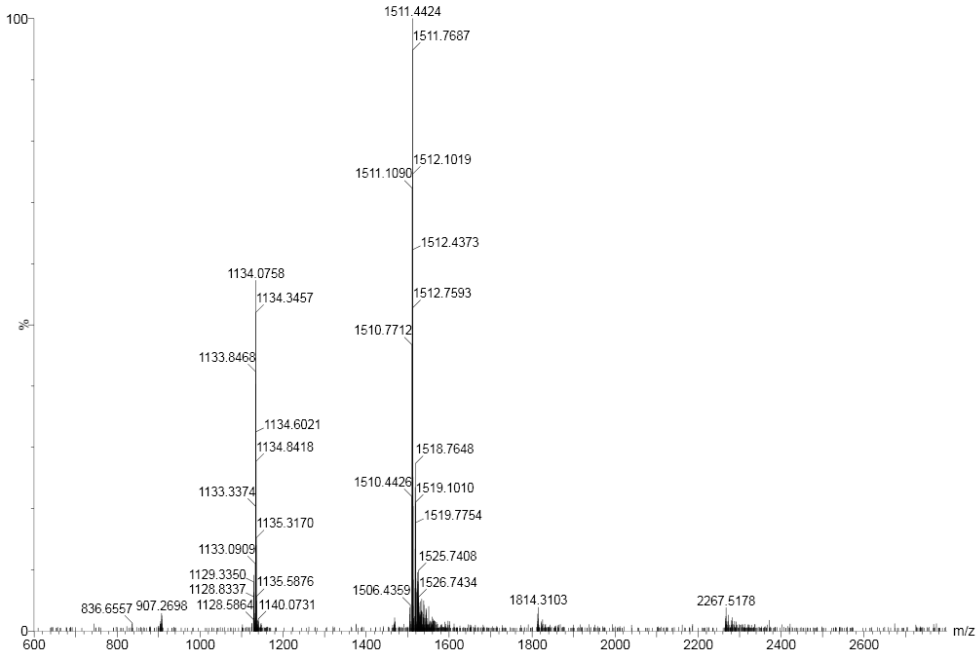

Supplementary Figure 55. Mass spectrum of (**4a**)$_9$ (retention time 6.53 min in Supplementary Figure 52e) from the LC-MS analysis of a DCL made from **4a** (2.0 mM). (**4a**)$_9$: m/z calculated: 1510.36 $[M+3H]^{3+}$, 1133.02 $[M+4H]^{4+}$; m/z observed: 1510.44 $[M+3H]^{3+}$, 1133.08 $[M+4H]^{4+}$.

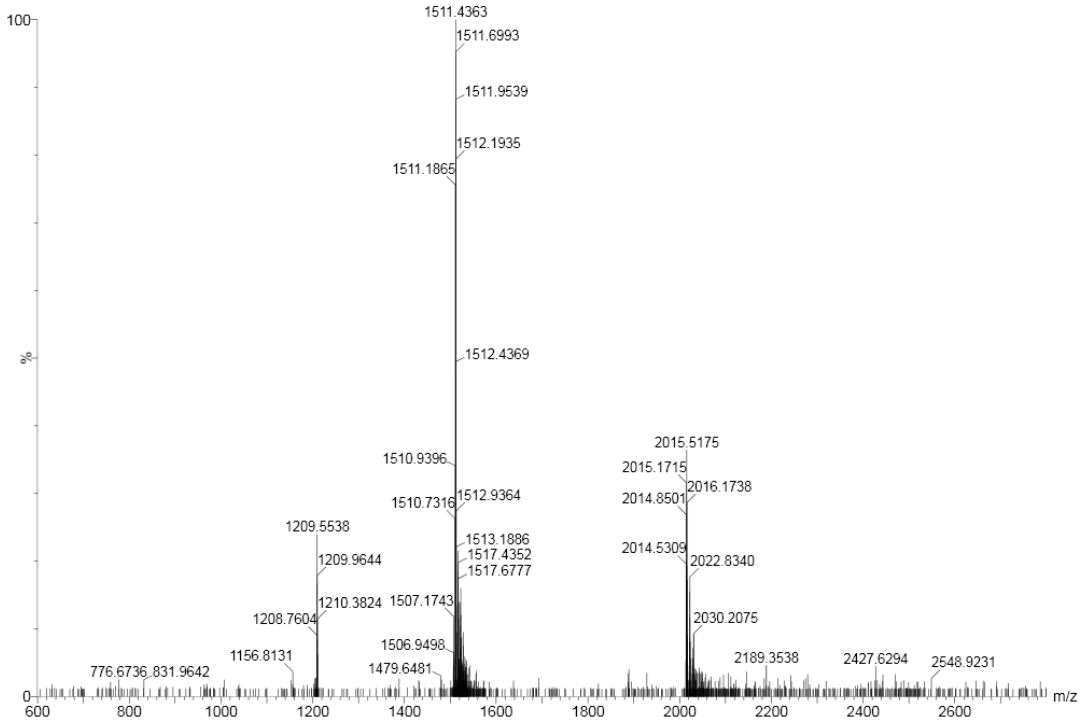

Supplementary Figure 56. Mass spectrum of $(\mathbf{4a})_{12}$ (retention time 6.67 min in Supplementary Figure 52e) from the LC-MS analysis of a DCL made from **4a** (2.0 mM). $(\mathbf{4a})_{12}$: m/z calculated: 1510.36 $[M+4H]^{4+}$, 1208.49 $[M+5H]^{5+}$; m/z observed: 1510.43 $[M+4H]^{4+}$, 1208.50 $[M+5H]^{5+}$.

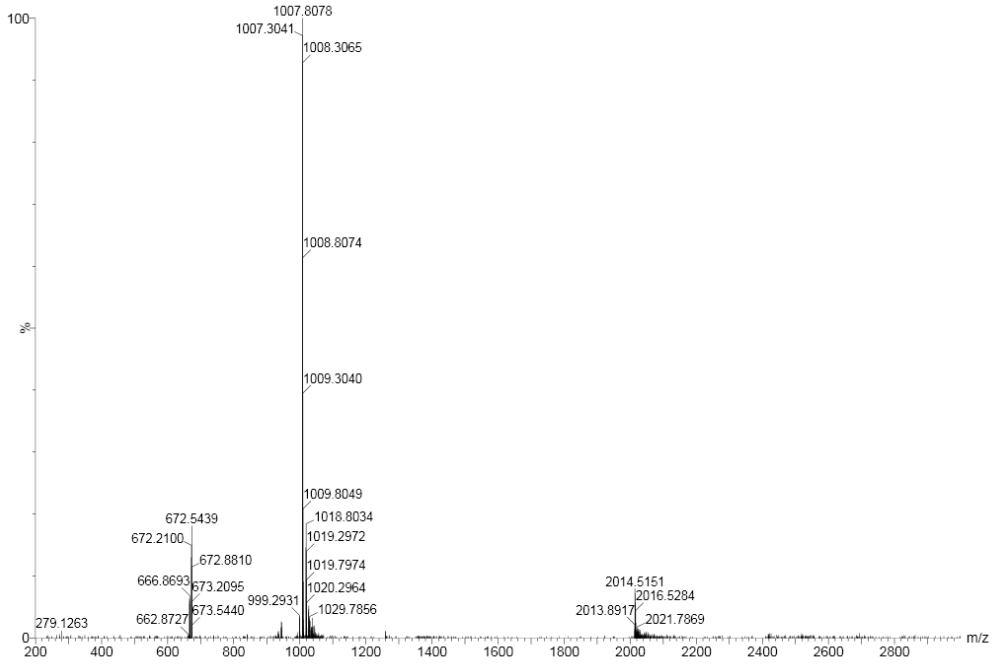

Supplementary Figure 57. Mass spectrum of (**4a**)$_4$ (retention time 7.52 min in Supplementary Figure 52e) from the LC-MS analysis of a DCL made from **4a** (2.0 mM). (**4a**)$_4$: m/z calculated: 1007.24 $[M+2H]^{2+}$; m/z observed: 1007.30 $[M+2H]^{2+}$.

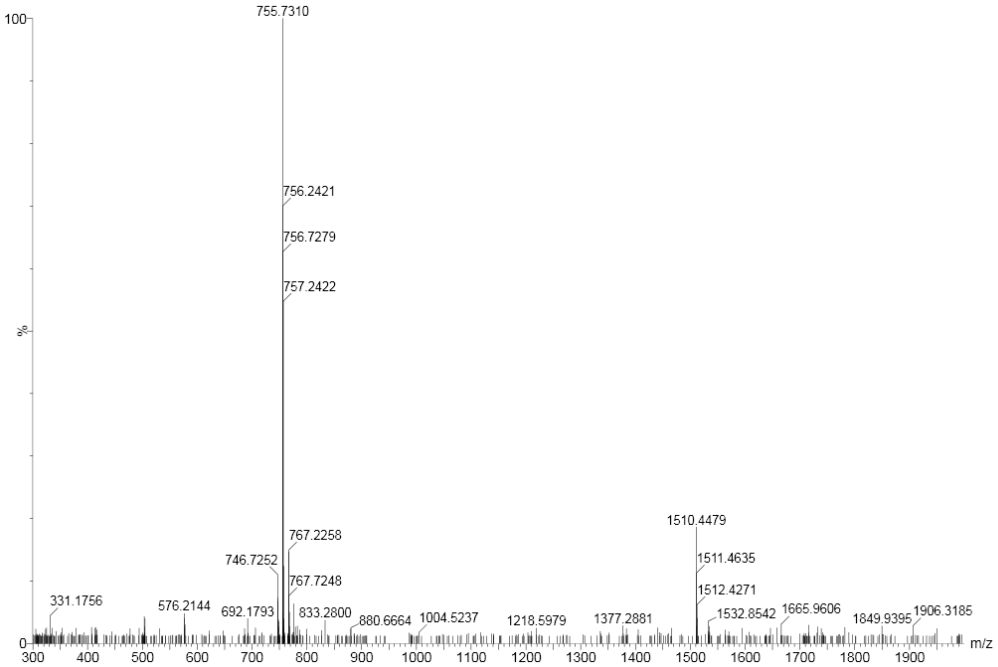

Supplementary Figure 58. Mass spectrum of $(\mathbf{4a})_3$ (retention time 8.81 min in Supplementary Figure 52e) from the LC-MS analysis of a DCL made from **4a** (2.0 mM). $(\mathbf{4a})_3$: m/z calculated: 1510.36 $[M+1H]^+$, 755.69 $[M+2H]^{2+}$; m/z observed: 1510.45 $[M+1H]^+$, 755.73 $[M+2H]^{2+}$.

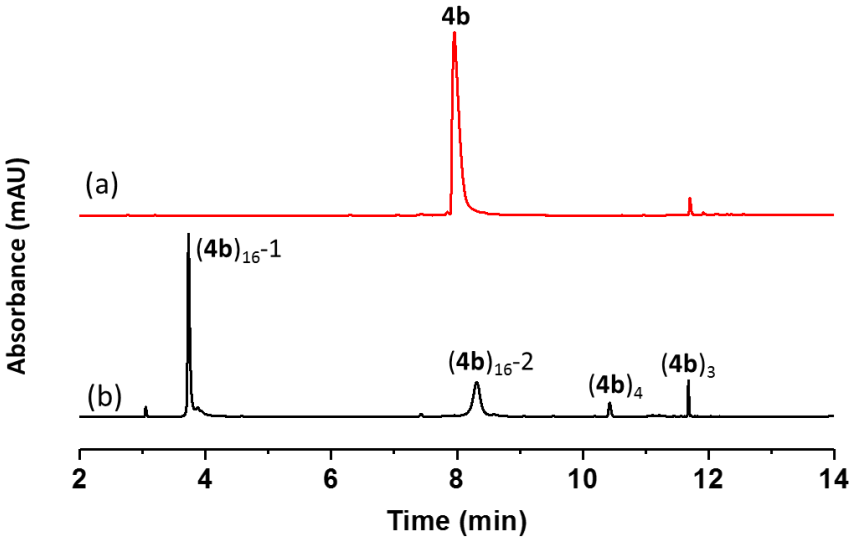

Supplementary Figure 59. UPLC analyses of a DCL made from **4b** (2.0 mM) in borate buffer (12.5 mM, pH = 8.0): (a) immediately after dissolving and (b) after stirring for 16 days.

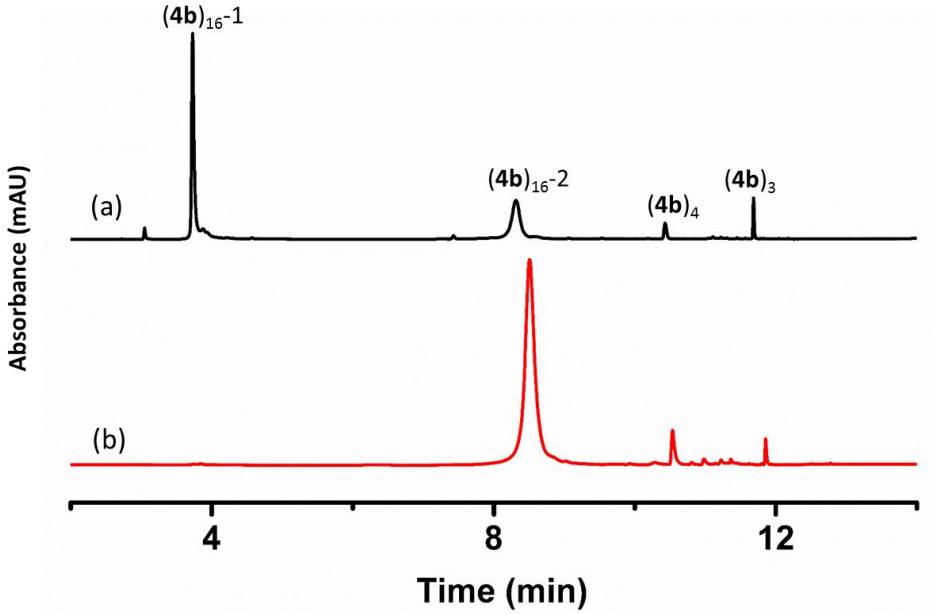

Supplementary Figure 60. UPLC analyses of the DCL made from $(\mathbf{4b})_{16}$ (a) after dissolving a freeze-dried library in buffer and (b) in DMF.

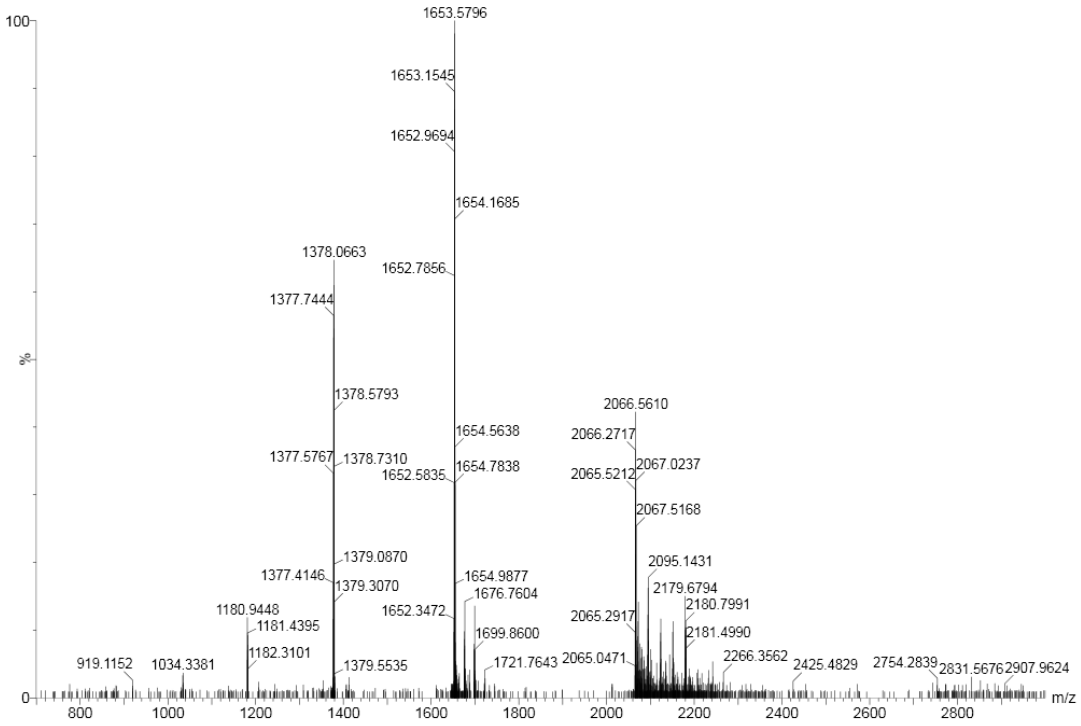

Supplementary Figure 61. Mass spectrum of $(\mathbf{4b})_{16}$ -1 (retention time 3.74 min in Supplementary Figure 59b) from the LC-MS analysis of a DCL made from **4b** (2.0 mM). $(\mathbf{4b})_{16}$-1: m/z calculated: 2065.65 $[M+4H]^{4+}$, 1652.72 $[M+5H]^{5+}$, 1377.44 $[M+6H]^{6+}$; m/z observed: 2065.52 $[M+4H]^{4+}$, 1652.78 $[M+5H]^{5+}$, 1377.41 $[M+6H]^{6+}$.

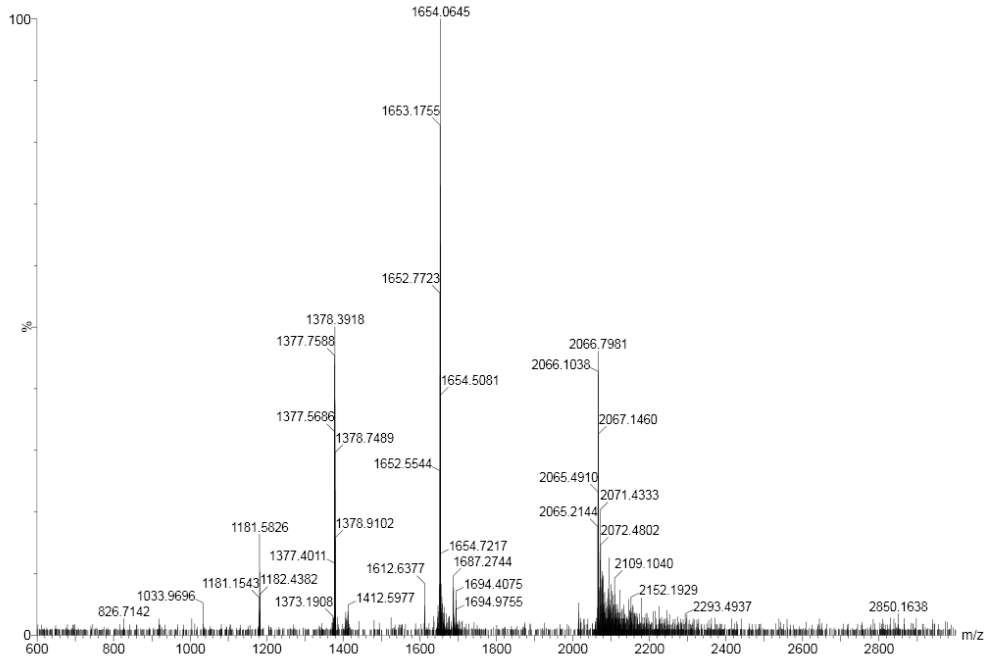

Supplementary Figure 62. Mass spectrum of $(\mathbf{4b})_{16}$ -2 (retention time 8.29 min in Supplementary Figure 59b) from the LC-MS analysis of a DCL made from **4b** (2.0 mM). $(\mathbf{4b})_{16}$ -2: m/z calculated: 2065.65 $[M+4H]^{4+}$, 1652.72 $[M+5H]^{5+}$, 1377.44 $[M+6H]^{6+}$; m/z observed: 2065.49 $[M+4H]^{4+}$, 1652.55 $[M+5H]^{5+}$, 1377.56 $[M+6H]^{6+}$.

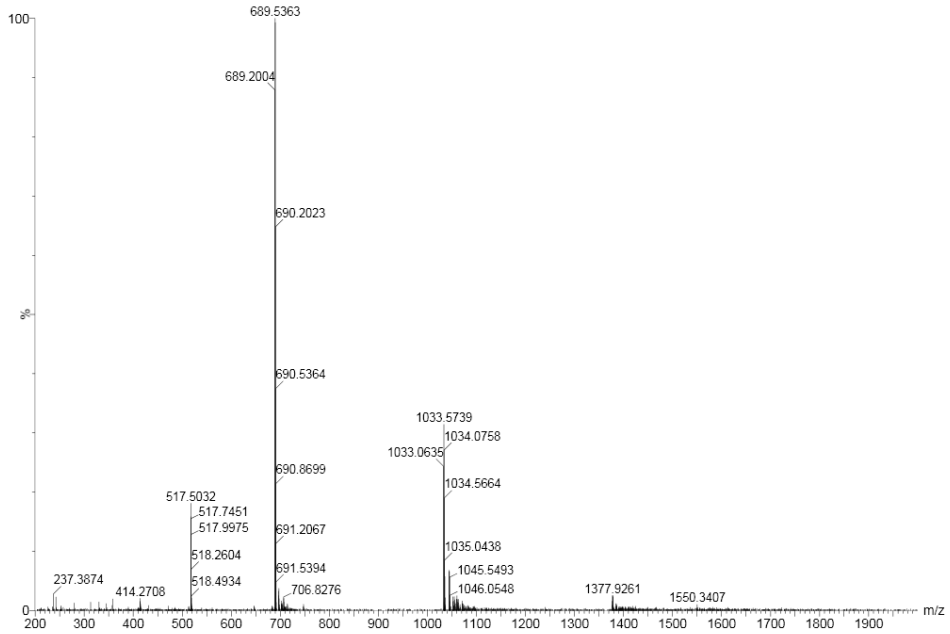

Supplementary Figure 63. Mass spectrum of $(\mathbf{4b})_4$ (retention time 10.44 min in Supplementary Figure 59b) from the LC-MS analysis of a DCL made from **4b** (2.0 mM). $(\mathbf{4b})_4$: m/z calculated: 1033.33 $[M+2H]^{2+}$, 689.22 $[M+3H]^{3+}$; m/z observed: 1033.06 $[M+2H]^{2+}$, 689.20 $[M+3H]^{3+}$.

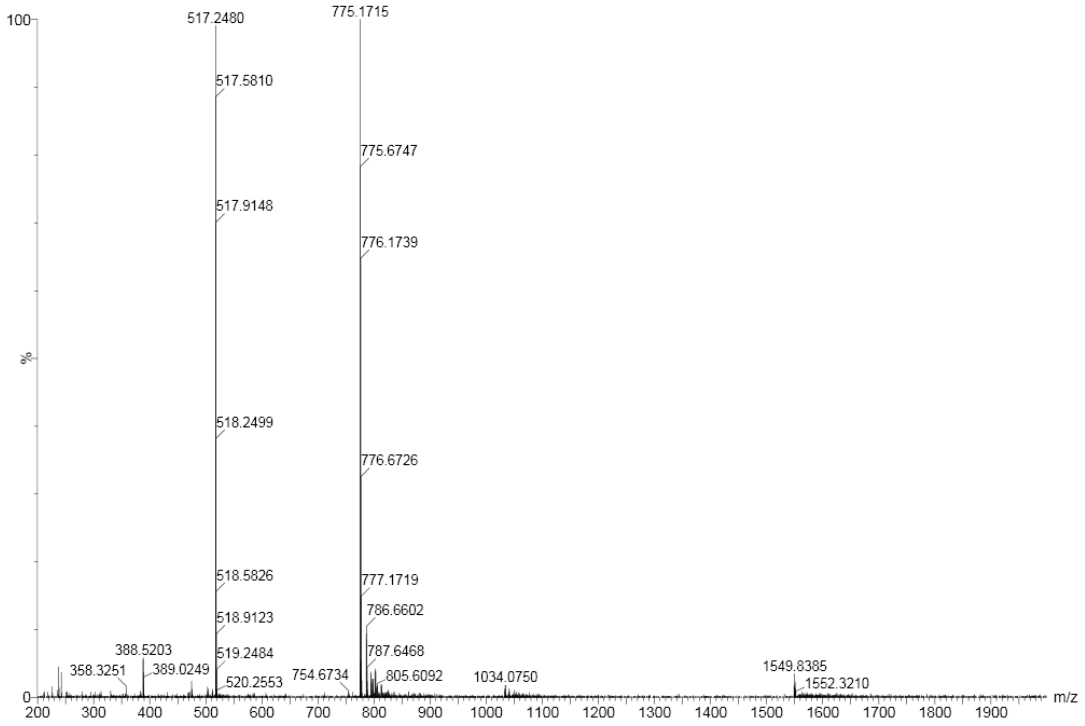

Supplementary Figure 64. Mass spectrum of (**4b**)$_3$ (retention time 11.67 min in Supplementary Figure 59b) from the LC-MS analysis of a DCL made from **4b** (2.0 mM). (**4b**)$_3$: m/z calculated: 775.25 $[M+2H]^{2+}$, 517.17 $[M+3H]^{3+}$; m/z observed: 775.17 $[M+2H]^{2+}$, 517.25 $[M+3H]^{3+}$.

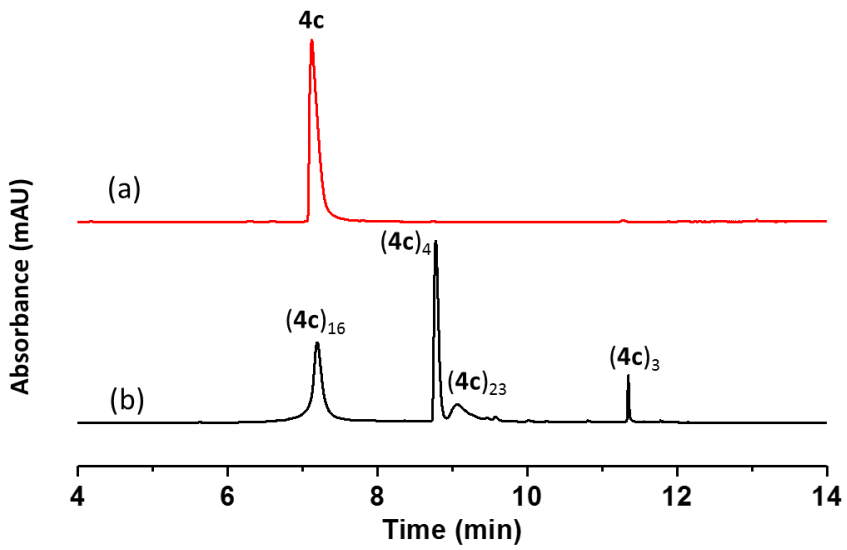

Supplementary Figure 65. UPLC analyses of a DCL made from **4c** (2.0 mM) in borate buffer (12.5 mM, pH = 8.0): (a) immediately after dissolving and (b) after stirring for 16 days.

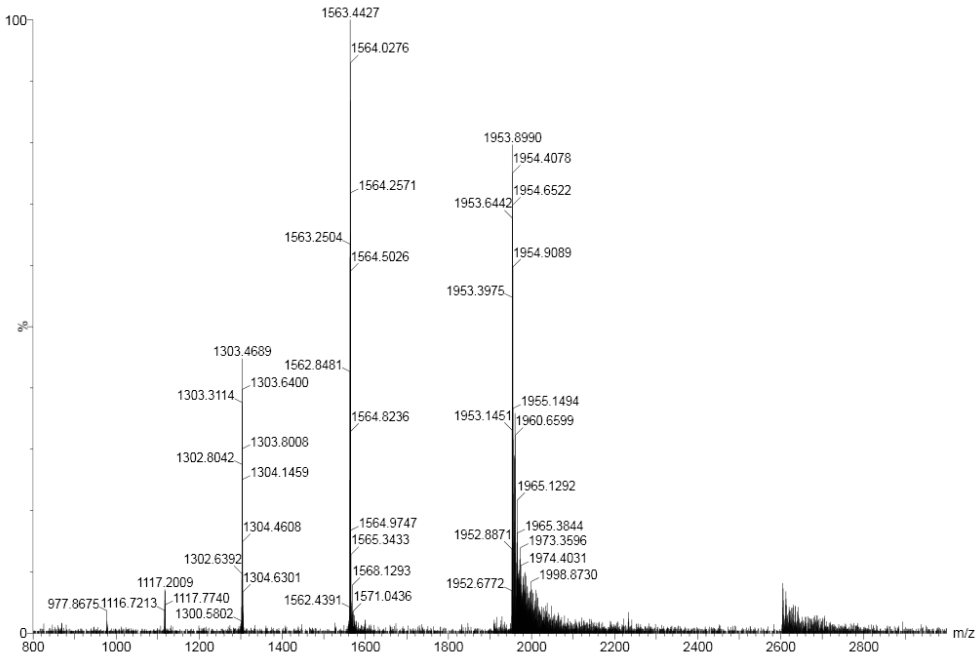

Supplementary Figure 66. Mass spectrum of $(\mathbf{4c})_{16}$ (retention time 7.21 min in Supplementary Figure 65b) from the LC-MS analysis of a DCL made from **4c** (2.0 mM). $(\mathbf{4c})_{16}$: m/z calculated: 1953.63 $[M+4H]^{4+}$, 1563.10 $[M+5H]^{5+}$, 1302.75 $[M+6H]^{6+}$; m/z observed: 1953.64 $[M+4H]^{4+}$, 1563.25 $[M+5H]^{5+}$, 1302.80 $[M+6H]^{6+}$.

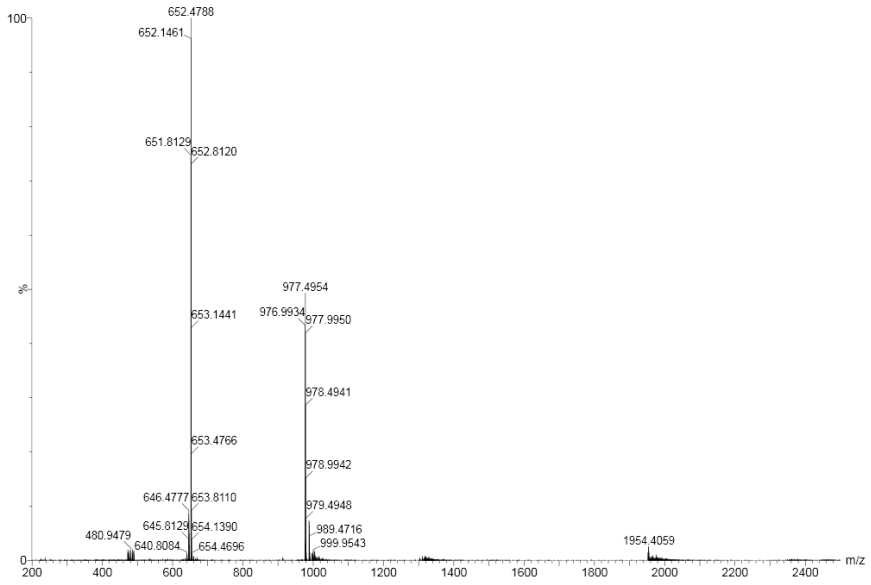

Supplementary Figure 67. Mass spectrum of (**4c**)$_4$ (retention time 8.76 min in Supplementary Figure 65b) from the LC-MS analysis of a DCL made from **4c** (2.0 mM). (**4c**)$_4$: m/z calculated: 977.32 $[M+2H]^{2+}$, 651.88 $[M+3H]^{3+}$; m/z observed: 977.50 $[M+2H]^{2+}$, 651.81 $[M+3H]^{3+}$.

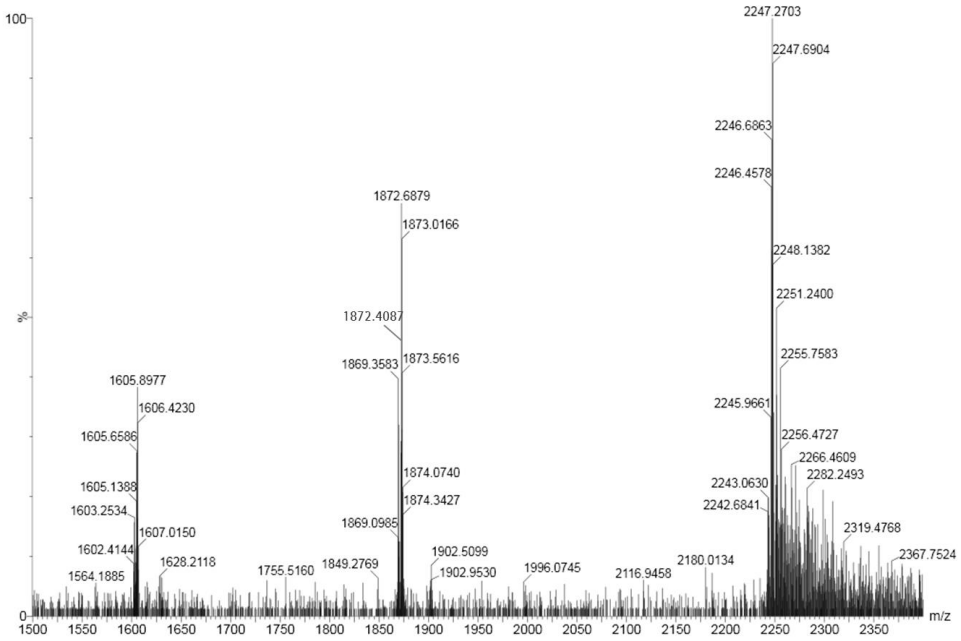

Supplementary Figure 68. Mass spectrum of $(\mathbf{4c})_{23}$ (retention time 9.10 min in Supplementary Figure 65b) from the LC-MS analysis of a DCL made from **4c** (2.0 mM). $(\mathbf{4c})_{23}$: m/z calculated: 2246.52 $[M+5H]^{5+}$, 1872.27 $[M+6H]^{6+}$, 1604.95 $[M+7H]^{7+}$; m/z observed: 2246.70 $[M+5H]^{5+}$, 1872.41 $[M+6H]^{6+}$, 1605.13 $[M+7H]^{7+}$.

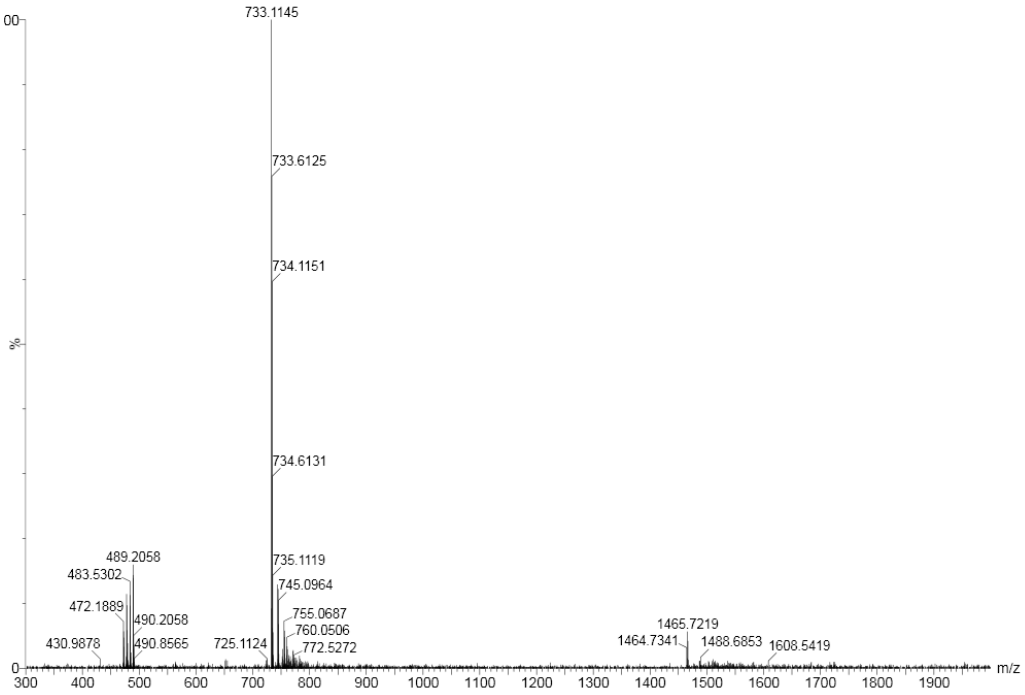

Supplementary Figure 69. Mass spectrum of (**4c**)$_3$ (retention time 11.34 min in Supplementary Figure 65b) from the LC-MS analysis of a DCL made from **4c** (2.0 mM). (**4c**)$_3$: m/z calculated: 733.24 $[M+2H]^{2+}$, 489.16 $[M+3H]^{3+}$; m/z observed: 733.11 $[M+2H]^{2+}$, 489.21 $[M+3H]^{3+}$.

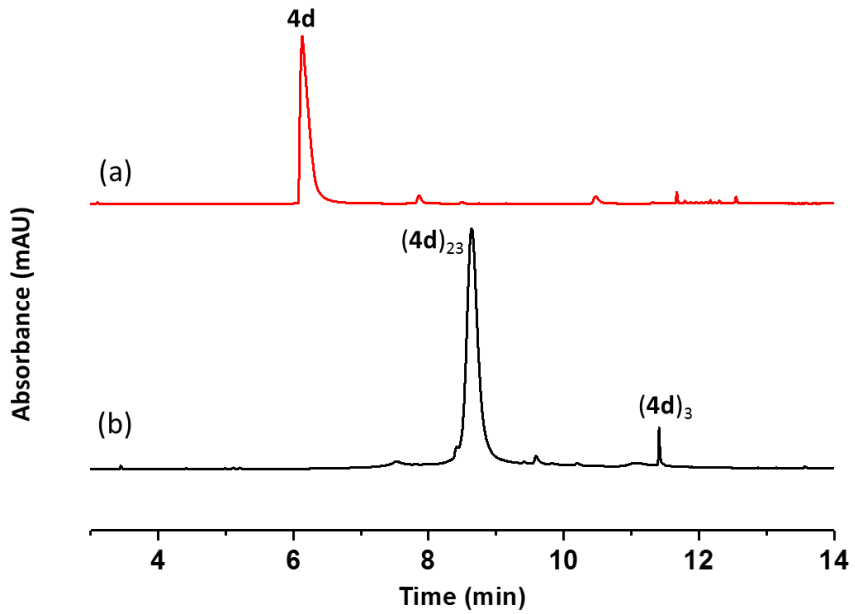

Supplementary Figure 70. UPLC analyses of a DCL made from **4d** (2.0 mM) in borate buffer (12.5 mM, pH = 8.0): (a) immediately after dissolving and (b) after stirring for 16 days.

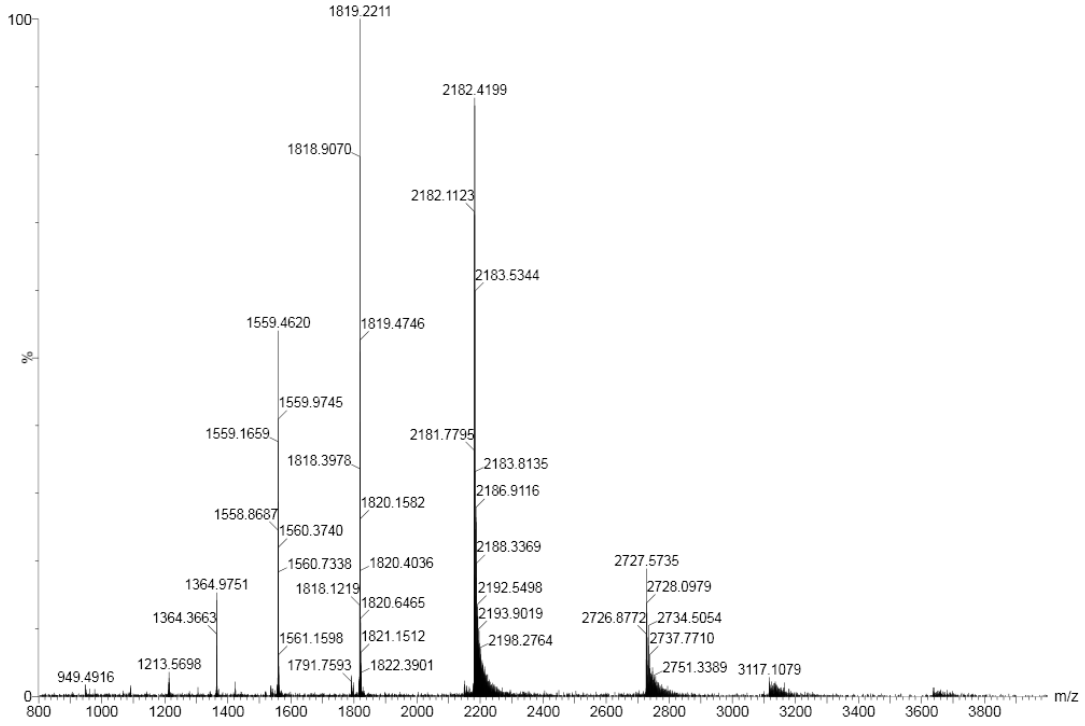

Supplementary Figure 71. Mass spectrum of $(\mathbf{4d})_{23}$ (retention time 8.62 min in Supplementary Figure 70b) from the LC-MS analysis of a DCL made from **4d** (2.0 mM). $(\mathbf{4d})_{23}$: m/z calculated: 2727.31 $[M+4H]^{4+}$, 2182.05 $[M+5H]^{5+}$, 1818.54 $[M+6H]^{6+}$, 1558.90 $[M+7H]^{7+}$, 1364.16 $[M+8H]^{8+}$; m/z observed: 2727.57 $[M+4H]^{4+}$, 2182.11 $[M+5H]^{5+}$, 1818.39 $[M+6H]^{6+}$, 1558.88 $[M+7H]^{7+}$, 1364.37 $[M+8H]^{8+}$.

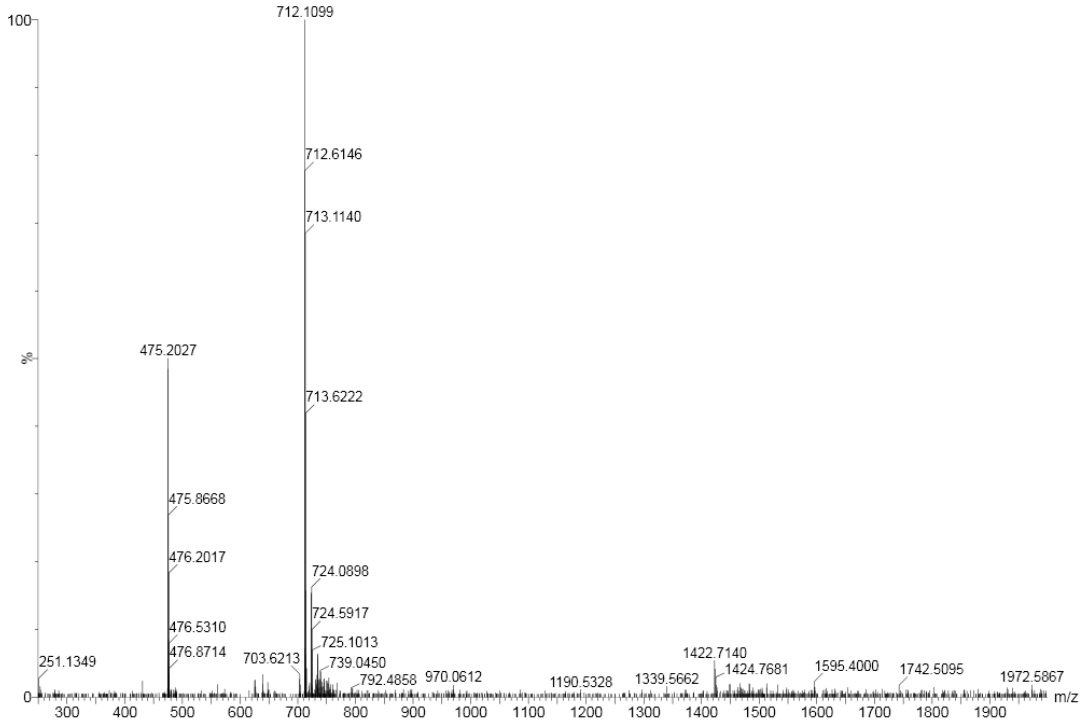

Supplementary Figure 72. Mass spectrum of $(\mathbf{4d})_3$ (retention time 11.34 min in Supplementary Figure 70b) from the LC-MS analysis of a DCL made from **4d** (2.0 mM). $(\mathbf{4d})_3$: m/z calculated: 712.22 $[M+2H]^{2+}$, 475.15 $[M+3H]^{3+}$; m/z observed: 712.11 $[M+2H]^{2+}$, 475.20 $[M+3H]^{3+}$.

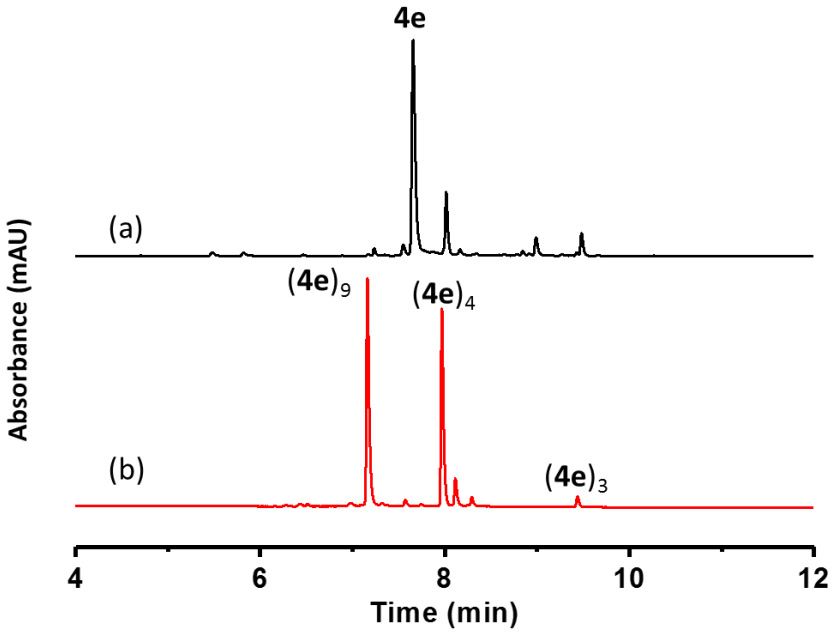

Supplementary Figure 73. UPLC analyses of the DCL made from **4e** (2.0 mM) in borate buffer (12.5 mM, pH = 8.0): (a) after stirring for 1 day and (b) after stirring for 16 days.

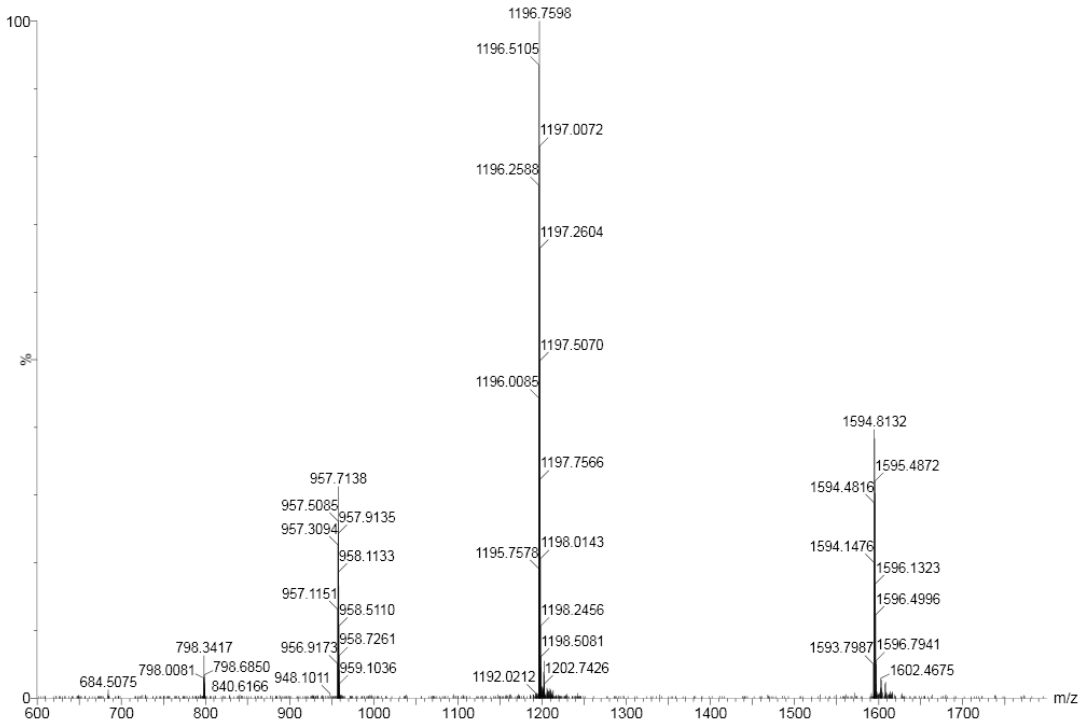

Supplementary Figure 74. Mass spectrum of $(\mathbf{4e})_9$ (retention time 7.15 min in Supplementary Figure 73b) from the LC-MS analysis of a DCL made from **4e** (2.0 mM). $(\mathbf{4e})_9$: m/z calculated: 1594.46 $[M+3H]^{3+}$, 1196.09 $[M+4H]^{4+}$, 957.08 $[M+5H]^{5+}$; m/z observed: 1594.48 $[M+3H]^{3+}$, 1196.26 $[M+4H]^{4+}$, 957.12 $[M+5H]^{5+}$.

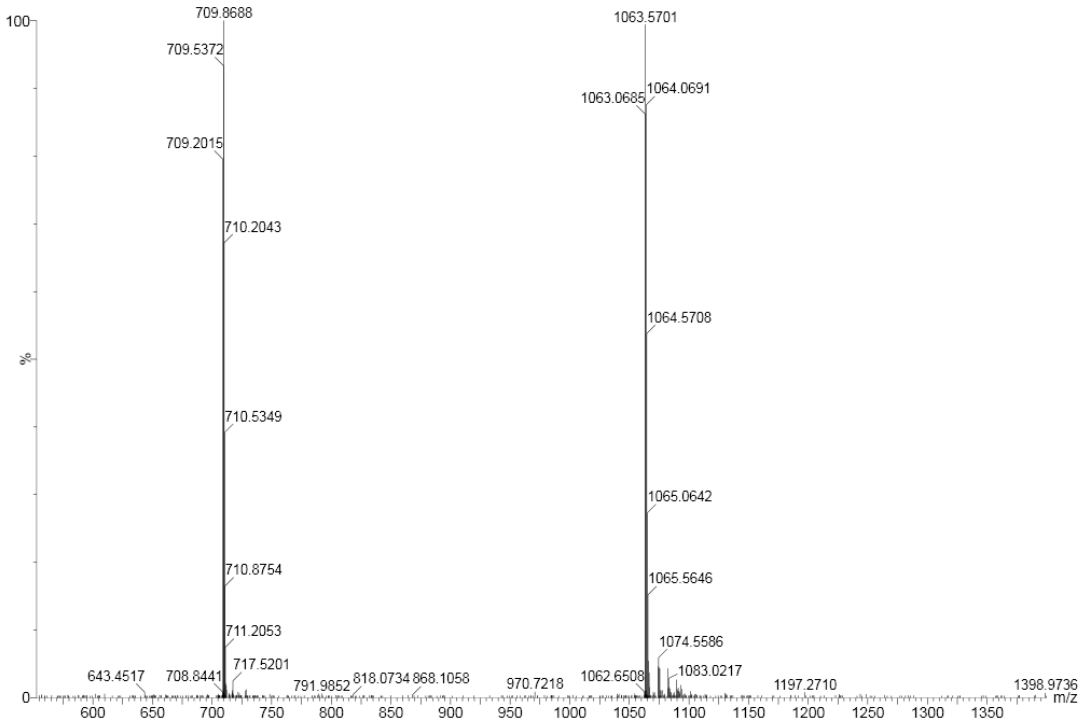

Supplementary Figure 75. Mass spectrum of (**4e**)$_4$ (retention time 7.97 min in Supplementary Figure 73b) from the LC-MS analysis of a DCL made from **4e** (2.0 mM). (**4e**)$_4$: m/z calculated: 1063.31 $[M+2H]^{2+}$, 709.21 $[M+3H]^{3+}$; m/z observed: 1063.57 $[M+2H]^{2+}$, 709.20 $[M+3H]^{3+}$.

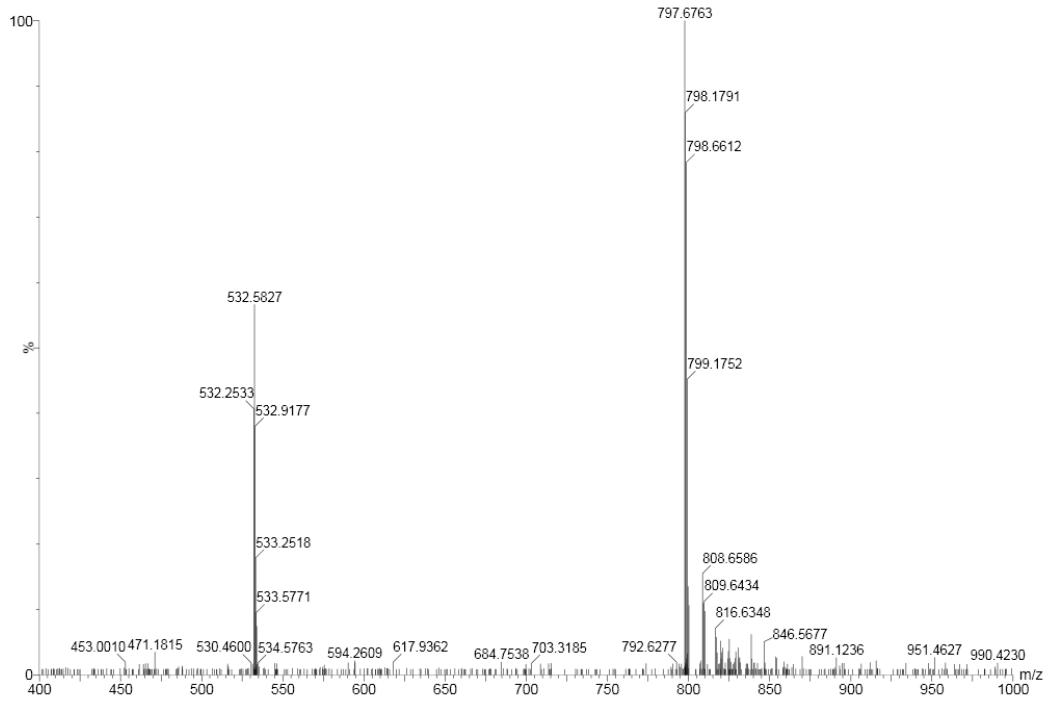

Supplementary Figure 76. Mass spectrum of $(\mathbf{4e})_3$ (retention time 9.45 min in Supplementary Figure 73b) from the LC-MS analysis of a DCL made from **4e** (2.0 mM). $(\mathbf{4e})_3$: m/z calculated: 979.73 $[M+2H]^{2+}$, 532.16 $[M+3H]^{3+}$; m/z observed: 979.68 $[M+2H]^{2+}$, 532.25 $[M+3H]^{3+}$.

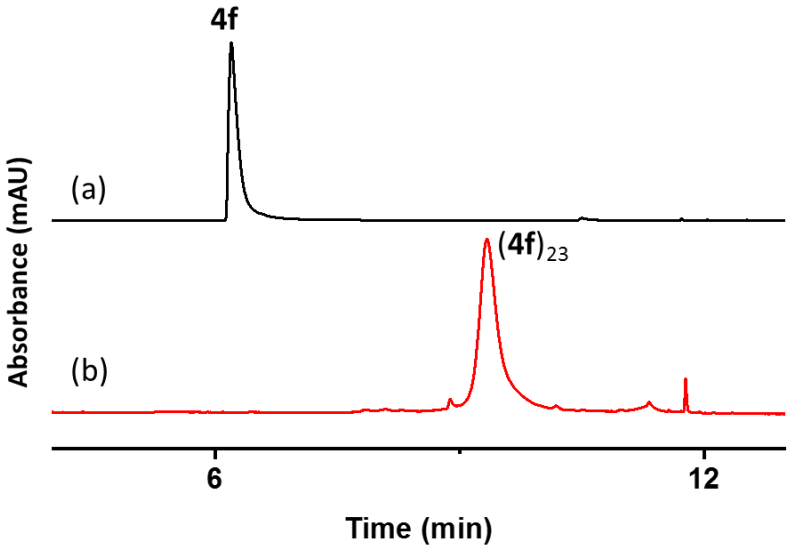

Supplementary Figure 77. UPLC analyses of the DCL made from **4f** (2.0 mM) in borate buffer (12.5 mM, pH = 8.0): (a) immediately after dissolving and (b) after stirring for 16 days.

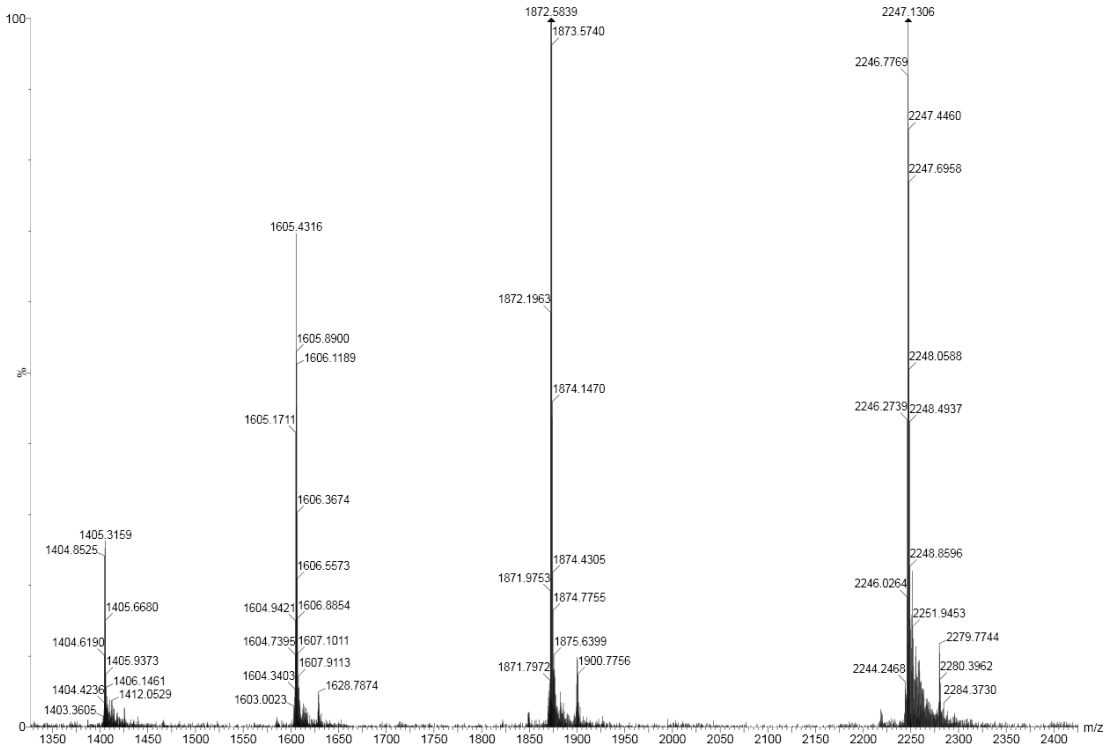

Supplementary Figure 78. Mass spectrum of $(\mathbf{4f})_{23}$ (retention time 9.34 min in Supplementary Figure 77b) from the LC-MS analysis of a DCL made from **4f** (2.0 mM). $(\mathbf{4f})_{23}$: m/z calculated: 2246.52 $[M+5H]^{5+}$, 1872.27 $[M+6H]^{6+}$, 1604.95 $[M+7H]^{7+}$, 1404.45 $[M+8H]^{8+}$; m/z observed: 2246.77 $[M+5H]^{5+}$, 1872.20 $[M+6H]^{6+}$, 1605.17 $[M+7H]^{7+}$, 1404.62 $[M+8H]^{8+}$.

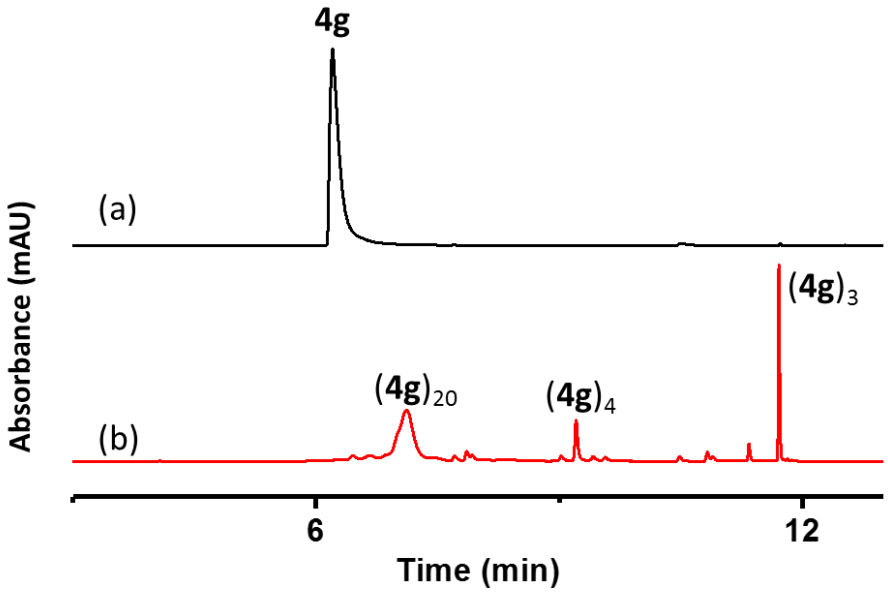

Supplementary Figure 79. UPLC analyses of the DCL made from **4g** (2.0 mM) in borate buffer (12.5 mM, pH = 8.0): (a) immediately after dissolving and (b) after stirring for 16 days.

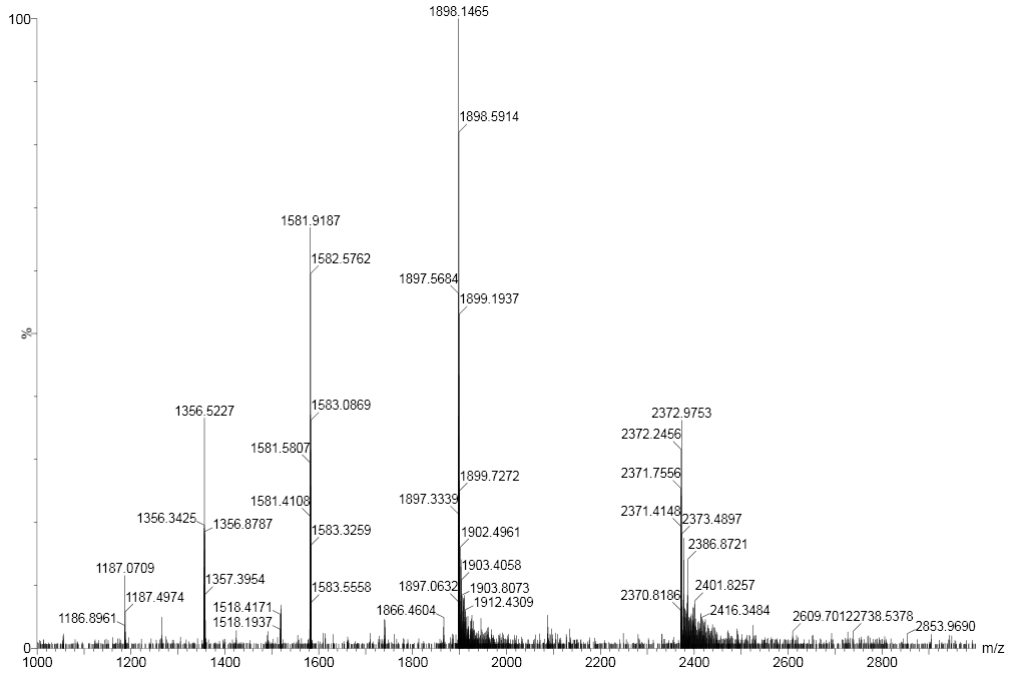

Supplementary Figure 80. Mass spectrum of $(\mathbf{4g})_{20}$ (retention time 7.1 min in Supplementary Figure 79b) from the LC-MS analysis of a DCL made from **4g** (2.0 mM). $(\mathbf{4g})_{20}$: m/z calculated: 2371.71 $[M+4H]^{4+}$, 1897.57 $[M+5H]^{5+}$, 1581.47 $[M+6H]^{6+}$; m/z observed: 2371.76 $[M+4H]^{4+}$, 1897.57 $[M+5H]^{5+}$, 1581.58 $[M+6H]^{6+}$.

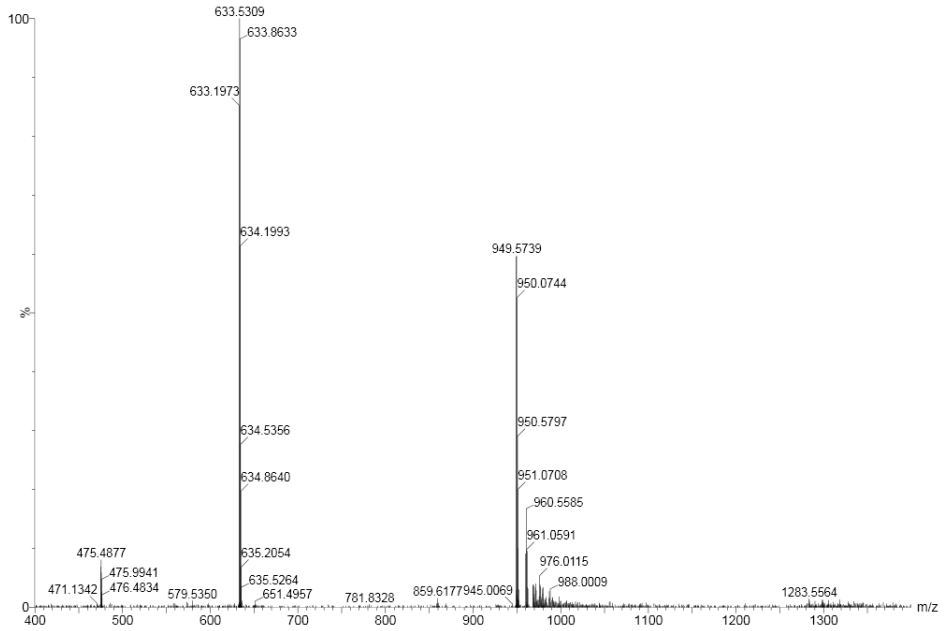

Supplementary Figure 81. Mass spectrum of $(\mathbf{4g})_4$ (retention time 9.2 min in Supplementary Figure 79b) from the LC-MS analysis of a DCL made from **4g** (2.0 mM). $(\mathbf{4g})_4$: m/z calculated: 949.29 $[M+2H]^{2+}$, 633.19 $[M+3H]^{3+}$; m/z observed: 949.57 $[M+2H]^{2+}$, 633.20 $[M+3H]^{3+}$.

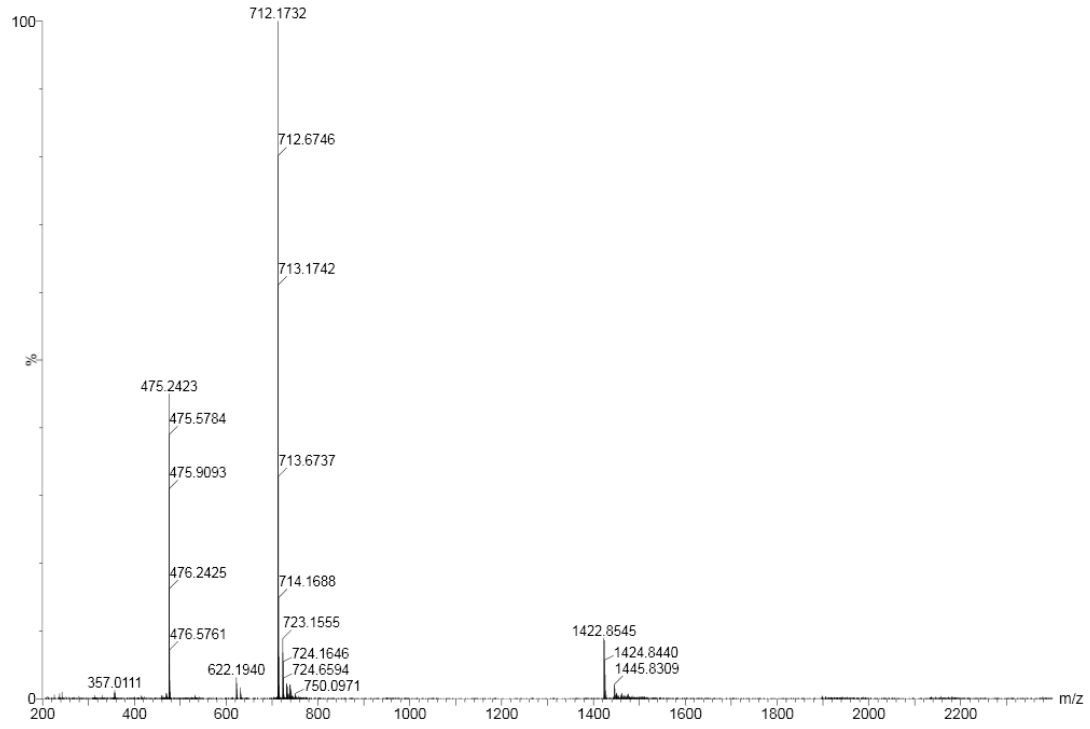

Supplementary Figure S82. Mass spectrum of (**4g**)$_3$ (retention time 11.7 min in Supplementary Figure 79b) from the LC-MS analysis of a DCL made from **4g** (2.0 mM). (**4g**)$_3$: m/z calculated: 712.22 $[M+2H]^{2+}$, 475.15 $[M+3H]^{3+}$; m/z observed: 712.17 $[M+2H]^{2+}$, 475.24 $[M+3H]^{3+}$.

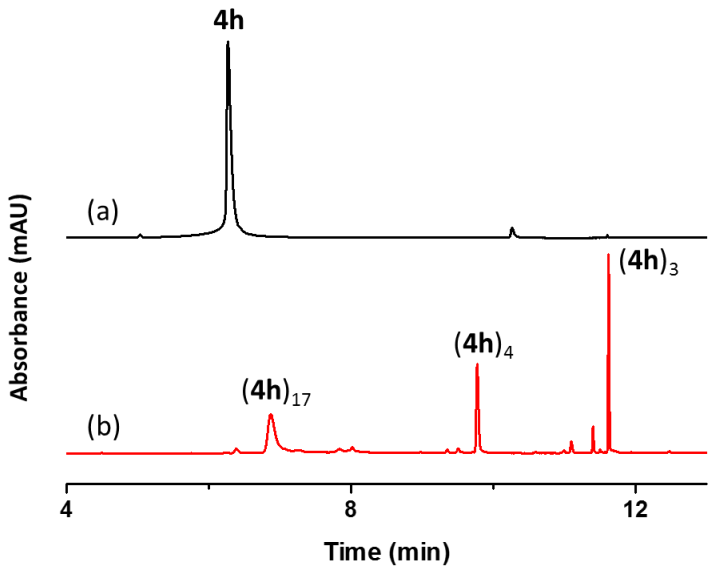

Supplementary Figure 83. UPLC analyses of the DCL made from **4h** (2.0 mM) in borate buffer (12.5 mM, pH = 8.0): (a) after stirring for 1 day and (b) after stirring for 16 days.

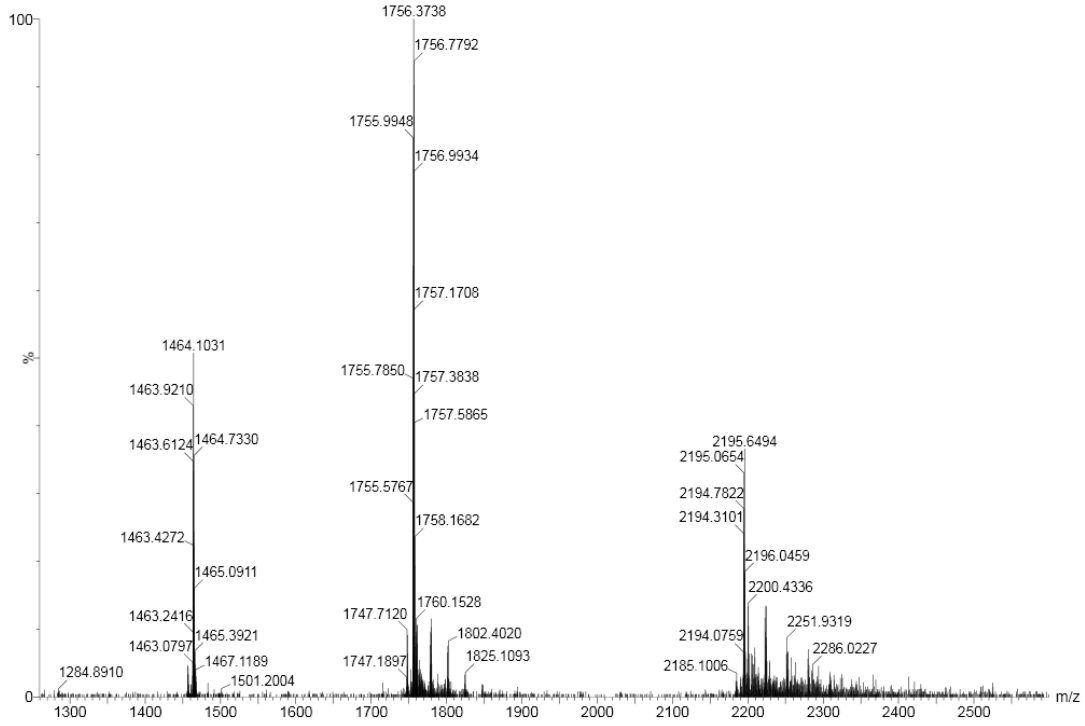

Supplementary Figure 84. Mass spectrum of $(\mathbf{4h})_{17}$ (retention time 6.86 min in Supplementary Figure 83b) from the LC-MS analysis of a DCL made from **4h** (2.0 mM). $(\mathbf{4h})_{17}$: m/z calculated: 2194.69 $[M+4H]^{4+}$, 1755.96 $[M+5H]^{5+}$, 1463.46 $[M+6H]^{6+}$; m/z observed: 2194.78 $[M+4H]^{4+}$, 1755.99 $[M+5H]^{5+}$, 1463.43 $[M+6H]^{6+}$.

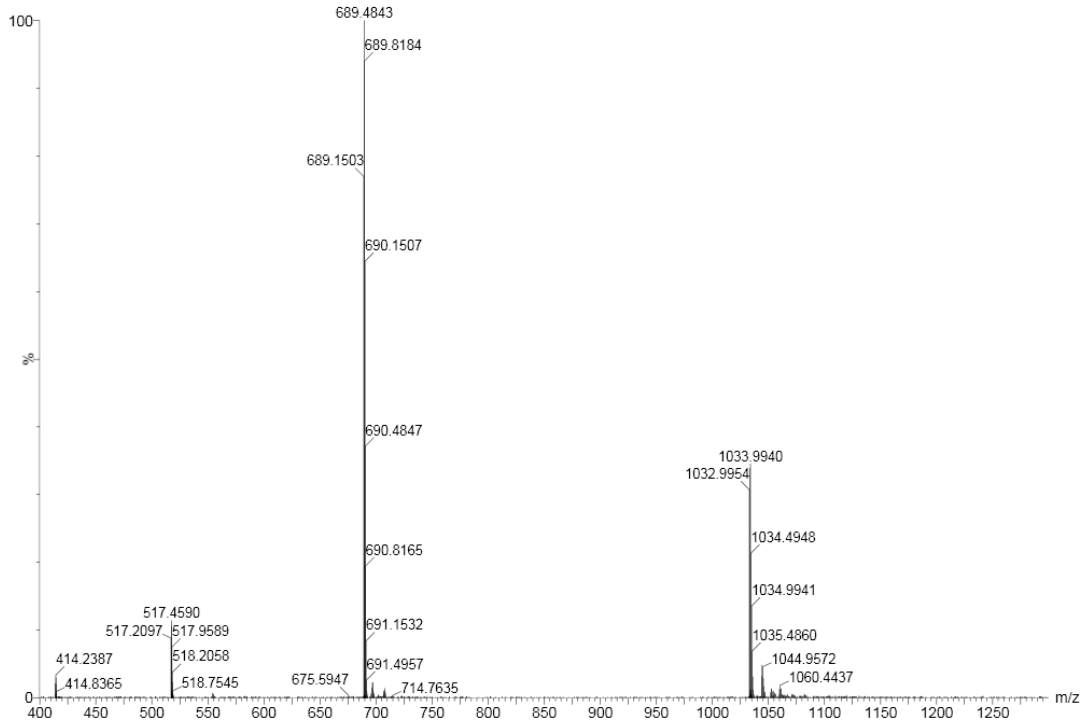

Supplementary Figure 85. Mass spectrum of (**4h**)$_4$ (retention time 9.77 min in Supplementary Figure 83b) from the LC-MS analysis of a DCL made from **4h** (2.0 mM). (**4h**)$_4$: m/z calculated: 1033.33 $[M+2H]^{2+}$, 689.22 $[M+3H]^{3+}$, 517.17 $[M+4H]^{4+}$; m/z observed: 1033.00 $[M+2H]^{2+}$, 689.15 $[M+3H]^{3+}$, 517.21 $[M+4H]^{4+}$.

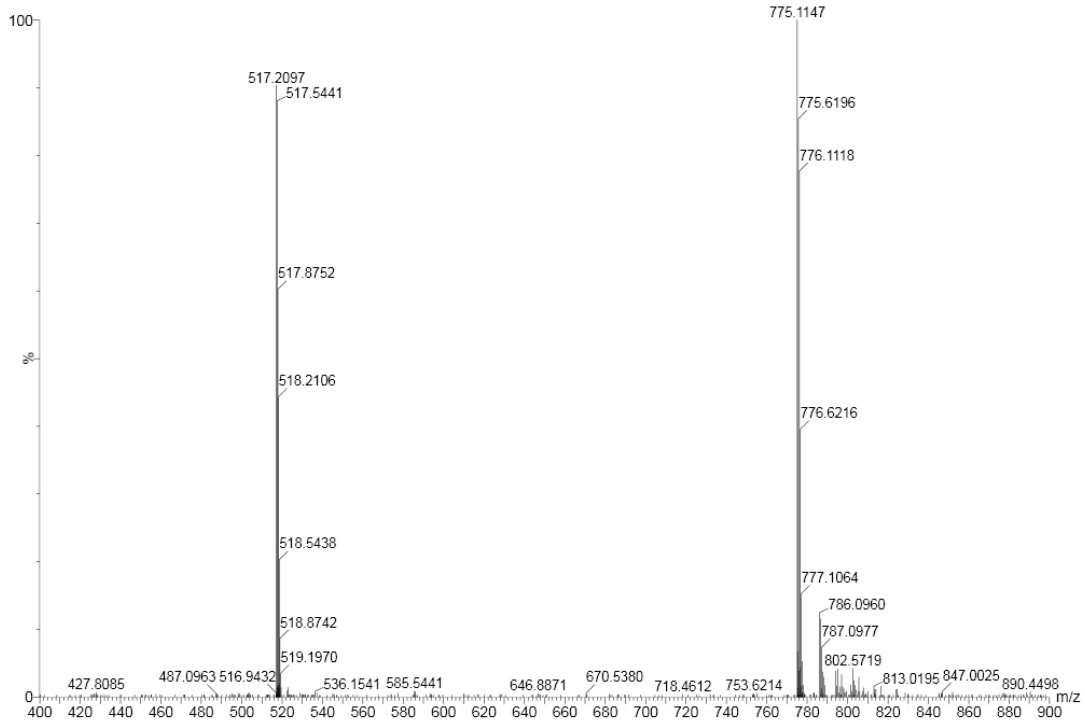

Supplementary Figure 86. Mass spectrum of (**4h**)$_3$ (retention time 11.67 min in Supplementary Figure 83b) from the LC-MS analysis of a DCL made from **4h** (2.0 mM). (**4h**)$_3$: m/z calculated: 775.25 $[M+2H]^{2+}$, 517.17 $[M+3H]^{3+}$; m/z observed: 775.11 $[M+2H]^{2+}$, 517.21 $[M+3H]^{3+}$.

3. Kinetic Profile and total UPLC peak areas for libraries prepared from building blocks 4a, 4b and 4d

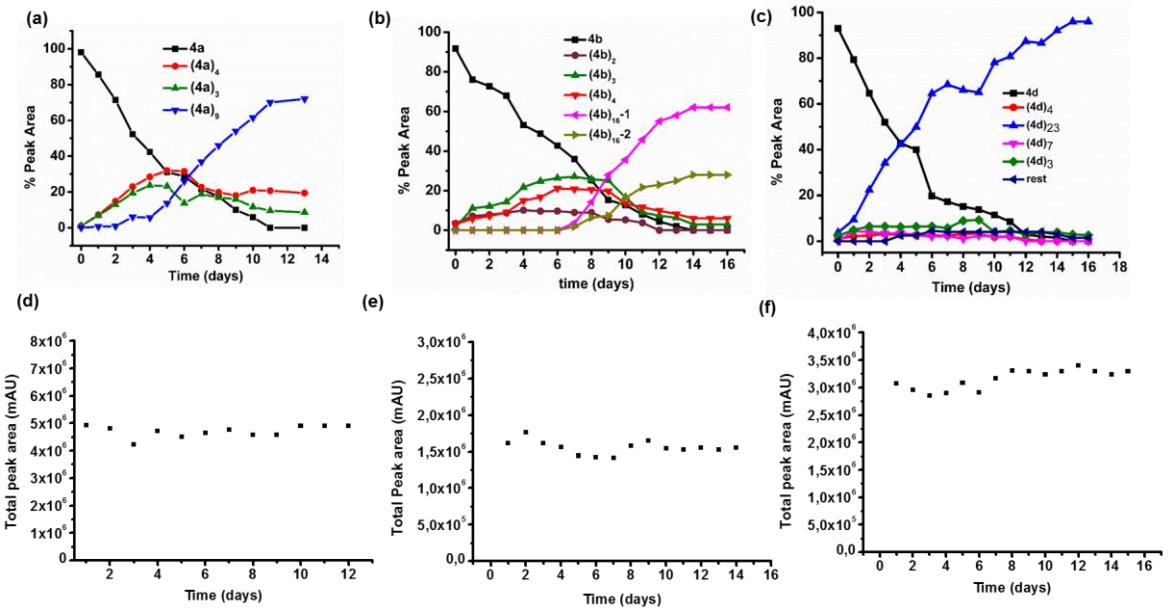

Supplementary Figure 87. Kinetic profiles of DCLs made by dissolving 2.0 mM building block in borate buffer (12.5 mM, pH = 8.0) for (a) **4a**, (b) **4b** and (c) **4d**. (d-f) Total UPLC peak areas for the libraries corresponding to the experiments in panels a-c, respectively.

4. NMR analysis of building blocks 4a, 4b and 4d and the foldamers made from these

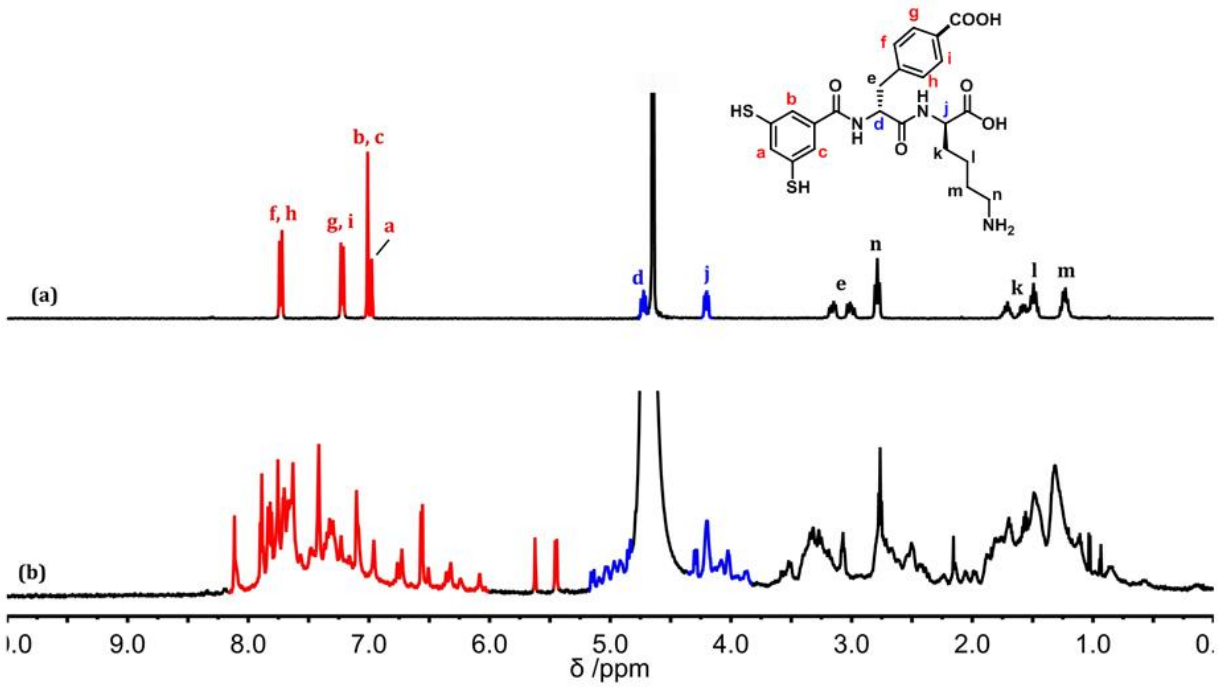

Supplementary Figure 88. ^{1}H-NMR spectra of (**a**) monomer **4a** and (**b**) foldamer (**4a**)$_9$ (20 days) in D_2O at room temperature (600 MHz).

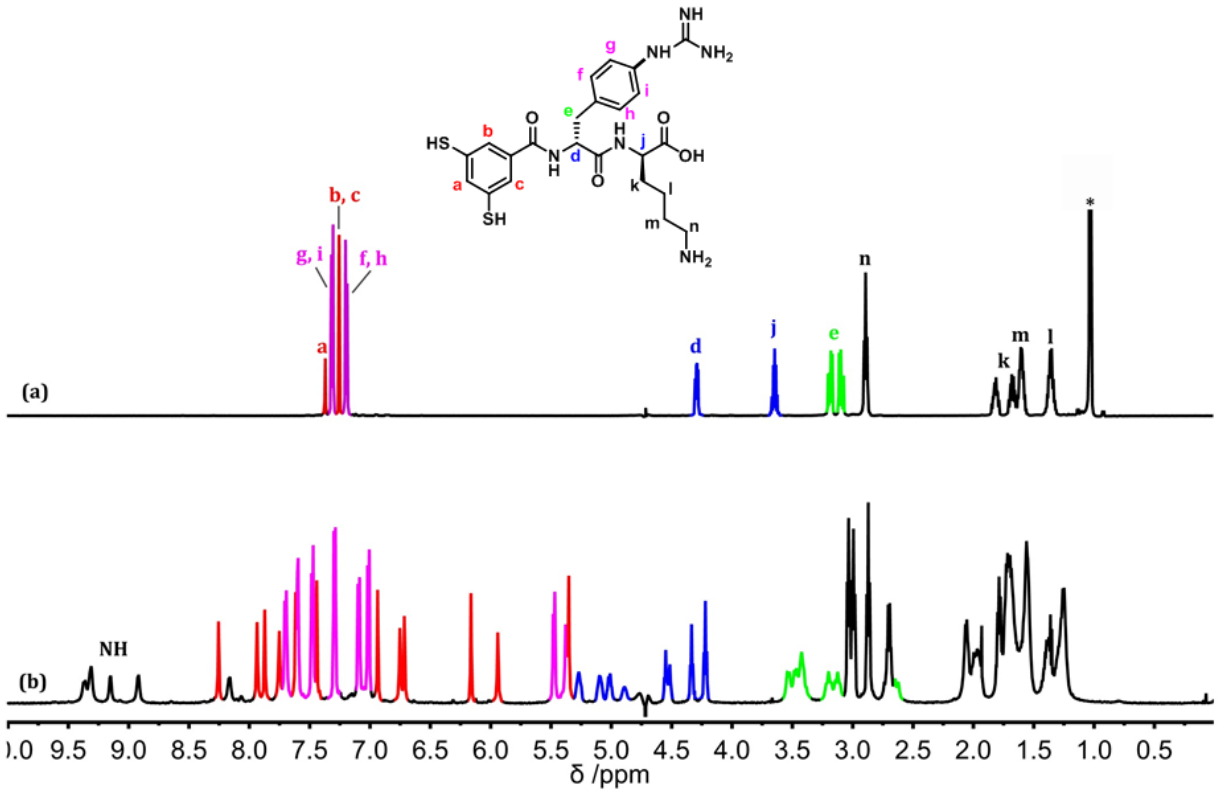

Supplementary Figure 89. ^{1}H-NMR spectra (water suppression) of (**a**) monomer **4b** and (**b**) early-eluting foldamer $(\mathbf{4b})_{16}$ in D_2O at room temperature (600 MH

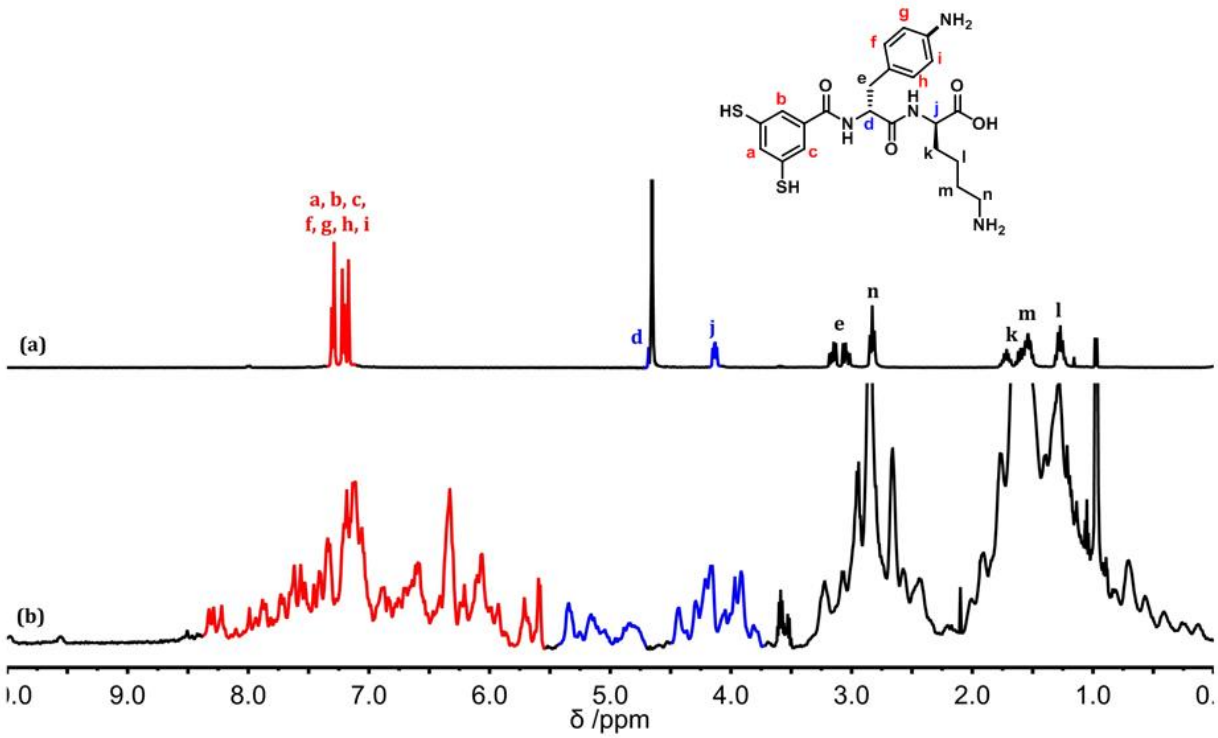

Supplementary Figure 90. ^{1}H-NMR spectra of (**a**) monomer **4d** and (b) foldamer (**4d**)$_{23}$ (23 days) in D_2O at room temperature (600 MHz).

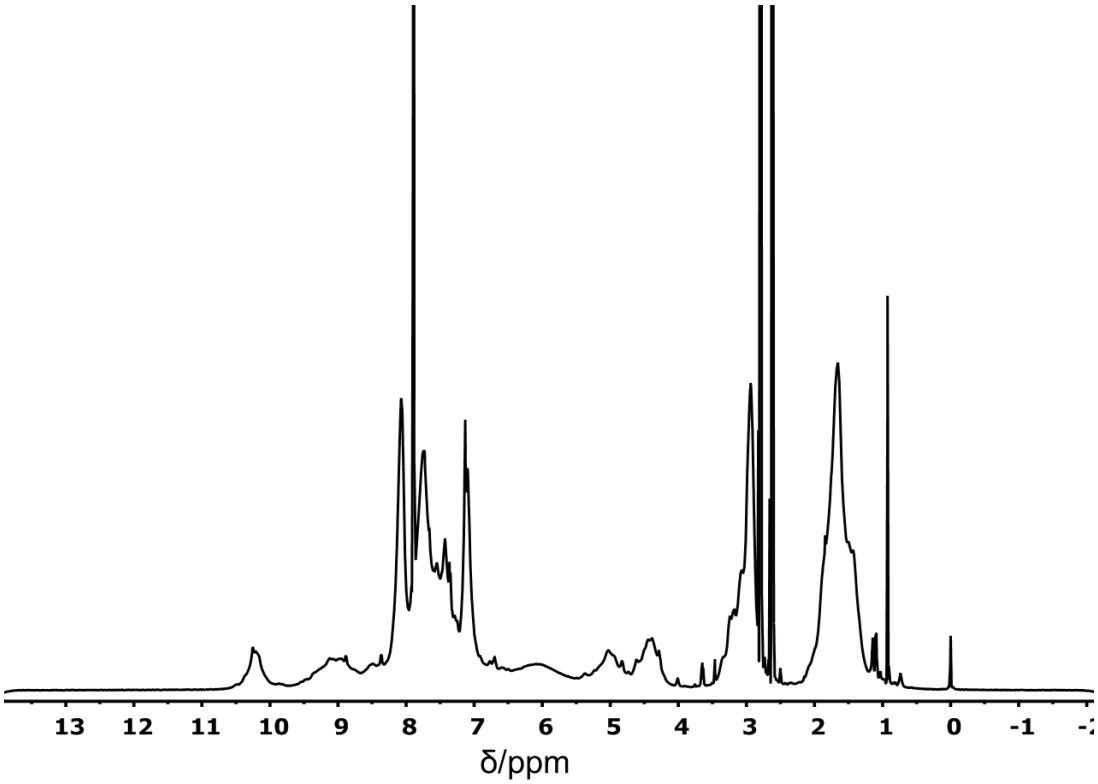

Supplementary Figure 91. ^{1}H-NMR spectra of the late-eluting foldamer (**4b**)$_{16}$ in DMF-d$_7$ at room temperature (600 MHz).

5. Temperature dependent NMR and CD for the foldamers made from building blocks 4a, 4b and 4d

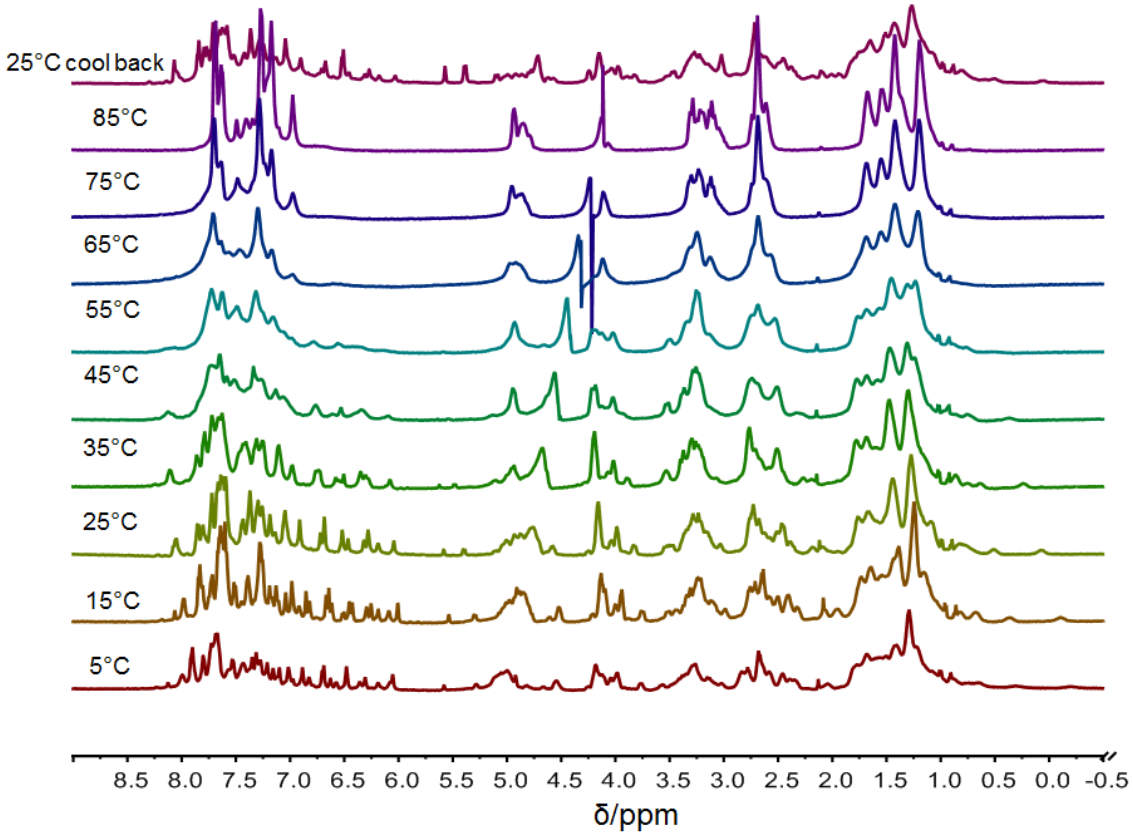

Supplementary Figure 92. Variable temperature ^{1}H-NMR (water suppression) spectra of foldamer (**4a**)$_9$ in D_2O from 5-85°C (500 MHz).

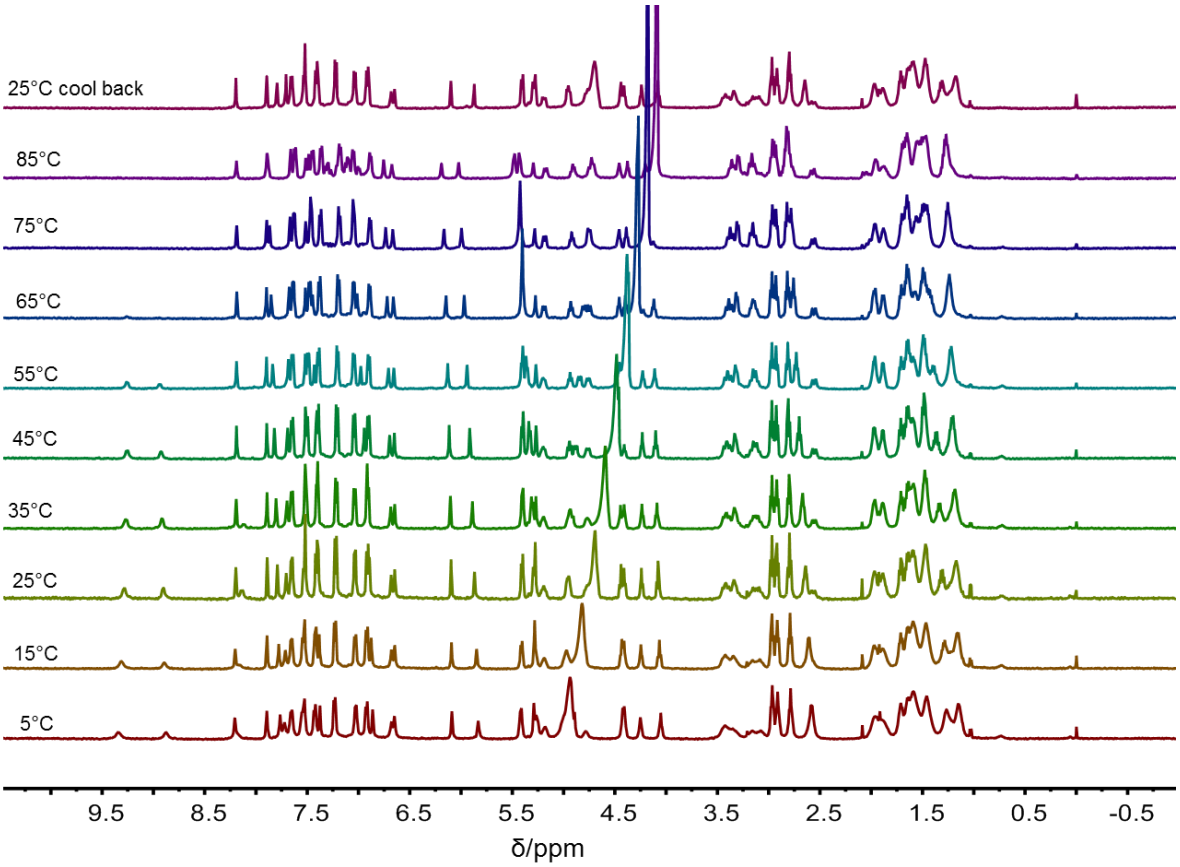

Supplementary Figure 93. Variable temperature ^{1}H-NMR (water suppression) spectra of foldamer (**4b**)$_{16}$ in D_2O from 5-85°C (500 MHz).

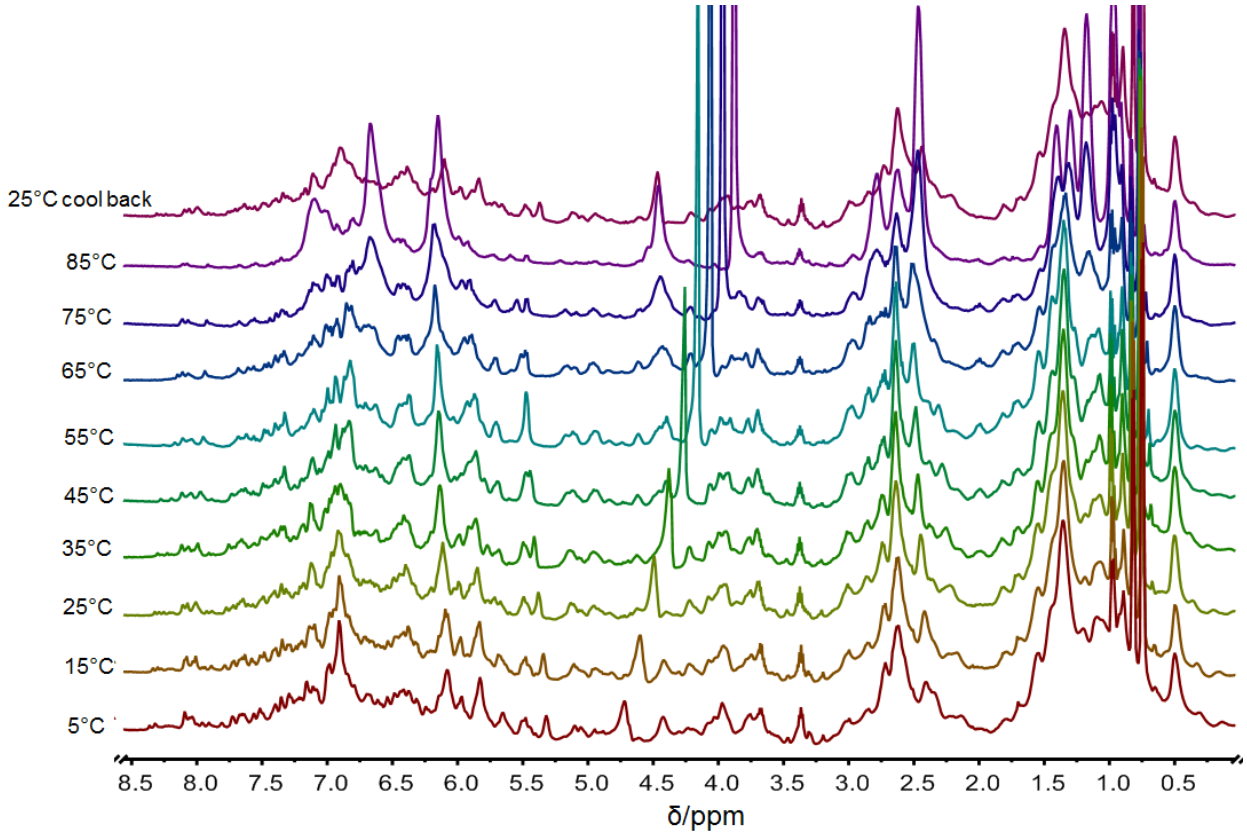

Supplementary Figure 94. Variable temperature ^{1}H-NMR (water suppression) spectra of foldamer **(4d)**$_{23}$ in D_2O from 5-85°C (500 MHz).

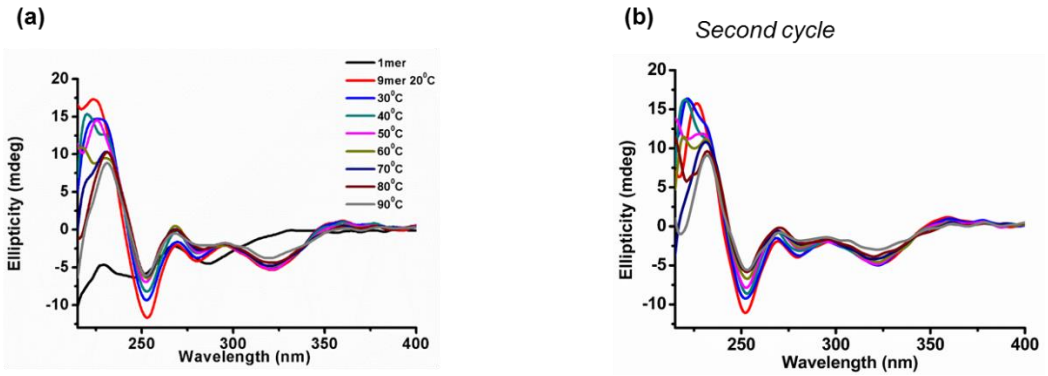

Supplementary Figure 95. Variable temperature CD spectra of foldamer (**4a**)$_9$ from 20-90°C. The spectrum of the monomer is shown for comparison.

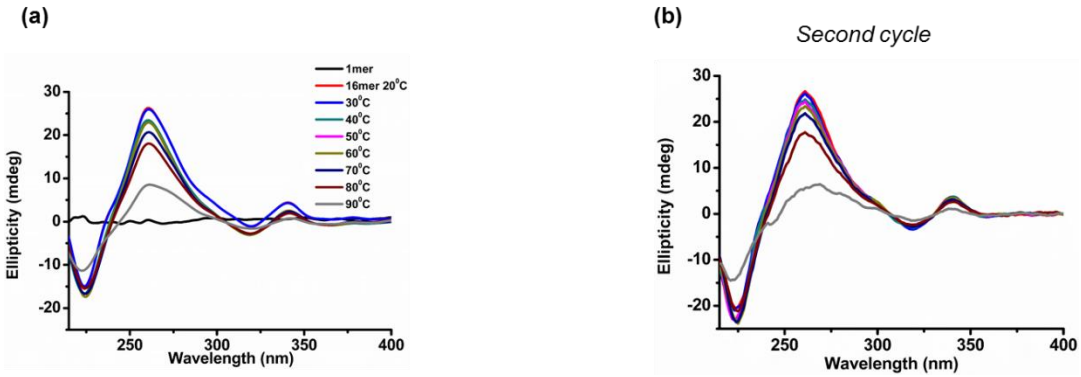

Supplementary Figure 96. Variable temperature CD spectra of foldamer $(\mathbf{4b})_{16}$ from 20-90°C. The spectrum of the monomer is shown for comparison.

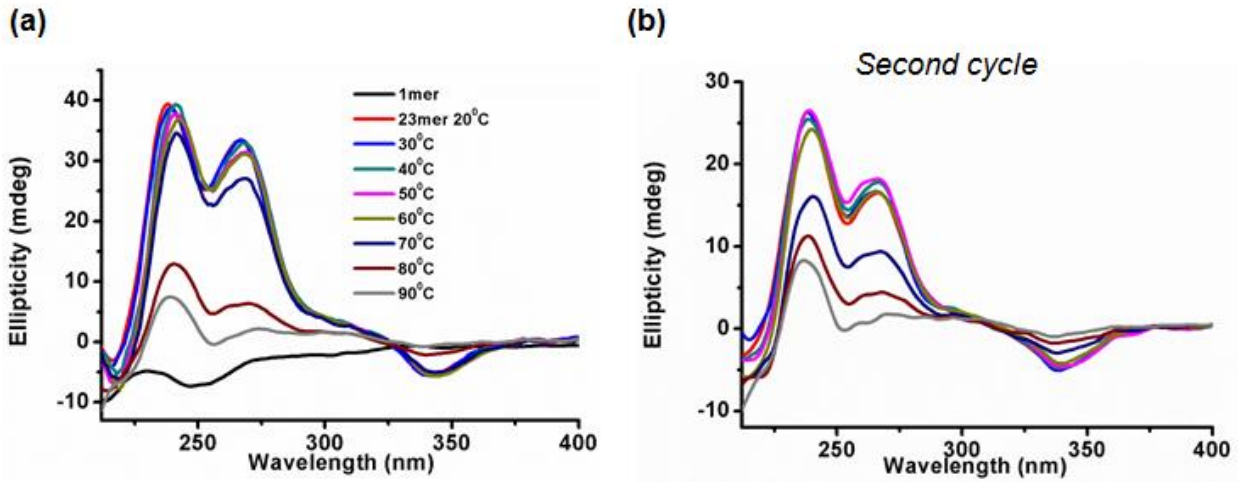

Supplementary Figure 97. Variable temperature CD spectra of foldamer (**4d**)$_{23}$ from 20-90°C. The spectrum of the monomer is shown for comparison.

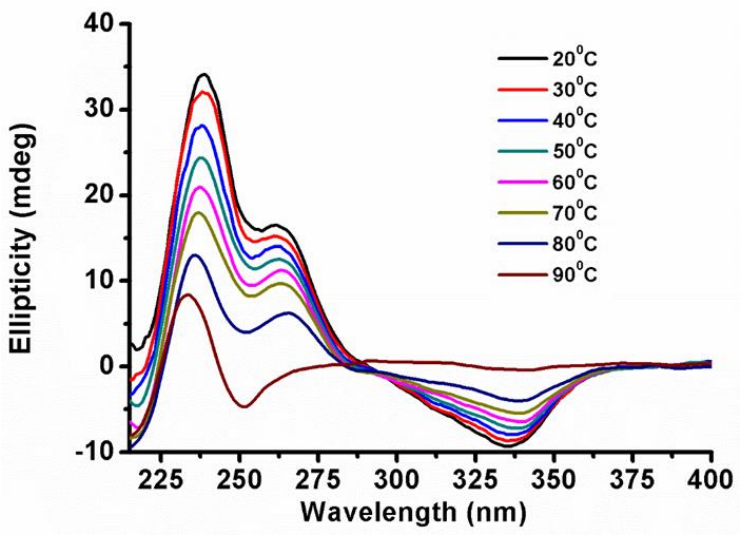

Supplementary Figure 98. Variable temperature CD spectra of foldamer (**4a**)$_{13}$ from 20-90°C.

6. Collision cross-sections for the macrocycles present in libraries prepared from building blocks 4a, 4b and 4d

Supplementary Table 1. Collision cross-sections $^{DT}\Omega_{He}$ (measured on the iMob and Synapt instruments utilizing a drift tube ion mobility cell and helium as a buffer gas) of the macrocycles with ring size *n* and charge state *z* present in the library prepared from building block **4a**.

n	*z*	$^{DT}\Omega_{He}$ (Å^2) iMob	$^{DT}\Omega_{He}$ (Å^2) Synapt
1	1		156
2	1		223
2	2		219
3	1		284
3	2	281	285
4	1		346
4	2	340 345	
4	3	374	
5	2		409
6	2		462
6	4	477	
9	3		593
9	4	582	600
9	5	604	

Supplementary Table 2. Collision cross-sections $^{DT}\Omega_{He}$ (measured on the iMob and Synapt instruments utilizing a drift tube ion mobility cell and helium as a buffer gas) of the macrocycles with ring size *n* and charge state *z* present in the library prepared from building block **4d**. The oligomers with ring sizes *n* = 12, 21 and 22 were not observed in the UPLC-MS analysis, but were detected in IM-MS experiments. This difference most likely reflects the difference in sensitivity of the different MS instruments used for these analyses. Data points for ring sizes *n* = 12, 21 and 22 were not included in Fig. 2 of the main text.

n	***z***	$^{DT}\Omega_{He}$ (Å^2) **iMob**	$^{DT}\Omega_{He}$ (Å^2) **Synapt**
1	1	149	
2	1	190	
2	2	224	
3	2	296	283
3	3	309 315	
4	2	314 332	339
4	3	348 372 380 394	368
5	3	398 413 427	396
5	4	466	
6	4	563	
12	6	879 904	
16	5		870
16	6		866
21	5		1030
22	6		1072
22	7		1023
23	5		1082
23	6	1083	1117
23	7	1094	1098
23	8	1109	1052

Supplementary Table 3. Collision cross-sections $^{DT}\Omega_{He}$ (measured on the iMob and Synapt instruments utilizing a drift tube ion mobility cell and helium as a buffer gas) of the macrocycles with ring size *n* and charge state *z* present in the library prepared from building block **4b**. The multiple conformers of the macrocycles with *n* = 16 represent (partially) unfolded species which is consistent with the presence of two peaks for the 16mer in the UPLC chromatogram. The more compact species correspond to the folded conformation, which also applies to the 16mers with more than six charges. Unfolding most likely results from intramolecular Coulomb repulsion, particularly at high charge density. Therefore, only the CCS value of the 16-mer of charge state 5^+ was included in Fig. 2 of the main text.

n	***z***	$^{DT}\Omega_{He}$ (Å^2) **iMob**	$^{DT}\Omega_{He}$ (Å^2) **Synapt**
1	2		161
2	1	191	
2	2	234	
3	2	297	288
3	3	326	
3	4		399
4	2	365	
4	3	338 368 396	392
4	4		455
4	5		469
5	3	429	447
5	4	453 481 508	493
6	3	422	
6	4	551	516
7	4		565
7	5		630
16	5		915
16	6	985	957 995
16	7	1026 1073	968 1057
16	8	1140	1174 1132
16	9	1208	1203

7. X-ray crystallography of $(4b)_{16}$ and $(4d)_{23}$

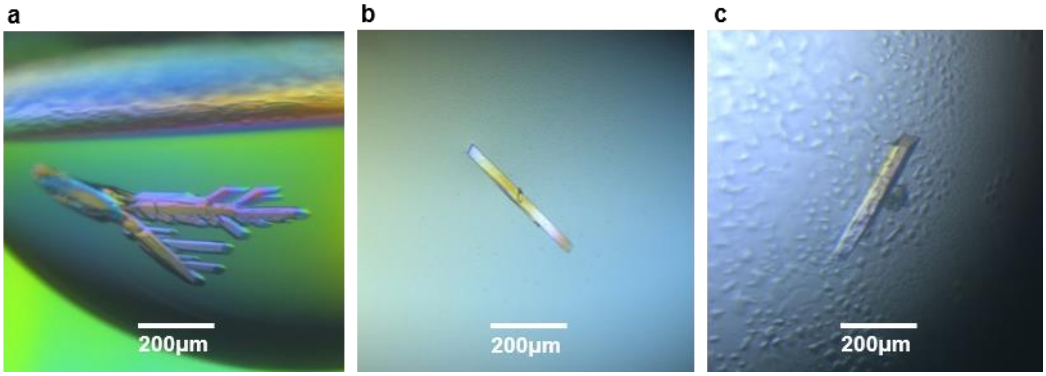

Supplementary Figure 99. Crystals of: **a** L-(**4b**)$_{16}$, and **b**, **c** L/D-(**4d**)$_{23}$ observed under crossed polarized microscopy. X-ray diffraction revealed space groups: (A) $P6_2$, (B) $P1$ and (C) $P2_1/n$ respectively. Structural elucidation at atomic resolution using ab initio methods was successful from (a) and (b) while (c) diffracted up to 1.6 Å.

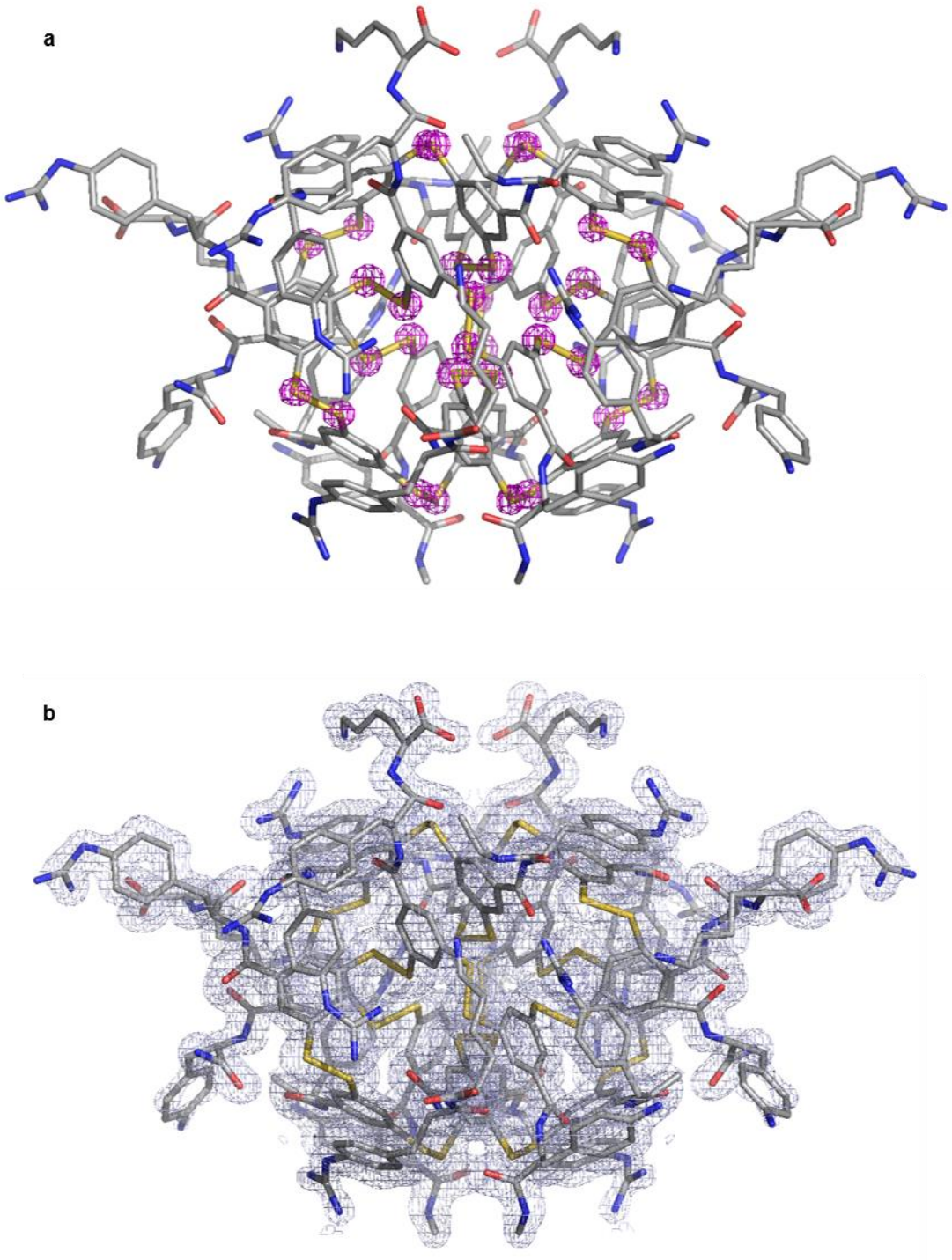

Supplementary Figure 100. Sigma weighted $2F_o$-F_c electron density map superimposed onto L-(**4b**)$_{16}$: **a** magenta mesh, contoured at 7σ level shows the position of sulfur atoms and **b** Grey mesh, contoured at 1σ level shows the macrocycle shape.

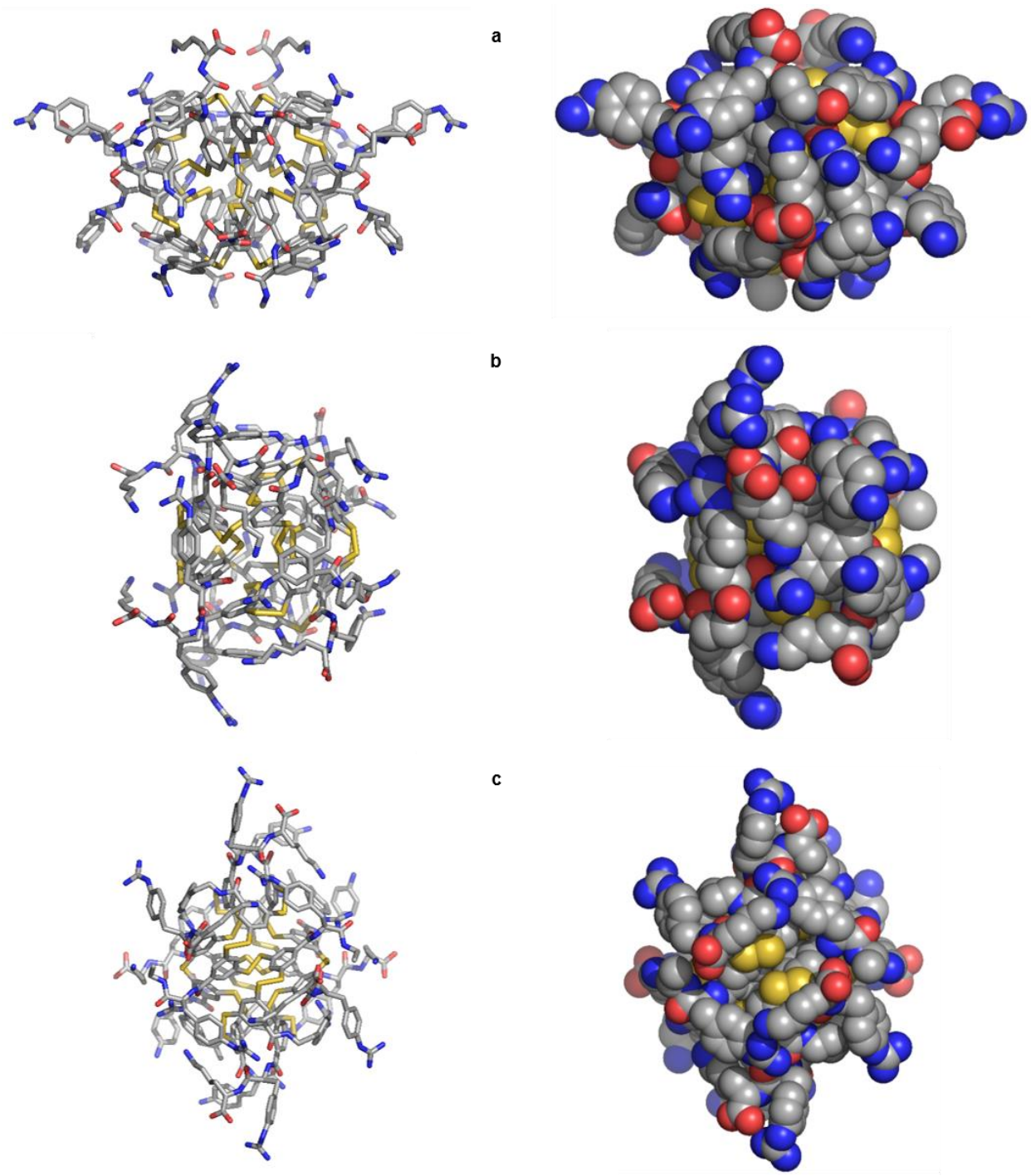

Supplementary Figure 101. Crystal structure of L-(**4b**)$_{16}$: view along the crystallographic: **a** *a*-axis; **b** *b*-axis; and **c** *c*-axis in stick and CPK representations.

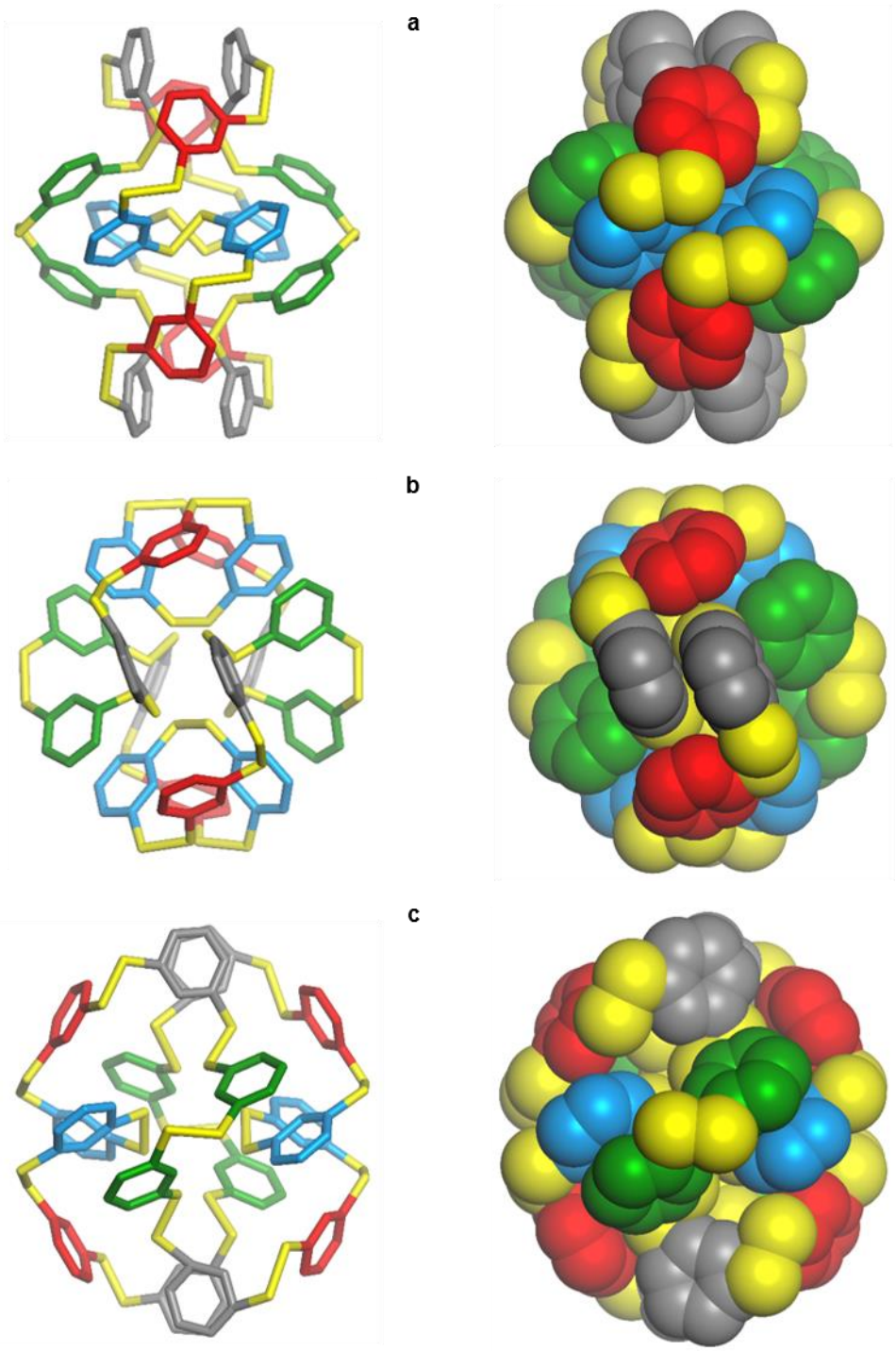

Supplementary Figure 102. Illustration of the hydrophobic core of L-(**4b**)$_{16}$, viewed across three (pseudo)-C_2 axes, in stick and CPK representations: **a** one crystallographic axis; **b**, **c** two non-crystallographic pseudo-C_2 axes. There are four equivalent phenyl rings colored grey, red, blue and green.

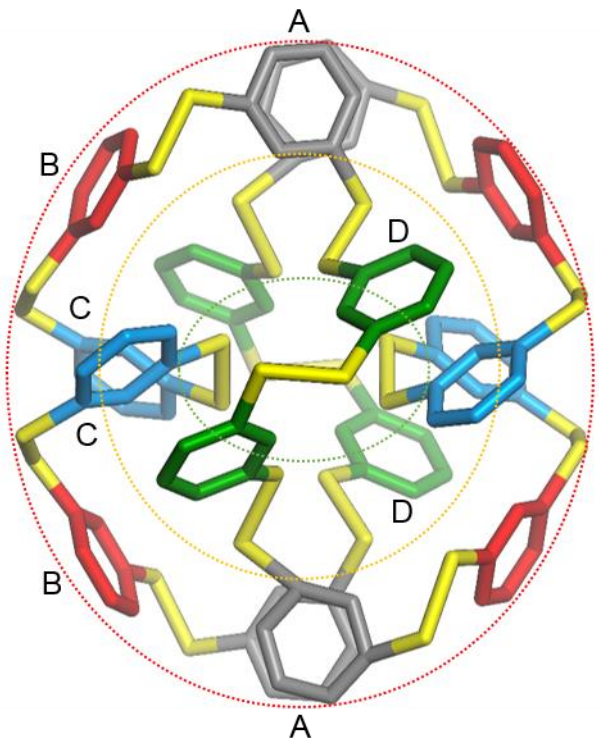

Supplementary Figure 103. Arrangement of equivalent phenyl rings A (grey), B (red), C (blue) and D (green) in the hydrophobic core of L-(**4b**)$_{16}$. The arrangement of sequence is complex [ABCCBADD]$_2$. Green dots show four (2 CC and 2 DD) inner core disulfide bridges. Orange dots show four (all AD) outer core disulfide bridges. Red dots show eight (4 AB and 4 BC) peripheral disulfide bridges.

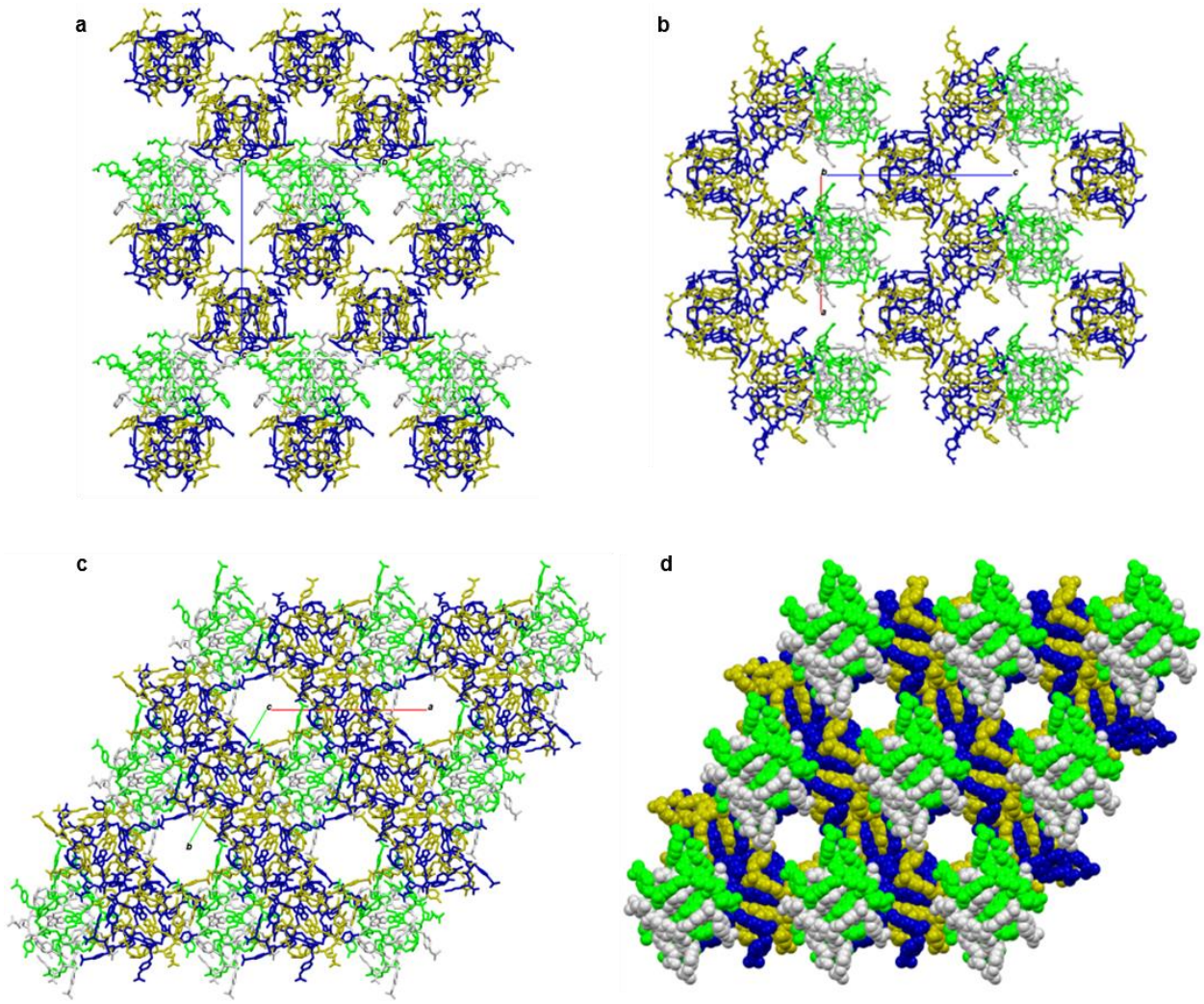

Supplementary Figure 104. Crystal arrangement of L-(**4b**)$_{16}$: views along the crystallographic: **a** *a*-axis; **b** *b*-axis; and **c** *c*-axis. The clusters are colored by symmetry operations. (d) Linear solvent channel-view down the *c*-axis.

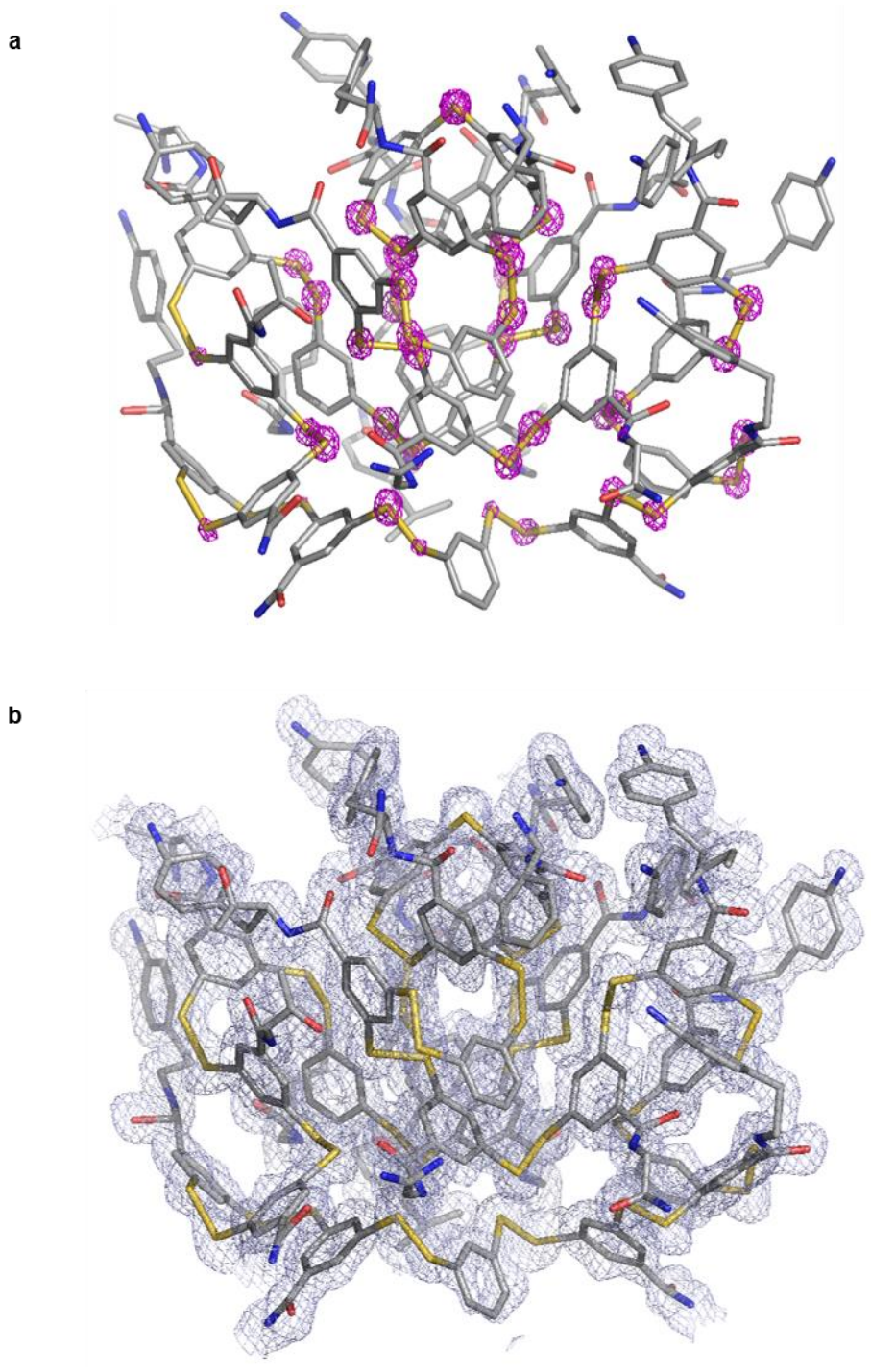

Supplementary Figure 105. Sigma weighted $2F_o$-F_c electron density map superimposed on one macrocycle from the crystal structure of L/D-(**4d**)$_{23}$: **a** magenta mesh, contoured at 7σ level shows the position of sulfur atoms and **b** grey mesh, contoured at 1σ level shows the overall macrocycle shape.

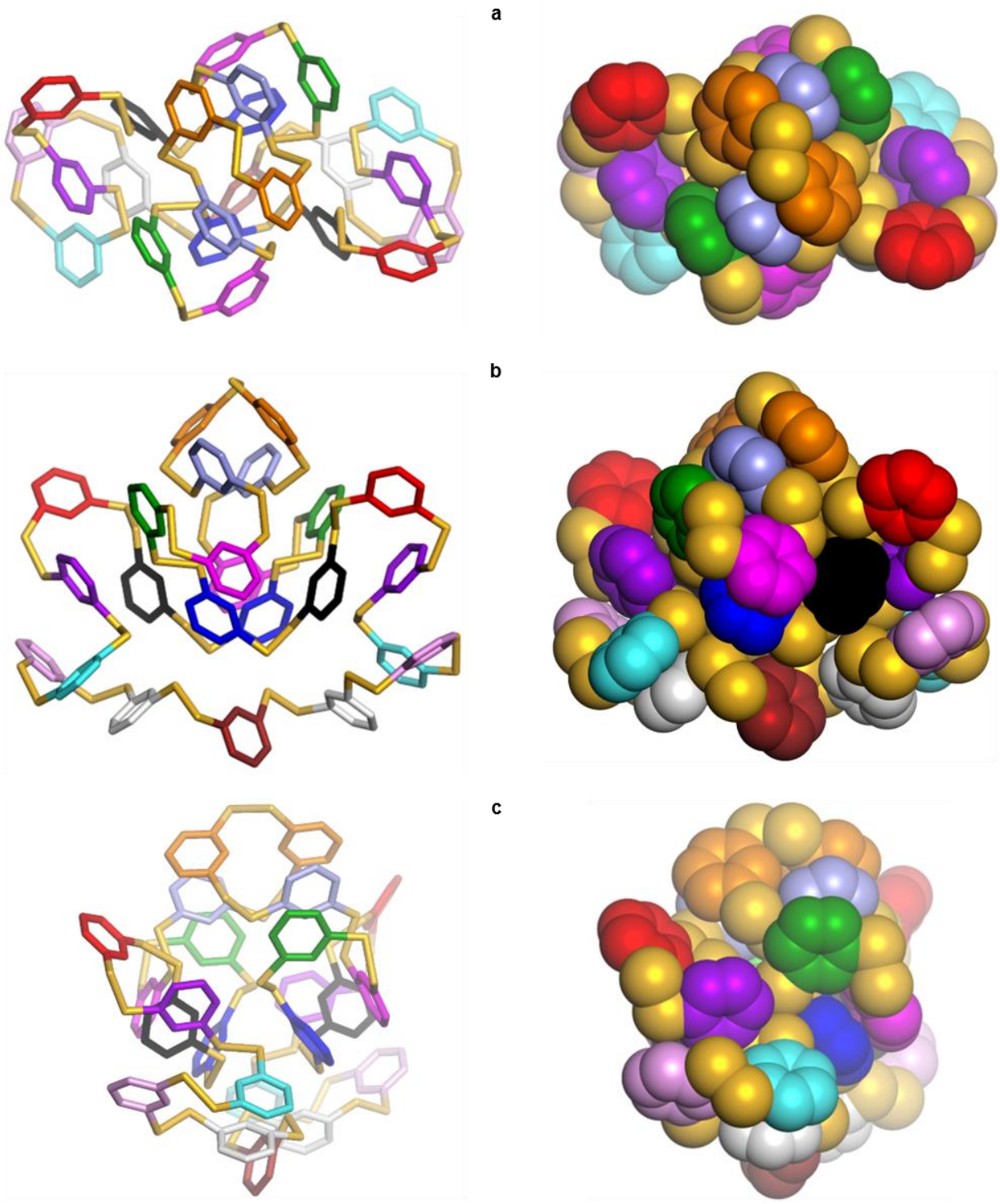

Supplementary Figure 106. Illustration of the hydrophobic core of L-(**4d**)$_{23}$ viewed along three perpendicular axes in stick and CPK representations (**a**, **b**, **c**). Phenyl rings equivalent with respect to the pseudo C_2 axis are color-coded except the five rings that constitute the bottom loop which are all shown in grey.

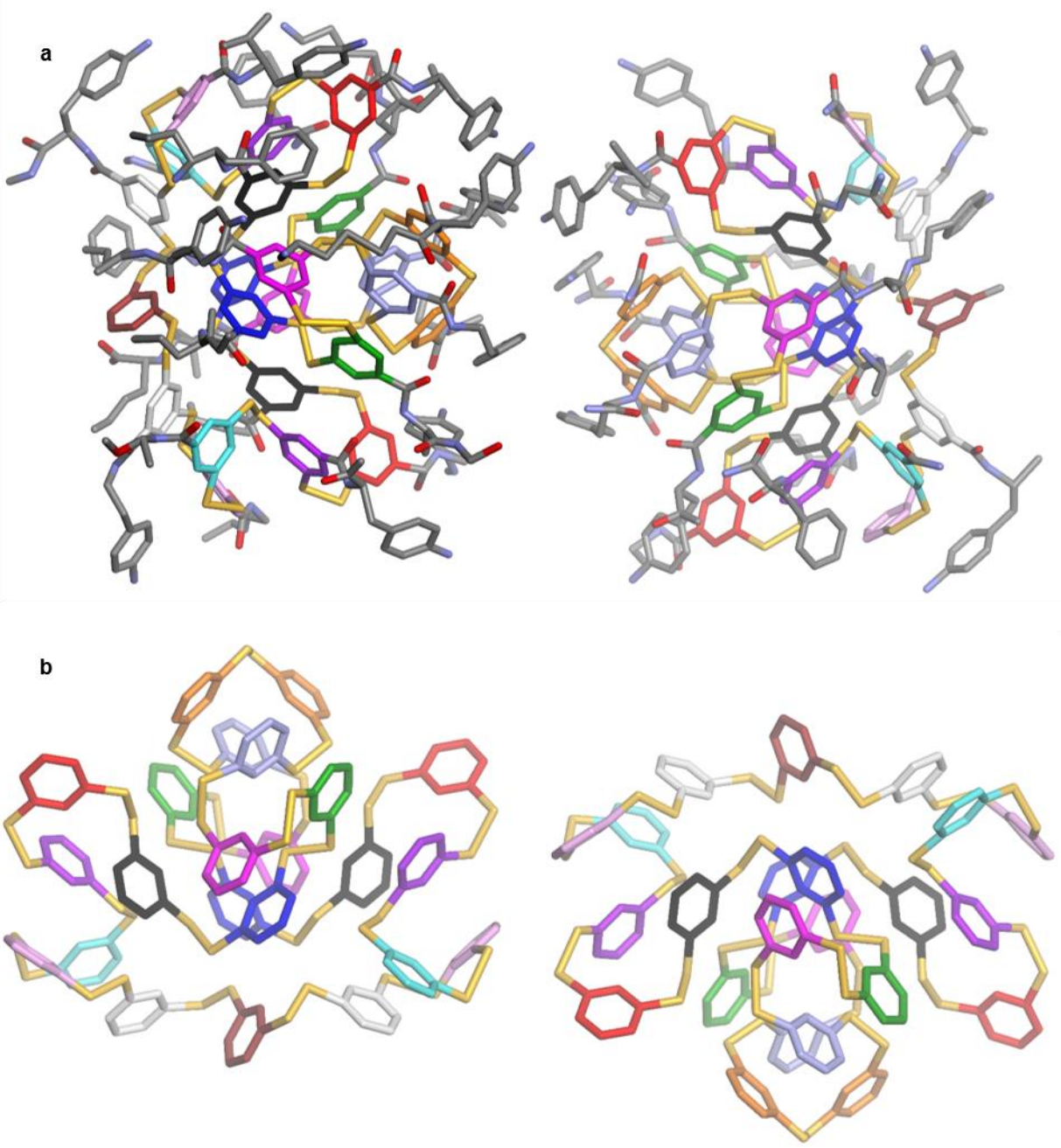

Supplementary Figure 107. Two distinct pairs of L-(**4d**)$_{23}$ and D-(**4d**)$_{23}$ related by pseudo-inversion centers in the structure L/D-(**4d**)$_{23}$. **a** one pair shows mainly side chain-mediated packing. **b** the other pair shows main chain-mediated packing (contacts between hydrophobic main chains).

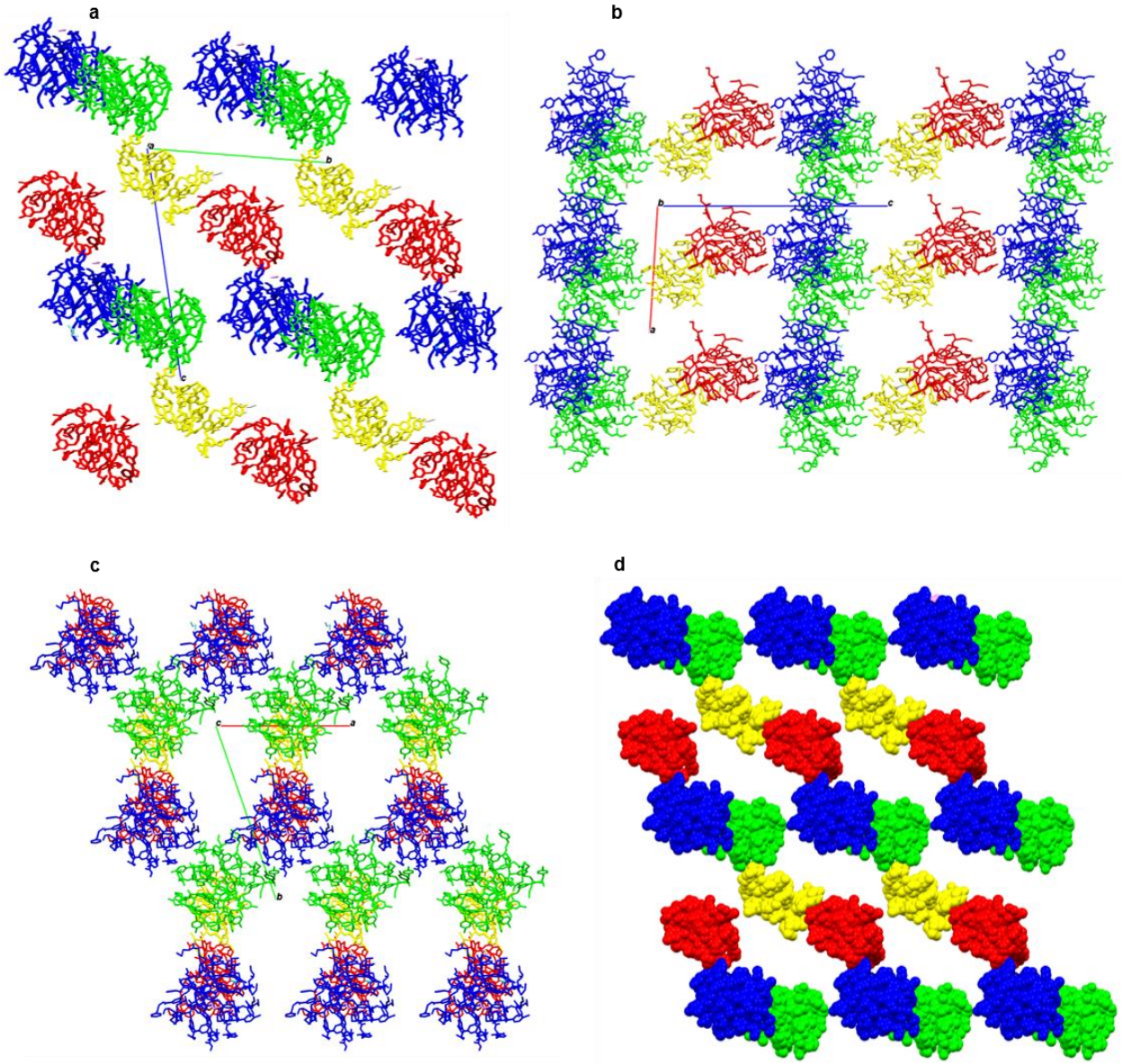

Supplementary Figure 108. Crystal packing arrangement of L/D-(**4d**)$_{23}$. Views along the crystallographic **a** *a*-axis; **b** *b*-axis; and **c** *c*-axis. The clusters are colored by pseudo symmetry operations. L-(**4d**)$_{23}$ in blue and yellow; D-(**4d**)$_{23}$ in green and red (d) Linear solvent channel-view down the *a*-axis.

Supplementary Table 4. Crystallographic data for L-(**4b**)$_{16}$ and L/D-(**4d**)$_{23}$.

Formula	$C_{289.5}H_{223}N_{56.5}O_{38.5}S_{32}$	$C_{301.75}N_{32.5}O_{21.25}S_{46}$
M	6129.10	5894.10
T/K	100	100
λ/Å	0.970	0.980
Crystal system	Hexagonal	Triclinic
Space group	$P6_2$	$P1$
a/Å	36.980 (5)	35.114 (2)
b/Å	36.980 (5)	49.232 (3)
c/Å	44.071 (9)	61.528 (5)
α/°	90.00	77.641 (1)
β/°	90.00	89.369 (1)
γ/°	120.00	71.229 (1)
V/Å^3	52194 (18)	98185.4 (14)
Z	3	4
ρ/g mm^{-3}	0.585	0.399
Color and shape	Colorless, prisms	Colorless, rod-like
Size (mm)	0.20 x 0.04 x 0.02	0.30 x 0.02 x 0.02
μ/mm^{-1}	0.332	0.316
Total reflections	89668	3777726
Unique reflections	22703	209616
R_{int}	0.0407	0.1082
Data/Restraints/Parameters	22703/1597/834	209616/584/5233
R1, wR2 (all data)	0.0833, 0.2401	0.1806, 0.3632
Goodness-of-fit	1.069	0.926
Largest diff. Peak/hole/e Å^{-3}	0.26/-0.18	1.46/-0.26

Supplementary Table 5. Containing Check cif alerts for L-(**4b**)$_{16}$ obtained from checkcif.iucr.org webpage and the authors'comments. Checkcif alerts for L/D-(**4d**)$_{23}$ could not be obtained from IUCr's checkcif algorithm.

Check cif alerts	Comments
The value of sine(theta_max)/wavelength is less than 0.550	Despite use of Synchrotron radiation, the diffraction limit was found to be 1.15 Å
Isotropic non-H Atoms in Main Residue(s) ..... 18 Report N0AA N10F N12F N13F N24 N25 etc.	The concerned atoms are side chain atoms of phenyl guanidium/ lysine that were severely disordered and very dynamic.
Too many H on C in C=N Moiety in Main Residue .. C2FA Check	This alert was checked.
Short Intra H...H Contact H19A ..H26A: 1.77 Å. x,y,z = 1_555 Check H19B ..H26B: 1.75 Å. x,y,z = 1_555 Check	This alert is generated due to large amount of disorder in the structure (side chains)
Short Inter D...A Contact O19 ..N2AA: 2.25 Å. 1-y,1+x-y,-1/3+z = 3_664 Check	This alert is generated due to large amount of disorder in the structure (side chains)
_diffrn_measured_fraction_theta_full value Low . 0.953 Why?	Despite use of Synchrotron radiation, the diffraction limit was found to be 1.15 Å
'MainMol' Ueq as Compared to Neighbors	This alert is generated due to large amount of disorder in the structure
Singly Bonded Carbon Detected (H-atoms Missing)	This alert is generated due to large amount of disorder in the structure (side chains)
Low Bond Precision on C-C Bonds 0.01931 Å	This alert is generated due to large amount of disorder in the structure
Long C(sp2)-C(sp2) Bond C4C - C7C 1.6 Å	This alert is generated due to large amount of disorder in the structure
Short Intra D-H..H-X H2E..H46 1.89 Å. x,y,z = 1_555 Check	This alert is generated due to large amount of disorder in the structure
Short Inter D...A Contact O2..N12F 2.78 Å. x+y,1-x,1/3+z = 5_565 Check	This alert is generated due to large amount of disorder in the structure

8. Salt effect on 4a

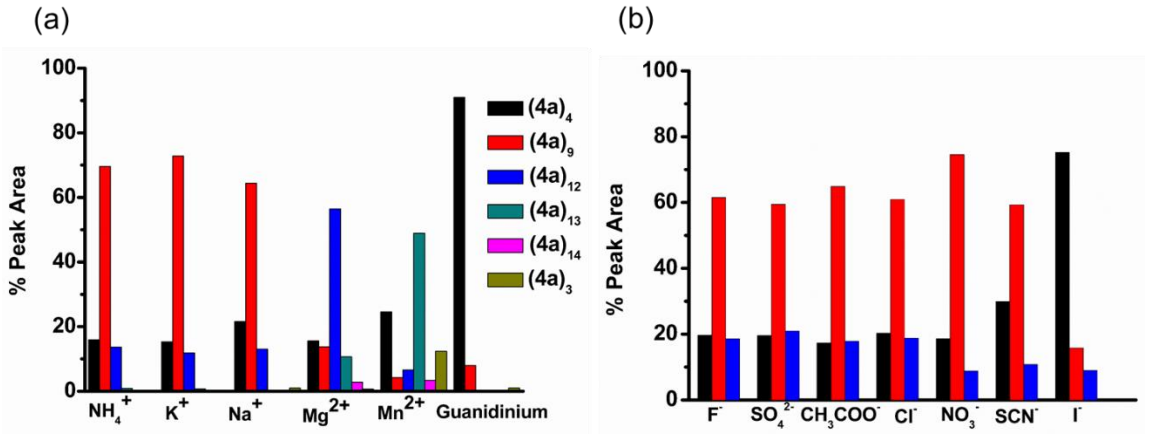

Supplementary Figure 109. Histograms showing product distributions of DCLs made from building block **4a** (2.0 mM) in borate buffer (12.5 mM, pH = 8.0) in the presence of 1.0 M of different (a) chloride and (b) sodium salts.

9. Isolation of $(4a)_{13}$

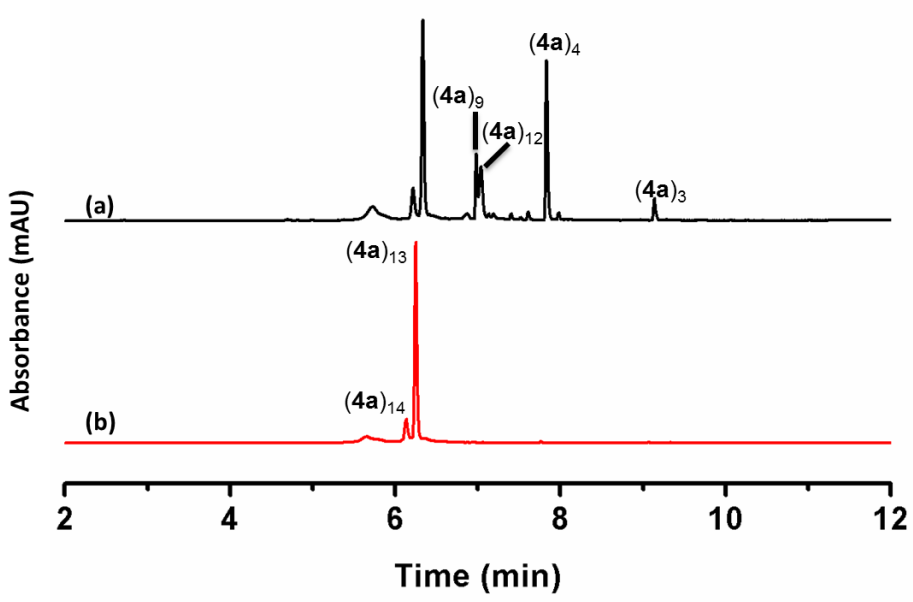

Supplementary Figure 110. UPLC analyses of the DCL made from **4a** (**a**) in the presence of 1.0 M $MnCl_2$ and (**b**) after flash column chromatography.

10. ITC data for titration of $(4a)_{13}$ with $MnCl_2$

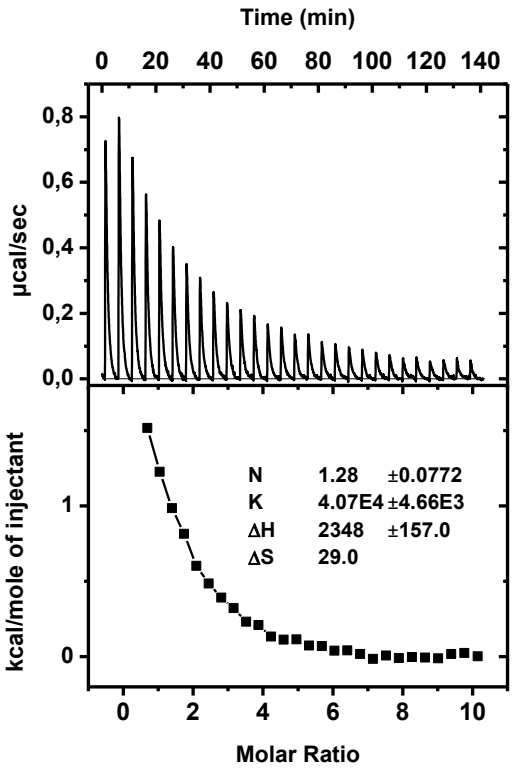

Supplementary Figure 111. ITC data of (**4a**)$_{13}$ (0.025 mM) titrated with a solution of 5.0 mM $MnCl_2$ in borate buffer (12.5 mM, pH = 8.0) at 25 °C. Repeating the data analysis after fixing the stoichiometry (N = 1.00) does not alter significantly the obtained value for the binding constant.

11. ITC data for titration of $(4a)_{13}$ with T1-T3

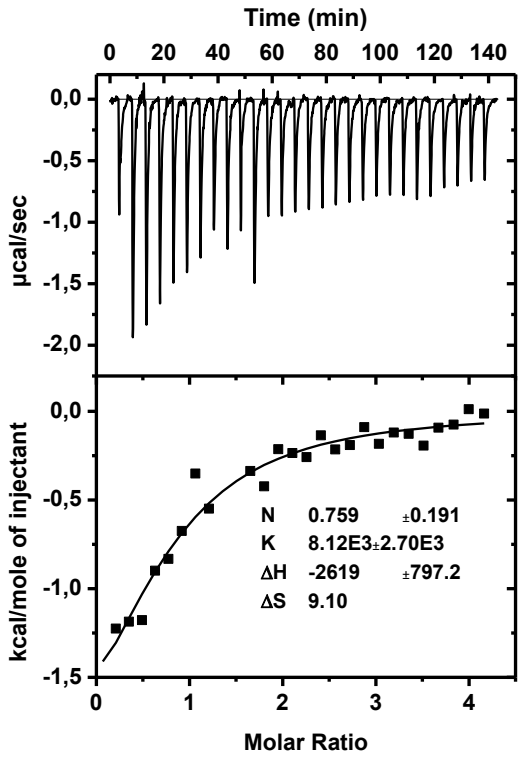

Supplementary Figure 112. ITC data of (**4a**)$_{13}$ (0.025 mM) titrated with a solution of 5.0 mM **T3** in borate buffer (12.5 mM, pH = 8.0) at 25 °C. Repeating the data analysis after fixing the stoichiometry (N = 1.00) does not alter significantly the obtained value of the binding constant.

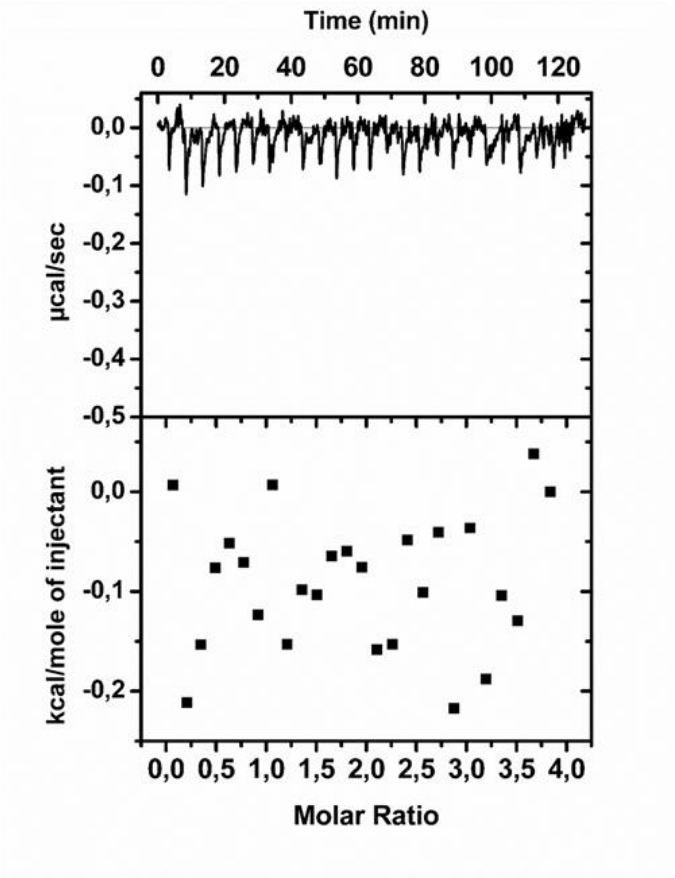

Supplementary Figure 113. ITC data of (**4a**)$_{13}$ (0.025 mM) titrated with a solution of 5.0 mM **T1** in borate buffer (12.5 mM, pH = 8.0) at 25 °C.

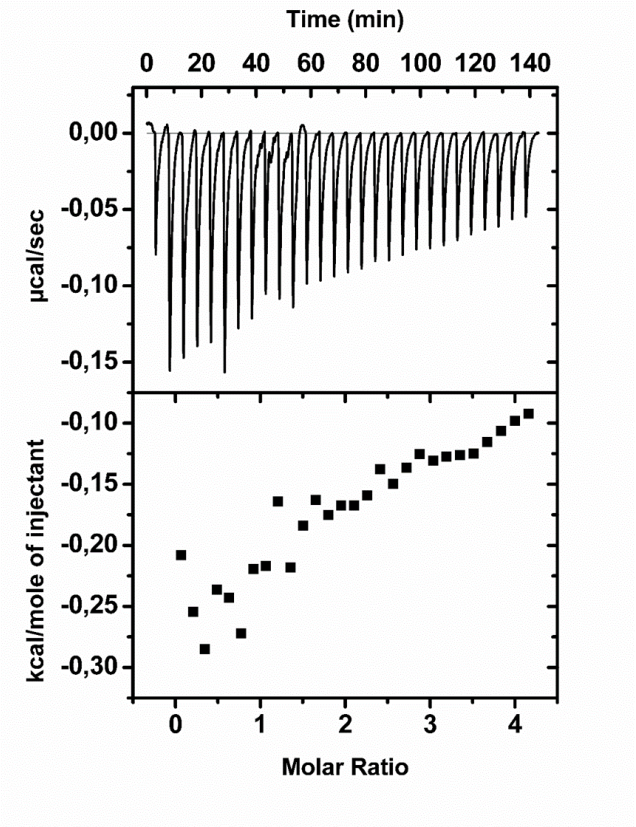

Supplementary Figure 114. ITC data of $(\mathbf{4a})_{13}$ (0.025 mM) titrated with a solution of 5.0 mM **T2** in borate buffer (12.5 mM, pH = 8.0) at 25 °C.

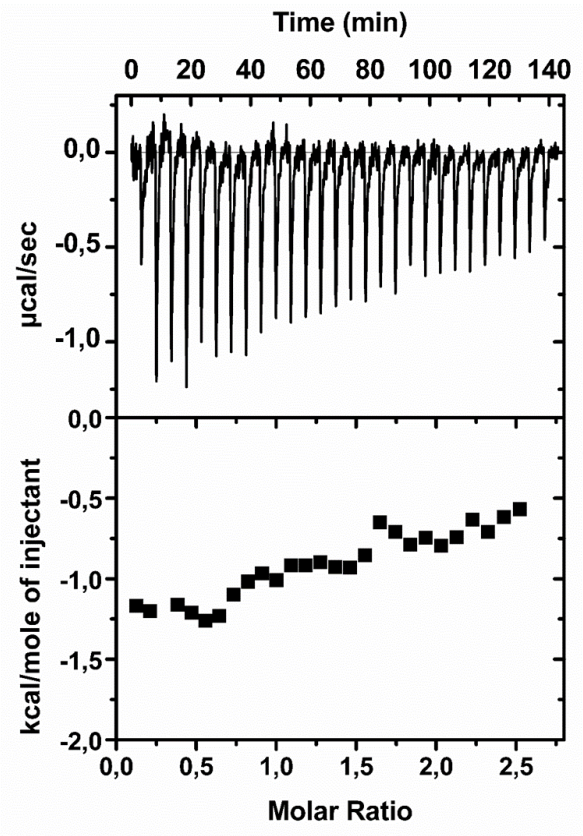

Supplementary Figure 115. ITC data of (**4a**)$_4$ (0.025 mM) titrated with a solution of 5.0 mM **T3** in borate buffer (12.5 mM, pH = 8.0) at 25 °C.

12. UPLC/MS analyses of peptide template effects

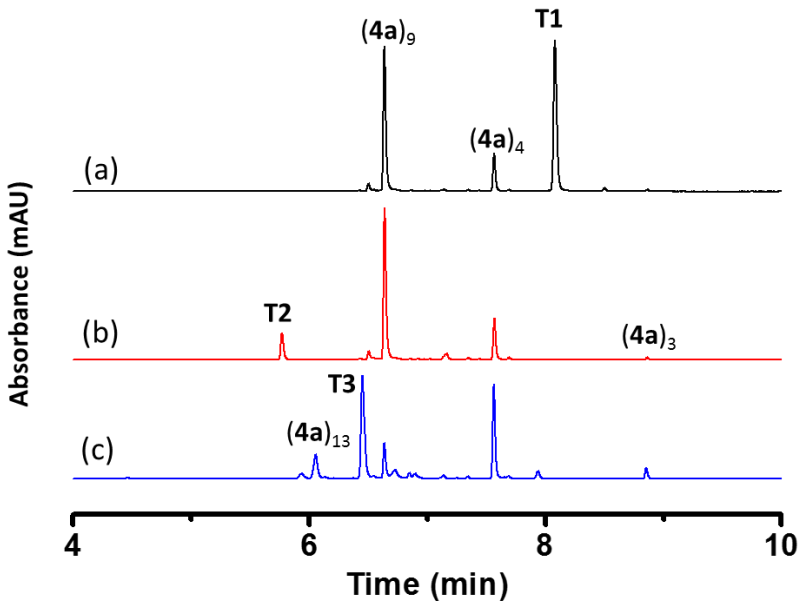

Supplementary Figure 116. UPLC analyses of the DCL made from 2.0 mM **4a** (**a**) in the presence of 2.0 mM template **T1** (**b**) template **T2** and (**c)** template **T3**.

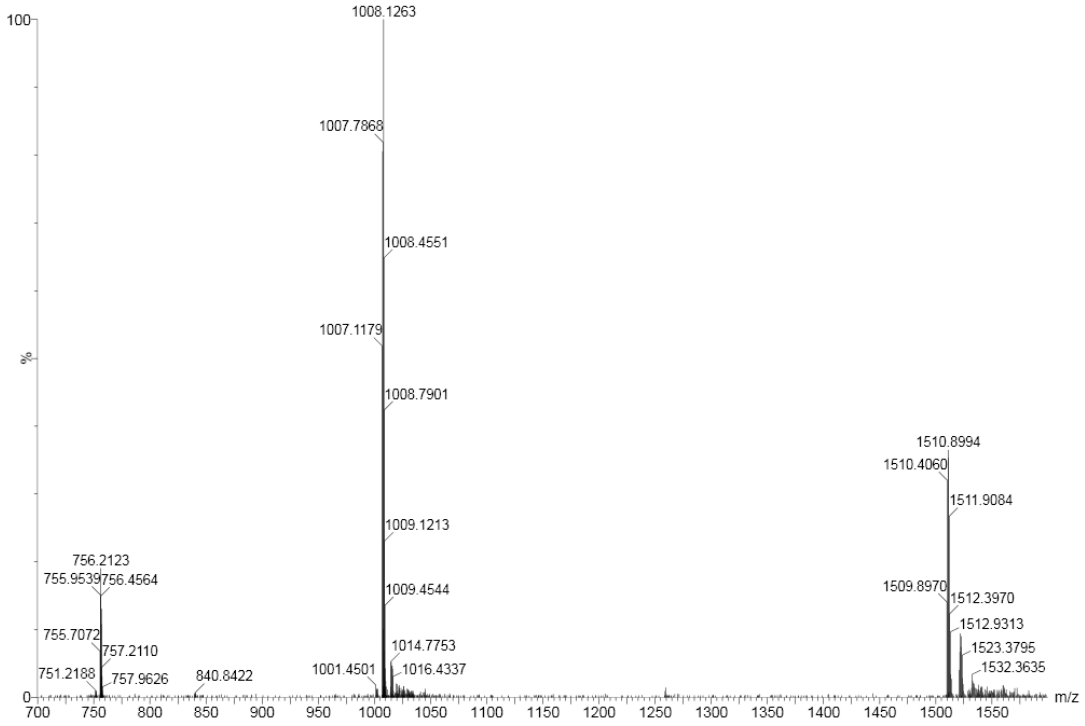

Supplementary Figure 117. Mass spectrum of (**4a**)$_6$ (retention time 7.70 min in Figure 2b) from the LC-MS analysis of a DCL made from **4a** (2.0 mM) in presence of 5.0 mM template **T3**. (**4a**)$_6$: m/z calculated: 1510.36 $[M+2H]^{2+}$, 1007.24 $[M+3H]^{3+}$, 755.69 $[M+4H]^{4+}$; m/z observed: 1510.41 $[M+2H]^{2+}$, 1007.12 $[M+3H]^{3+}$, 755.71 $[M+4H]^{4+}$.

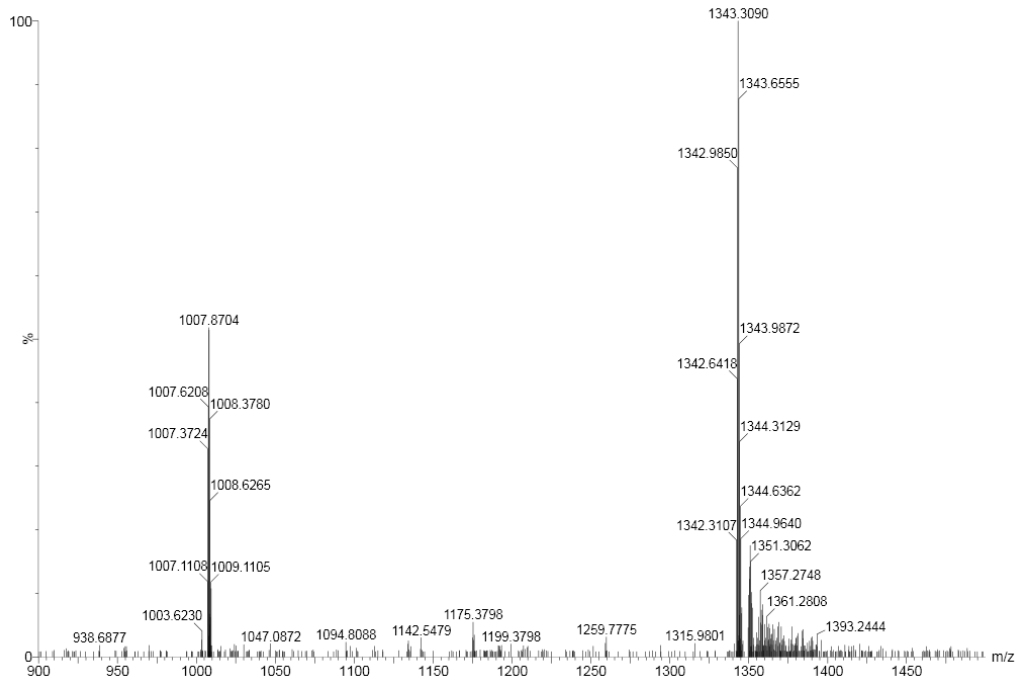

Supplementary Figure 118. Mass spectrum of $(\mathbf{4a})_8$ (retention time 7.27 min in Figure 2b) from the LC-MS analysis of a DCL made from **4a** (2.0 mM) in presence of 5.0 mM template **T3**. $(\mathbf{4a})_8$: m/z calculated: 1342.66 $[M+3H]^{3+}$, 1007.24 $[M+4H]^{4+}$; m/z observed: 1342.64 $[M+3H]^{3+}$, 1007.37 $[M+4H]^{4+}$.

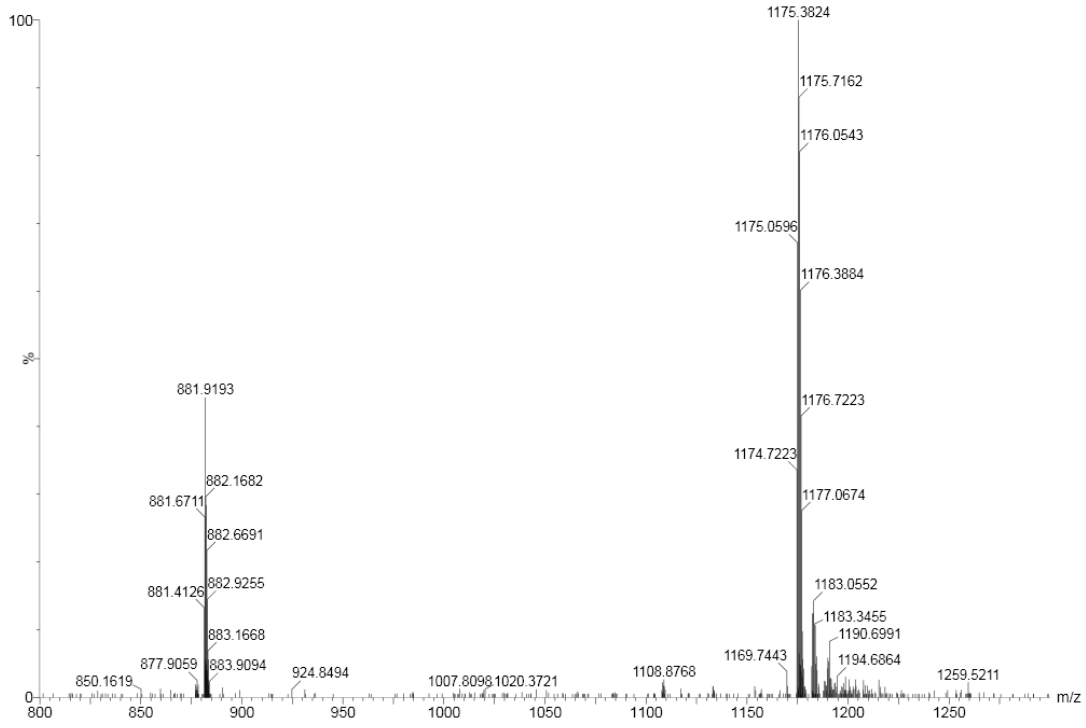

Supplementary Figure 119. Mass spectrum of (**4a**)$_7$ (retention time 6.93 min in Figure 2b) from the LC-MS analysis of a DCL made from **4a** (2.0 mM) in presence of 5.0 mM template **T3**. (**4a**)$_7$: m/z calculated: 1174.95 $[M+3H]^{3+}$, 881.46 $[M+4H]^{4+}$; m/z observed: 1175.06 $[M+3H]^{3+}$, 881.41 $[M+4H]^{4+}$.

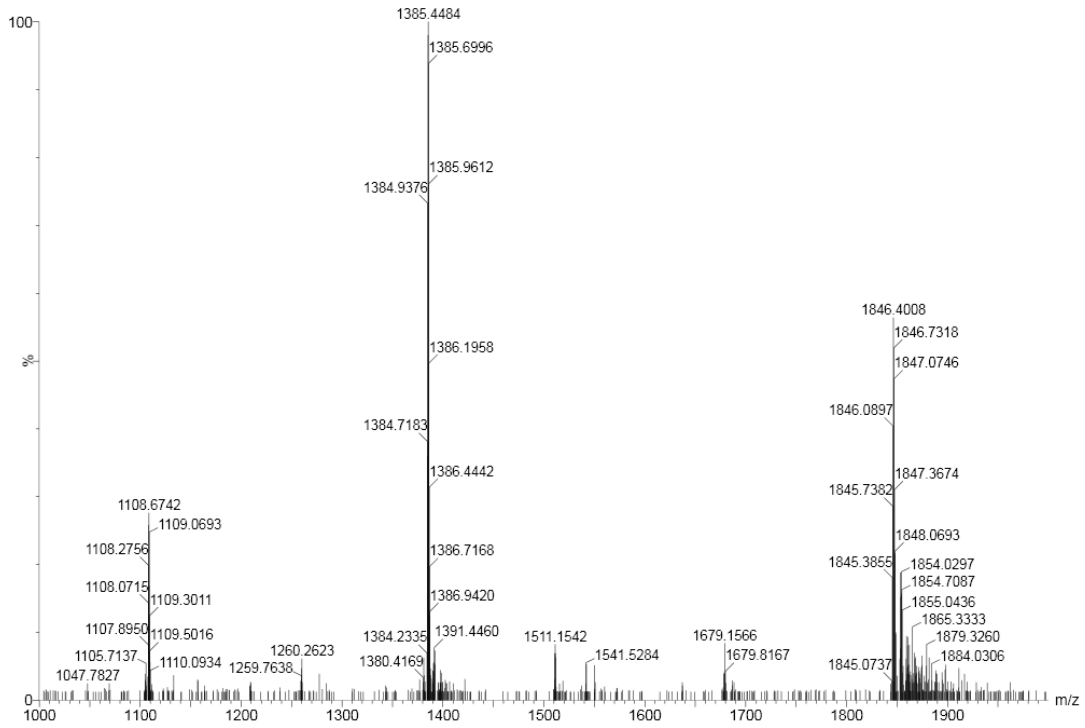

Supplementary Figure 120. Mass spectrum of $(\mathbf{4a})_{11}$ (retention time 6.86 min in Figure 2b) from the LC-MS analysis of a DCL made from **4a** (2.0 mM) in presence of 5.0 mM template **T3**. $(\mathbf{4a})_7$: m/z calculated: 1845.78 $[M+3H]^{3+}$, 1384.58 $[M+4H]^{4+}$, 1107.87 $[M+5H]^{5+}$; m/z observed: 1845.74 $[M+3H]^{3+}$, 1384.72 $[M+4H]^{4+}$, 1107.90 $[M+5H]^{5+}$.

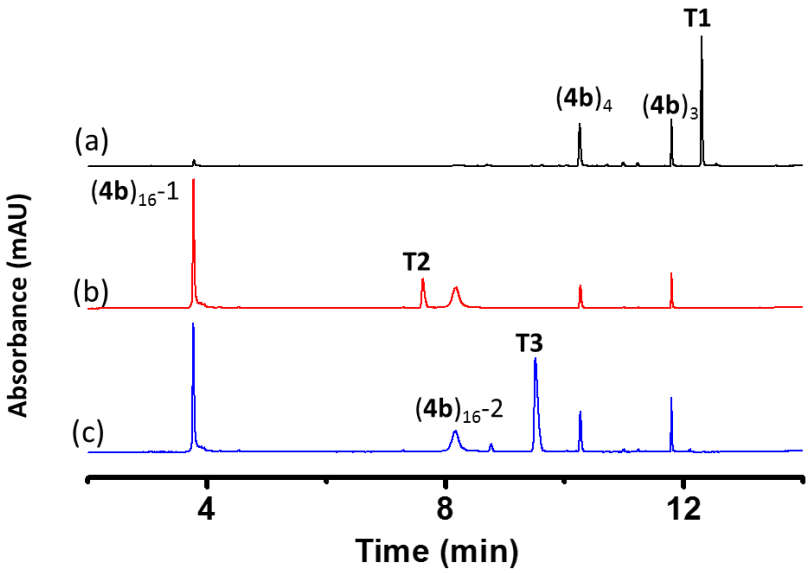

Supplementary Figure 121. UPLC analyses of the DCL made from 2.0 mM **4b** (**a**) in the presence of 2.0 mM template **T1** (**b**) template **T2** and (**c)** template **T3**.

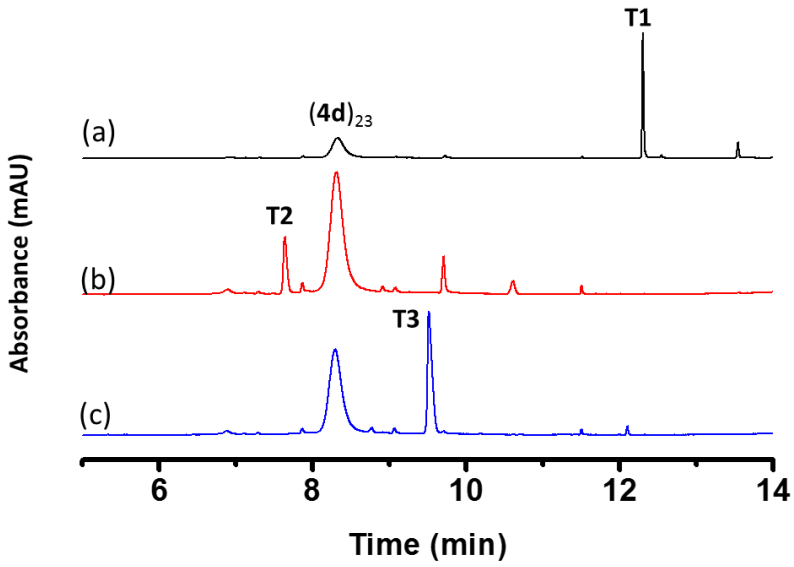

Supplementary Figure 122. UPLC analyses of the DCL made from 2.0 mM **4d** (**a**) in the presence of 2.0 mM template **T1** (**b**) template **T2** and (**c**) template **T3**.

References

For building block **3d**: Bartolec, B.; Altay, M.; Otto, S. Template-promoted self-replication in dynamic combinatorial libraries made from a simple building block. *Chem. Commun.*, **2018**, 54, 13096-13098.

For building block **1b**: Liu, B.; Pappas, C. G.; Zangrando, E.; Demitri, N.; Chmielewski, P. J.; Otto, S. Complex Molecules That Fold Like Proteins Can Emerge Spontaneously. *J. Am. Chem. Soc.*, **2019**, 141, 1685-1689.